AIRCRAFT OPTIMIZATION FOR MINIMAL ENVIRONMENTAL IMPACT

A DISSERTATION
SUBMITTED TO THE DEPARTMENT OF AERONAUTICS AND ASTRONAUTICS
AND THE COMMITTEE ON GRADUATE STUDIES
OF STANFORD UNIVERSITY
IN PARTIAL FULFILLMENT OF THE REQUIREMENTS
FOR THE DEGREE OF
DOCTOR OF PHILOSOPHY

Nicolas Eugene Antoine
August 2004

I certify that I have read this dissertation and that, in my opinion, it is fully adequate in scope and quality as a dissertation for the degree of Doctor of Philosophy.

Ilan M. Kroo
(Principal Adviser)

I certify that I have read this dissertation and that, in my opinion, it is fully adequate in scope and quality as a dissertation for the degree of Doctor of Philosophy.

Juan J. Alonso

I certify that I have read this dissertation and that, in my opinion, it is fully adequate in scope and quality as a dissertation for the degree of Doctor of Philosophy.

Sanjiva Lele

Approved for the University Committee on Graduate Studies.

"C'est l'aviation qui m'a fait découvrir mon royaume intérieur."

– Adrienne Bolland
Test Pilot and Aviation Pioneer (1895-1975)

"My airplane is quiet, and for a moment still an alien,
still a stranger to the ground, I am home."

– Richard Bach
Stranger to the Ground

"The 50-year exception is now over and aviation should grow up and play its full role in delivering a responsible and intelligent sustainable development plan for the future. At the core of this plan will be less flying, less freight carried by air, and an end to airport expansion plans."

– John Whitelegg
Liverpool John Moores University

Abstract

While aircraft environmental performance has been important since the beginnings of commercial aviation, continuously increasing passenger traffic and a rise in public awareness have made aircraft noise and emissions two of the most pressing issues hampering commercial aviation growth today. This research explores the feasibility of integrating noise and emissions as optimization objectives at the aircraft conceptual design stage, thereby allowing a quantitative analysis of the trade-offs between environmental performance and operating cost. Beyond meeting regulations and establishing environmental performance trades, the design tool allows the generation of extremely low-noise and low-emissions designs that could, in the future, dramatically decrease the environmental impact of commercial aviation, albeit at the expense of increased operating cost. To these ends, a preliminary design tool was developed that uses a multiobjective genetic algorithm to determine optimal aircraft configurations and to estimate the sensitivities between the conflicting objectives of low noise, low emissions, and operating costs. The design tool incorporates ANOPP, a detailed noise prediction code developed at NASA Langley, and NASA Glenn's NEPP engine simulator, as well as aircraft design, analysis, and optimization modules developed at Stanford.

Acknowledgements

For someone passionate about aviation, joining the Aircraft Aerodynamics and Design Group at Stanford University was a privilege. During my four years with the group, I have had the pleasure to work closely with and alongside Stefan Bieniawski, Martin Chan, Takumi Kobayashi, Peter Kunz, Hak-Tae Lee, Yoshi Makino, and Peter Sturdza: thanks for the stimulating conversations and exchanges of ideas. I will miss them.

Of course, a research group is only as good as its leader. My work owes much to the inspirational guidance and the peerless advice Professor Ilan Kroo provided tirelessly throughout my Ph.D. program. I am in his debt and will always be grateful to have had the opportunity to learn from the best. I hope that I was able to make a modest contribution to the fertile research environment he fostered.

David Rodriguez at Desktop Aeronautics and Scott Jones at NASA Glenn helped me get started with NEPP, while John Rawls, Jr. at NASA Langley patiently provided much-needed tutoring with ANOPP. My thanks also to MIT Professors Karen Willcox and Ian Waitz, and their student Garrett Barter for their contributions through the joint NASA-Stanford-MIT EDS program.

Jane Lintott was a wonderful administration assistant and always went the extra mile, with a smile, to be helpful. Her replacement after she retired, Nandita Pakrasi, was also a model of efficiency.

I am grateful to Professors Juan Alonso and Sanjiva Lele for reading this thesis and providing extensive feedback. Professor Chris Edwards, who acted as chair for my defense, was an excellent resource for the emissions chapter. Thanks also to Professor George Springer for agreeing to serve as a defense examiner.

A balanced life would be impossible without friends and family. I am fortunate to have been surrounded by some amazing people during my years at Stanford. To Alexandre Bayen, Cathy Chou, Wilf Knecht, Justin Kuck, Mayana Malik, Andrés Mediavilla, Karen Nelson, Andrew O'Brien, Francis Sweeney, Peter Syré, Caroline Vialard-Goudou, John Wilde, and Joe Wolski: thank you for your enduring friendships. You've kept me sane.

It is in California that I rediscovered my passion for the outdoors that I thought I had lost after leaving Kenya. To my great friends Joaquim Martins and Jamie Nam, thanks for getting me hooked on mountain biking, running, skiing, and surfing — the essentials of a proper California lifestyle. It did more good than you can imagine!

One of the happiest events during my time at Stanford occurred when my brother, François, moved to the Bay Area with Amada, now my very own *cuñada*. We have had plenty of laughs together, with hopefully many more to come. To both of them, thank you for your support and for putting things in perspective when needed. Not to mention keeping your fridge fully stocked for the 'starving student' of the family.

Guy and Jacqueline Antoine-Mathy, my parents, always thought it a little strange that I could identify various sub-types of aircraft from the age of four, but they never failed to support my addiction to everything airplane-related. I was extremely fortunate to be able to rely on them for emotional support during the inevitable highs-and-lows that accompany a long-term project such as a Ph.D. In the process, they taught me the most important lesson of all: *primum vivere*. This thesis is dedicated to them.

Contents

List of Tables

List of Figures

Chapter 1

Introduction

1.1 Aviation and the Environment

Aircraft noise and emissions have been of concern since the beginning of commercial aviation. The continuing growth in air traffic and increasing public awareness have made environmental considerations one of the most critical aspects of commercial aviation today. It is generally accepted that significant improvements to the environmental acceptability of aircraft will be needed if the long-term growth of air transport is to be sustained. This is an open issue. The Intergovernmental Panel of Climate Change (IPCC) has projected that, under an expected 5% annual increase in passenger traffic, the growth in aviation-related nuisances will outpace improvements that can be expected through evolutionary changes in engine and airframe design [1].

1.1.1 Noise

While considerable progress has been made to reduce the noise signature of airliners, the public's perception of noise continues to grow, as illustrated by the ever-increasing number of public complaints. This can be attributed to increasing air traffic as well as further encroachment by airport-neighboring communities. As a result, noise has become a major constraint to air traffic, with 60% of all airports considering it a major problem and the nation's fifty largest airports viewing it as their biggest issue [2].

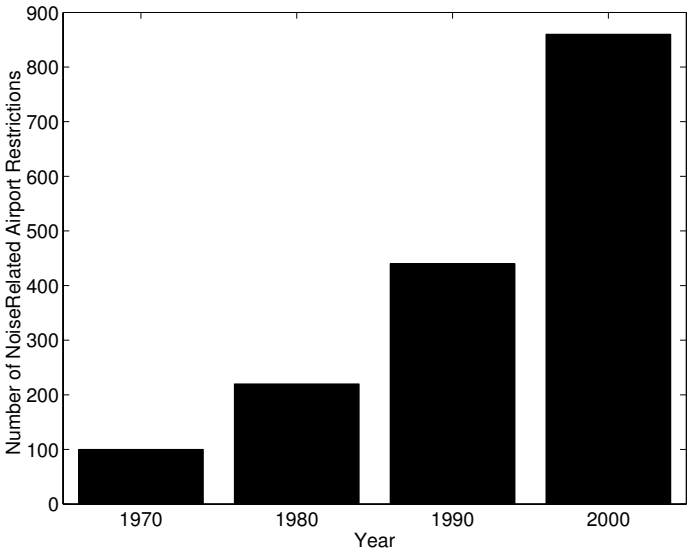

Figure 1.1: The world-wide increase in airport-enforced noise restrictions.

The construction of new runways and airports raises massive issues due to public fears of increased air traffic and the associated louder, or more frequent, noise. In response to these public concerns, airports have adopted operational restrictions on top of the International Civil Aviation Organization (ICAO) certification guidelines. A survey of the world's airports reveals a two-fold increase in the number of noise-related restrictions in the past ten years [3]. These include curfews, fines, operating restrictions, and quotas (Figure 1.1).

The historical trend in aircraft noise has shown a reduction of approximately 20dB since the 1960s [4] largely due to the adoption of high bypass turbofans and more effective lining materials. Reductions since the mid-eighties have not been as dramatic (Figure 1.2). The point seems to have been reached where future improvements through technological advances will be possible only by significantly trading off operating costs for environmental performance. As shown on the notional graph in Figure 1.3, the outlook is that further reductions in the environmental impact of commercial aircraft will exact increasingly severe penalties in operating costs. Quantifying the terms of this trade-off — critical for the efficient design of future aircraft — is one of the main topics addressed by this research.

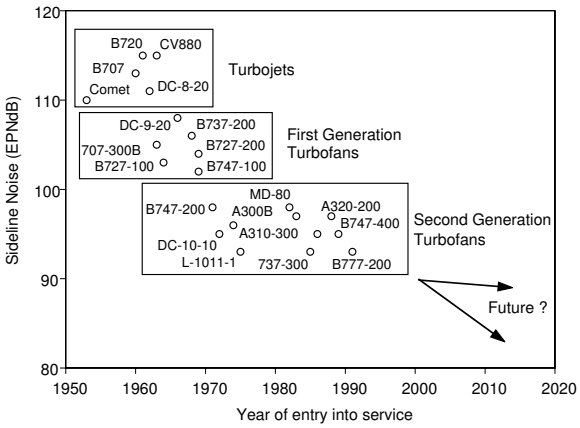

Figure 1.2: The progress in noise reduction is illustrated by a select number of commercial aircraft of the past 50 years.

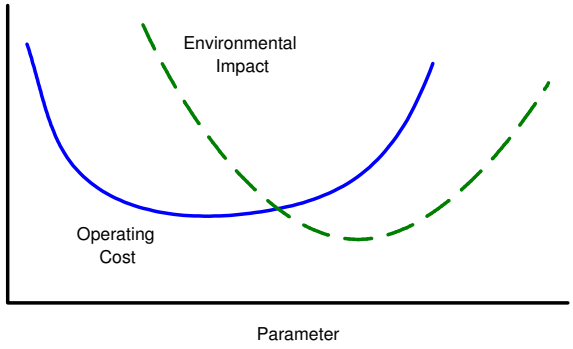

Figure 1.3: Technological advances reduce the environmental impact of aircraft, but only at rising operating costs. The challenge is to determine the designs offering the optimal trade-off between operating and environmental performances.

The ICAO Assembly has endorsed the concept of a 'Balanced Approach' that aims to address noise issues by working simultaneously on four parameters: aircraft noise at the source, flight and operating procedures, operating restrictions at airports, and land-use planning and management (Figure 1.4). While the focus of this research is firmly on the first two parameters, it should be kept in mind that significant reductions in acoustic nuisances around airports will also require contributions from airports, regulating authorities and local land planners.

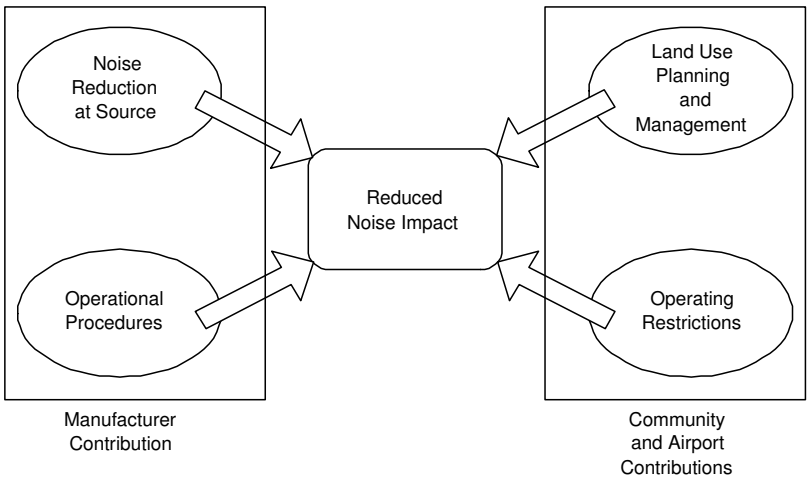

Figure 1.4: The ICAO Balanced Approach: successfully reducing the noise impact of commercial aircraft on communities must include contributions from the manufacturers, airports, and communities.

1.1.2 Emissions

The release of exhaust gasses in the atmosphere is the second major environmental issue associated with commercial airliners. The world fleet releases approximately 13% of CO_2 emissions from all transportation sources, or 2% of all anthropogenic sources [5]. The expected doubling of the fleet in the next twenty years [6] will certainly exacerbate the issue: the contribution of aviation is expected to increase by a factor of 1.6 to 10, depending on the fuel use scenario. Conscious of this problem, engine manufacturers have developed low-emission combustors, and made them available as options. These combustors have been adopted by airlines operating in European airports with strict emissions controls, in Sweden [7] and Switzerland, for example.

Current emissions regulations have focused on local air quality in the vicinity of airports. Emissions released during cruise in the upper atmosphere are recognized as an important issue with potentially severe long-term environmental consequences, and ICAO is actively seeking support for regulating them as well. However, political and diplomatic considerations compound the difficulty of reaching an agreement on emissions levels in international airspace.

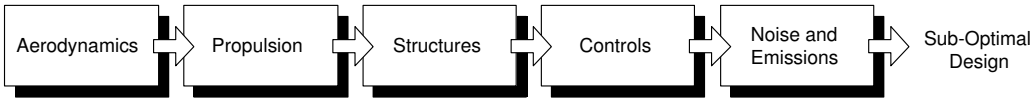

Figure 1.5: Sequential optimization is unable to produce truly optimal designs.

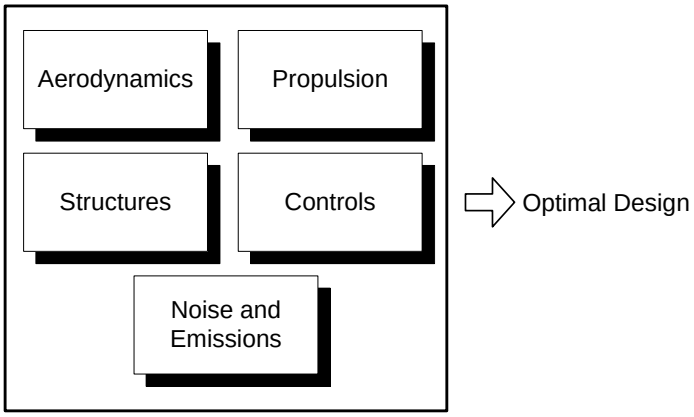

Figure 1.6: Simultaneous consideration of all aspects of aircraft design can yield truly optimal designs.

1.2 An Integrated Approach

Commercial aircraft design processes have focused primarily on producing airplanes that meet performance goals at minimum operating costs. Environmental performance has been considered mostly at a post-design analysis phase, during which adjustments are made to satisfy the noise and emissions requirements of individual airlines or airports. This sequential design approach does not guarantee that the final aircraft is of overall optimal design, but it served its purpose as long as only localized, minor adjustments were necessary to bring aircraft into environmental compliance. However, following the gradual tightening of environmental requirements, the cost and complexity of achieving compliance has increased significantly.

To illustrate the point, consider the Airbus A380, which had to be modified well into the design phase, at the request of airlines, to meet nighttime restrictions at London Heathrow airport. The modification involved using an engine fan substantially larger than required for lowest fuel consumption, necessitating a redesign of the engine, nacelle, pylon and wing.

These modifications resulted in a 1-2% increase in fuel burn for a 1-2 dB noise reduction [8], considered a very expensive trade-off. Such sub-optimal solutions are the unavoidable outcome of a sequential optimization process that is still the norm in the industry (Figure 1.5).

On the emissions front, the ICAO's Committee on Aviation Environmental Protection, at its 6th meeting in early 2004, concluded that it could not demand, for new aircraft entering service in 2008, a reduction of aircraft NO_x of more than 12% relative to today's aircraft [9]. The issue was not related to technology risk: existing combustors can today attain this level of emissions performance. The reason was a lack of information regarding interrelationships: the impact of further NO_x reductions on noise and other emissions was not fully understood. It was agreed that demanding a reduction in one type of emissions only to obtain an increase in another — by an unknown quantity — was not a viable solution.

Clearly, there is a need for integrating environmental considerations at an earlier stage of the aircraft design process, and for more systematic investigation and quantification of the tradeoffs involved in meeting specific noise/emissions constraints. This research intends to contribute by proposing a conceptual design tool structured to generate optimized preliminary aircraft designs based on specified mission parameters. Existing aircraft design codes were extensively modified to incorporate the parameters required to model environmental performance. Various optimizers were also created to explore the design space, while noise prediction codes and an engine simulator were integrated into the automated design process.

The design tool enables users, *inter alia*, to evaluate the sensitivity of optimized aircraft to variations in operating and environmental requirements, and to compare the merits of various trade cases. Because all aspects of the aircraft are considered simultaneously, the tool allows for truly optimal designs to be obtained (Figure 1.6).

The research also briefly explores the implications of introducing environmentally optimized aircraft into existing fleets and route networks. It proposes a simple aircraft allocation model that, in conjunction with the aircraft design tool, allows the user to determine the optimal fleet mix and size of future low-noise aircraft in their fleets.

1.3 Organization of Thesis

Chapters 2 and 3 discuss noise and emissions sources, their modeling, and potential reduction scenarios. Chapter 4 introduces the concept, structure, and codes of the design tool. Optimization methods are discussed in Chapter 5. The focus of Chapter 6 is a discussion of results generated by the design tool for trade studies of noise, cost, and emissions. Chapter 7 addresses the operational considerations of introducing lower-noise airplanes into a fleet. Finally, Chapter 8 concludes the research and includes possible topics for future work.

Chapter 2

Aircraft Noise

2.1 Noise and the Public

2.1.1 The Noise Issue

While aircraft noise has been a problem since the beginnings of aviation (Figure 2.1), the introduction in the late 1950s of jet-powered aircraft, with their excruciatingly loud turbojets, led the Federal Aviation Administration (FAA) to adopt noise certification regulations in 1971. The expansion, as well as the construction, of airports, has brought high levels of noise to communities that had traditionally enjoyed a certain level of serenity.

It is the responsibility of the aircraft and engine manufacturers to ensure that an airplane meets certification standards in noise. However, communities living in the vicinity of airports have been pushing hard for tight restrictions on total air traffic noise, leading to additional requirements on top of certification standards.

Night operations, in particular, have been increasingly restricted. At London Heathrow airport, for example, only the quietest aircraft are allowed to operate at nighttime, and flights are further restricted through a points system, known as the Quota Count system [11]. Each landing and takeoff costs points based on the certification noise of the airplane, and the cumulative points cannot exceed a certain total over specific time periods.

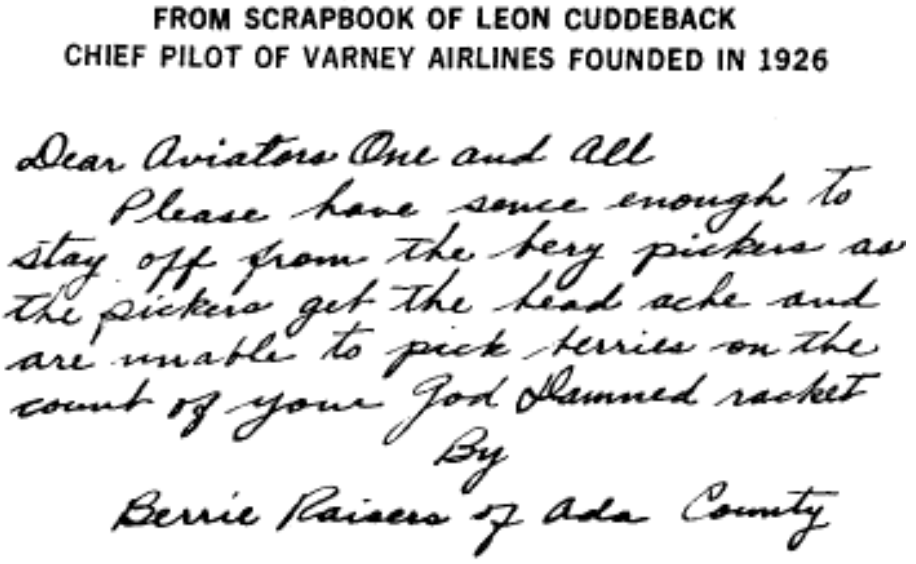
FROM SCRAPBOOK OF LEON CUDDEBACK
CHIEF PILOT OF VARNEY AIRLINES FOUNDED IN 1926

Dear Aviators One and All
Please have sence enough to
stay off from the hey pickers as
the pickers get the head ache and
are unable to pick berries on the
count of your God dammed racket
By
Berrie Raisers of Ada County

Figure 2.1: Aircraft noise complaints predate mass commercial transport [10].

Consequently, during sensitive periods, the only solution to allow more flights is to use quieter planes, with the result that airlines, especially those operating at night (especially cargo operators), face equipment and scheduling constraints. Recognizing the importance of such restrictions, manufacturers have adopted the London system as a benchmark for the noise levels of their aircraft — and strive to build planes exceeding FAA certification requirements.

The trend towards tighter noise restrictions, and stiff penalties for breaking them, is expected to continue: in Europe, many airports charge landing and takeoff fees that are based in part on the certification noise of the aircraft. The noise-related component of the fees is significant, and can result in a 100% increase in takeoff/landing fees for noisier aircraft. While such fees are currently illegal in the United States, affected communities have used other means to demand improvements in noise levels: in-depth environmental impact studies, covering all affected neighborhoods, are now the norm for most airport expansions that are allowed to proceed only if the public will not suffer a measurable increase in noise (or emissions).

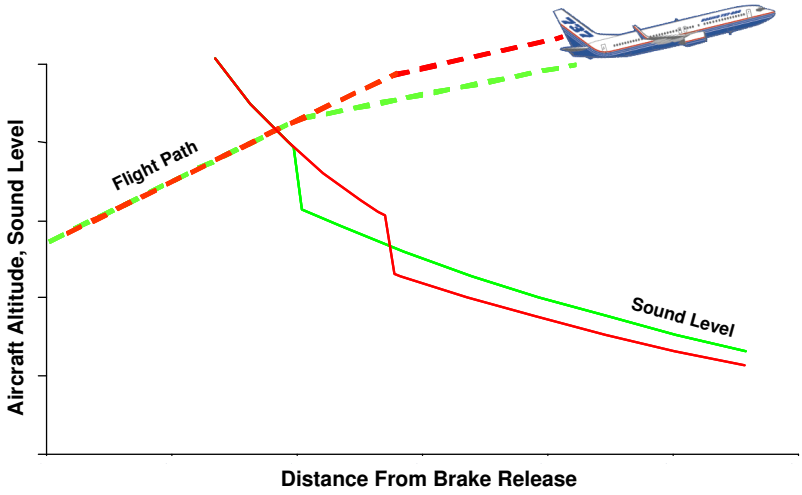

Figure 2.2: Thrust cutback on take-off: noise is displaced from the airport-neighboring communities [12].

2.1.2 Mitigation Measures

Investing in technology to reduce noise at the source is most promising but will have effects only in the long-term. Design decisions made today on noise performance will only have a gradual impact due to the relatively slow renewal rate of the worldwide airliner fleet — and the increasing lifespan of new models.

For the short term, considering the size of the current US fleet (5,100 aircraft), and the urgent need to increase capacity at airports to meet growth in traffic demand, the most effective method of complying with community noise regulations has been via noise mitigation procedures that can be adopted by existing aircraft.

Thrust cutback on takeoff (Figure 2.2) has been used since the early days of the turbojet as a method to minimize the noise exposure of adjacent communities. This method is still widely used although it has lost some of its former importance following the development of high-bypass turbofans whose noise emissions are less affected by throttling than those of earlier engines. Because a fixed amount of energy is required to bring an aircraft to cruise altitude, the total noise generated during the climb is fixed too, so that thrust cutback during the takeoff phase primarily displaces the noise to a different location.

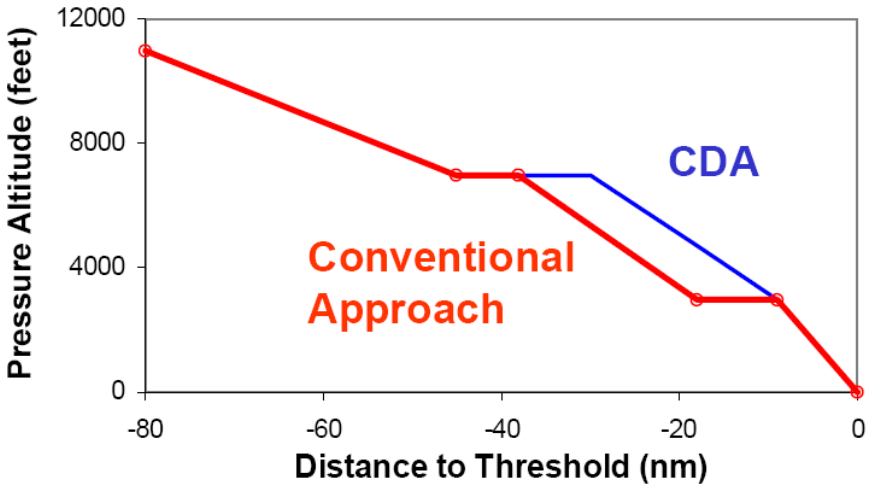

Figure 2.3: Continuous descent approach (CDA): the distance from the aircraft to the ground is increased during descent, reducing measured noise [15].

Thrust cutbacks to lower noise in the immediate vicinity of airports are counterbalanced by a reduction in the aircraft climb angle — increasing the area exposed to takeoff noise — and an increase in noise when the engines are returned to full power, that may affect other, more distant communities. As a result, thrust cutback is ideal at airports located close to low-population density areas, such as seaside airports (e.g. Orange County in California) where the procedure lowers noise substantially in the vicinity of the airport, but aircraft can resume full climb rapidly, without causing nuisance, once the ocean is reached. The ICAO and FAA allow pilots to execute thrust cutback between the altitudes of 800 ft (240 m) and 3000 ft (900 m).

On approach, commercial aircraft fly at altitudes around 3,000 ft for extended periods of time before intercepting the final glide slope. This has the effect of exposing a large amount of ground area to aircraft noise for extended periods of time. Considerable work is being done in developing continuous descent approaches (CDA), in which this plateau is eliminated altogether [13, 14]. The FAA and the airlines are in the process of certifying CDA approaches (Figure 2.3).

2.2 Noise Metrics

2.2.1 The deciBel

The passage of air over the aircraft structure or through the powerplants causes fluctuating pressure disturbances that propagate to an observer and are perceived as noise. These pressure disturbances are created by airflow discontinuities that occur in the engines — where power generation demands significant changes in pressure and temperature — and on the airframe: high-lift devices and landing gears, as well as the significant wetted area associated with these commercial aircraft, create considerable turbulence.

The human ear has a highly non-linear response, and is sensitive to a wide range of frequencies and million-fold changes to pressure levels. One of the most challenging aspects of noise abatement research is the taking into account of the observers' subjectivity. A logarithmic unit, the deciBel (dB) was developed to measure noise intensity, defined as the logarithmic ratio between actual sound pressure level (SPL) and a reference value, usually the threshold of hearing:

$$\mathrm{dB} = 10\log_{10}\frac{\mathrm{SPL}}{\mathrm{SPL}_{ref}} \tag{2.1}$$

Illustrating the challenge of decreasing noise, halving the sound intensity is reflected by a change of only 3 dB:

$$\mathrm{dB}_{half} = \log_{10}(2/1) = 3.01\mathrm{dB} \tag{2.2}$$

Similarly, computing the total noise from various source underlines the fact that reducing the noise from one source below the level of another has little beneficial effect on total noise. For example, with two sources $\mathrm{dB}_1 = 80$ dB and $\mathrm{dB}_2 = 95$ dB, the total noise perceived is imperceptibly louder than the loudest source:

$$\text{Total Noise} = 10\log_{10}(10^{0.1\mathrm{dB}_1} + 10^{0.1\mathrm{dB}_2}) = 95.13 \text{ dB} \tag{2.3}$$

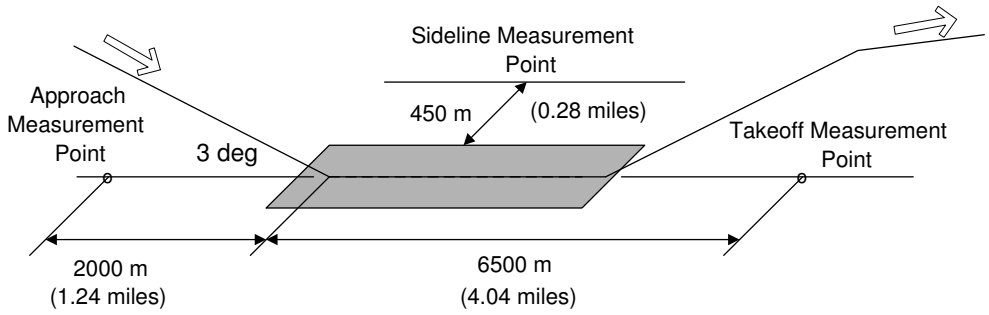

Figure 2.4: ICAO certification noise measurement points.

2.2.2 Aircraft Certification Noise

For certification purposes, a commercial aircraft must meet FAA Part 36 regulations, based on ICAO Annex 16 guidelines [16]. Noise certification is issued based on measurements made at three points during the takeoff and the landing procedures (Figure 2.4). Noise is recorded continuously at these points during takeoff and landing. Time-integrated sideline, climb, and approach noise — known as Effective Perceived Noise Levels (EPNL) — must not exceed a set limit, based on the maximum takeoff weight of the airplane and the number of engines. Jet noise typically dominates in sideline and climb noise. On approach at low power, the use of high bypass ratios diminishes engine contribution to noise, making aerodynamic noise a major component.

Current aircraft must meet so-called Chapter 3 noise regulations at the time of certification. Beginning in 2006, new aircraft will have to meet stricter Chapter 4 certification rules that dictate a cumulative noise reduction of at least 10 EPNdB relative to Chapter 3. Community noise is typically reported in Day-Night Levels, a metric that averages the total sound energy (in A-weighted dB) over 24 hours. DNLs are particularly suited for reporting overall airport operations to the public because they give a picture of the total noise exposure, including the effects of the mix of the fleet operating from the airport, as well as runway usage and operational procedures.

Because the focus of this research is on aircraft, EPNLs are used as the noise metric. This manufacturer-reported number is independent of airport, fleet mix and operational factors.

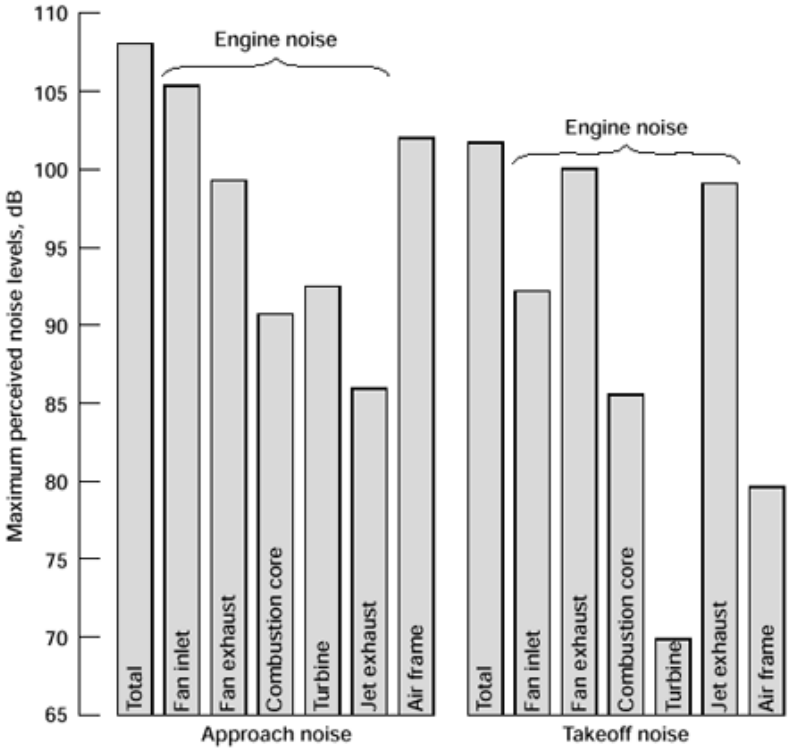

Figure 2.5: Breakdown of noise sources for a modern commercial aircraft [10].

2.3 Noise Modeling

2.3.1 ANOPP Overview

The Aircraft Noise Prediction Program (ANOPP) is a semi-empirical code that incorporates publicly available noise prediction schemes and is continuously updated by NASA Langley [17]. As progress is made in the field of aeroacoustics, ANOPP is enhanced with the latest prediction methods. Hence, using ANOPP involves accepting a certain technology level – all designs considered feature the same noise prediction methodology: a "state-of-the-art" is assumed. As part of this research, three noise sources are considered: fan turbomachinery, jet, and airframe. Other noise sources, such as combustion, turbines, and compressors were not considered because of their relatively minor contribution to total aircraft noise for most engines (Figure 2.5).

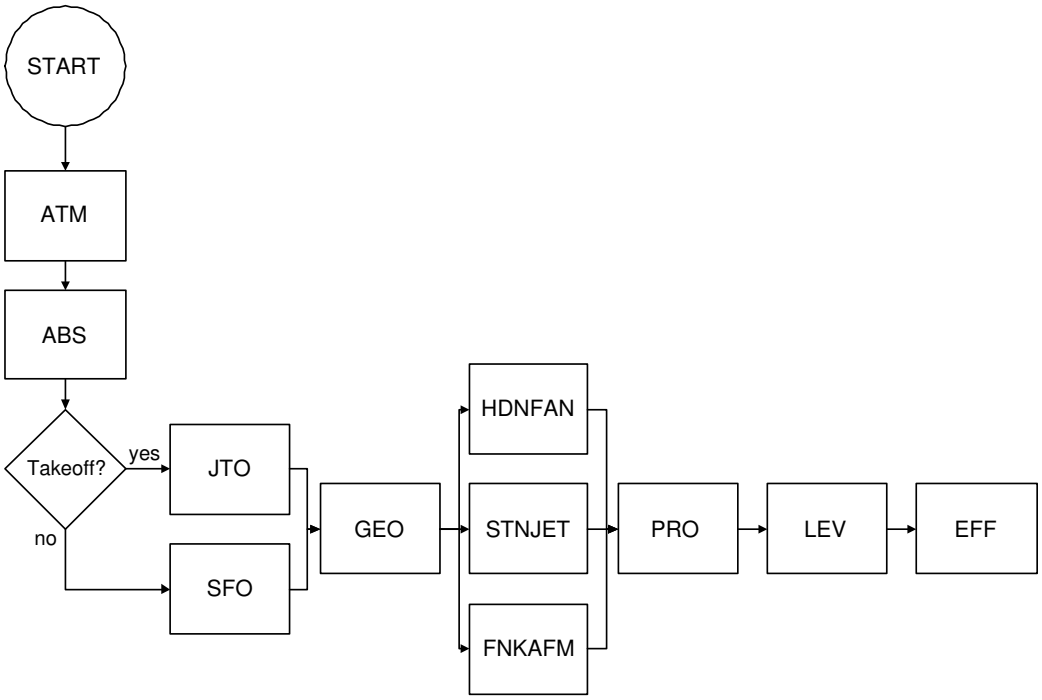

Figure 2.6: Flow chart of ANOPP program modules.

A flow chart of the ANOPP system is shown in Figure 2.6. The procedure begins by defining an atmosphere using the Atmosphere Module (ATM), followed by the atmospheric absorption module (ABS). The steady flyover module (SFO) is used for the approach measurement point, and the jet takeoff module (JTO)for sideline and takeoff measurement points. The geometry module (GEO) computes the range and directivity angles from the observer to the noise source. At this point, the various noise sources modules are run: Heidmann's for fan noise (HDNFAN), Stone's for coaxial jet noise (STNJET) and Fink's for airframe noise (FNKAFM).

Once data has been generated by the noise source modules, the propagation module (PRO) applies corrections to the noise data in the source frame of reference to transfer it to the observer frame of reference. Atmospheric absorption effects are applied at this point. The noise levels module (LEV) computes the Tone-corrected Perceived Noise (PNLdB), and the effective noise level module (EFF) is run next to compute the EPNdB levels used as noise metrics in this research.

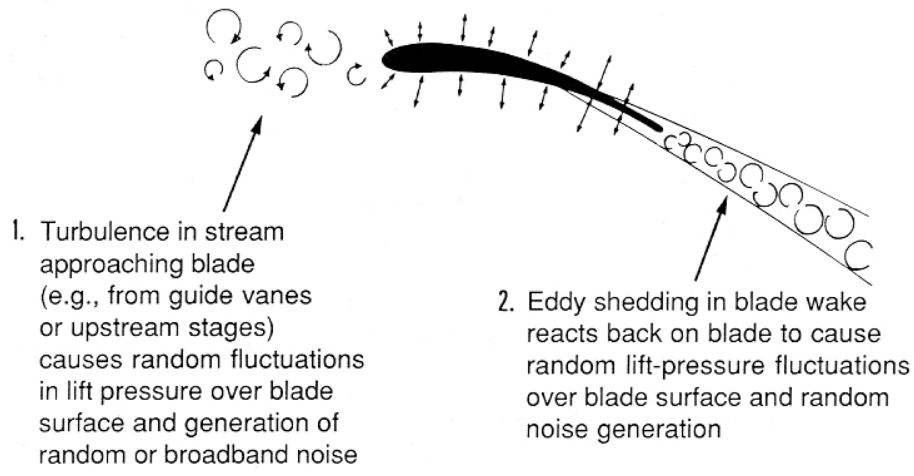

Figure 2.7: Fan broadband noise [18].

2.3.2 Fan Turbomachinery Noise

Fan turbomachinery noise includes both tonal and broadband components. The broadband noise is generated by the movement of the fan tip within the turbulent boundary layer close to the wall of the inlet duct (Figure 2.7). Turbulence present in the wakes of the fan blades also contribute to the total noise. This aspect of fan noise is expected to gain in importance, as there is a trend towards larger diameter fan blades.

Engine manufacturers are also studying multi-stage fans in order to minimize the fan frontal area, which has grown dramatically with increasing bypass ratios. The resulting complications in the flow between the fan stages is considered an important broadband noise issue. Fan trailing edge blowing could be used to delay the onset of separation and is under consideration to reduce wake noise.

Essentially, discrete tones are generated by the interaction between airflow perturbations (for example, a wake) and blade stages. The pressure field generated by each blade is unique due to very slight variations in manufacturing, fatigue, and damage — the result being that the observer will hear a characteristic “buzzsaw” noise, indicating supersonic airflow at the fan tip region, and the propagation of shocks (Figure 2.8).

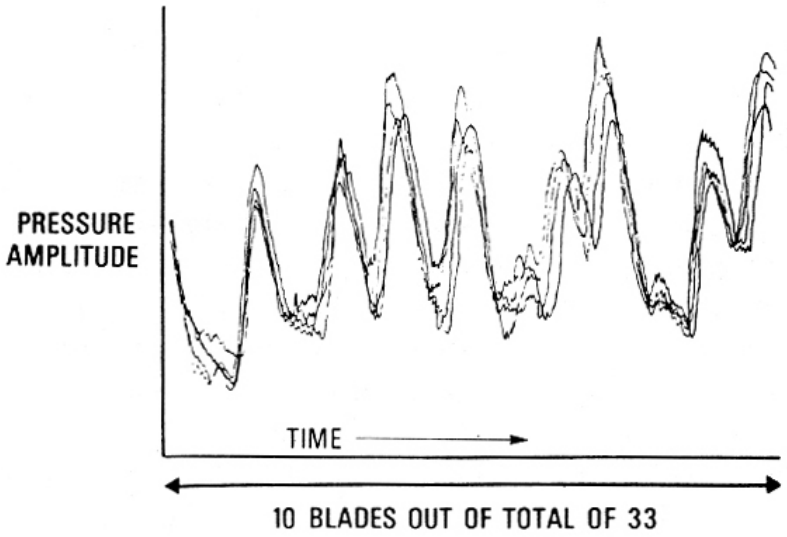

Figure 2.8: Pressure-time signature ahead of a fan operating with supersonic tip speed [19].

The broadband and tonal components of fan noise are predicted using a model developed by M. F. Heidman [20]. The components include inlet broadband noise, inlet rotor-stator interaction noise, discharge broadband noise, and discharge rotor-stator interaction noise. The method employs empirical correlations to predict the sound spectra as a function of frequency and directivity angle.

Inlet broadband noise is associated with random unsteadiness or turbulence in the flow passing the blades. Sources of this unsteadiness includes turbulence in the boundary layers, blade wakes and resulting vortices, and inlet flow effects. Acoustic power varies inversely with the rotor-stator spacing.

The discrete tones generated due to rotor-stator interaction are linked to the lift fluctuations on the blades. They are generated as the wakes from the blades impinges on the guide vanes. Distortion of the inlet flow has an effect on both broadband and tonal components; the unsteady lift that these distortions can create produce additional pure tone noise. The discharge rotor-stator interaction tones are created through a mechanism similar to the inlet interaction tones.

2.3.3 Coaxial Jet Noise

Jet noise covers the sources associated with the mixing process between the engine exhaust flow and the atmosphere, and those associated with the shocks created by a supersonic jet. The exhaust flow is conceptually divided into three regions: the primary (core) jet, the secondary (bypass) jet, and the mixed (merged) jet. Each region generates a component of jet noise and has its own noise source distribution.

Lighthill's theory shows that the fluctuating shear and normal stresses in the exhaust mixing process causes broadband noise – and that it varies according to the 8th power of the jet velocity. For pure turbojets or very-low bypass ratio turbofans at take-off conditions, the core jet exhaust velocity varies between 500 and 600 m/s, and is by far the dominant source of noise. High-bypass ratio engines have greatly reduced the contribution of core jet noise to total jet noise — exhaust velocities are as much as 50% lower than in turbojets. For an equivalent thrust level this reduction in velocity yields a 21 dB reduction in mixing noise, reflecting the high-power dependence between noise and jet velocities.

Stone's method [21] is used to predict the coaxial circular jet noise. Because only moderate and high-bypass ratio engines with subsonic exhaust flows are under consideration in this research, shock turbulence interference is not relevant, and this leaves mixing noise as the only significant jet noise component.

2.3.4 Airframe Noise

With the advent of very-high bypass ratio engines, airframe noise is expected to become the major contributor to total noise energy — and the limiting factor in noise reduction — during approach and landing, when the aircraft is in high-lift, high-drag configuration. While a clean airframe produces a broadband source, strong tones may be observed due to the wing trailing edge vortex shedding. Low-frequency tones have also been identified in association with cavities or gaps in the airframe.

Wing anti-icing exhaust vents on the Boeing 777, for example, were redesigned to eliminate a discrete tone that was louder than either the landing gear or lifting surfaces sources [12].

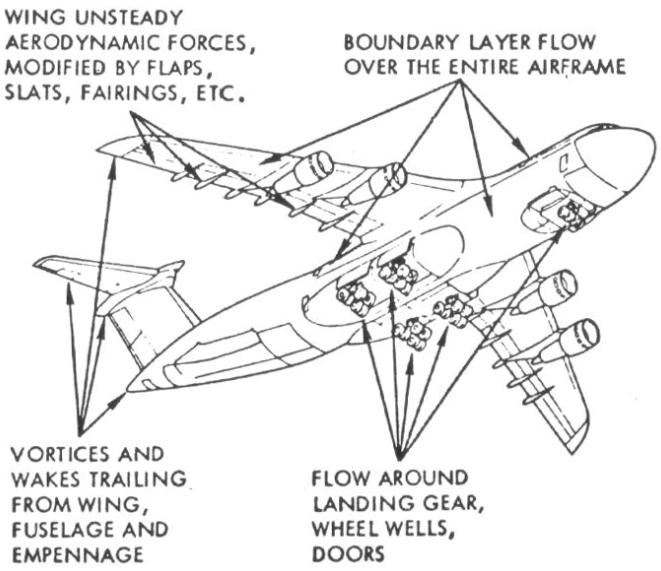

Figure 2.9: Airframe noise sources [10].

Advances in acoustic camera technologies have greatly contributed to solving such problems and reducing the level of "annoyance" associated with tone noise sources.

Airframe noise sources include the wings, tail, landing gear, flaps, and slats. Noise from the boundary layer shear and vortices shedding from the landing gear, high-lift devices, and other flow separation mechanisms contribute a significant portion of the total aircraft noise (Figure 2.9).

In theory, the source intensity should vary according to the fifth or sixth power of aircraft speed. Experimental studies, involving the identification and separation the various noise sources for analysis, seem to indicate that the velocity dependence may be of lower power dependence. Broadband noise is computed using Fink's methodology [22] to produce sound spectra as a function of frequency, polar directivity angle, and azimuth directivity angle. In some cases, a significant source of airframe noise is the sound generated by the side edges of the flaps [23, 24]. However, the version of ANOPP used in this research does not support flap side-edge noise.

Manufacturer	Engine	SLS Thrust	OPR	BPR
Rolls-Royce	Trent 892	92,500 lbs	41.38	5.70
Pratt & Whitney	PW4090	88,800 lbs	39.16	6.10
General Electric	GE90-90B	94,000 lbs	39.80	8.36

Table 2.1: Data for three engines available on the Boeing 777-200ER [29].

	FAA Data			Predicted			Error		
Engine	FO	SL	AP	FO	SL	AP	FO	SL	AP
Trent 892	91.50	95.70	98.30	95.10	95.07	106.86	3.60	-0.63	8.56
PW4090	93.90	98.20	99.20	96.69	95.19	108.31	2.69	-3.01	9.11
GE90-90B	94.00	97.70	99.50	96.70	95.44	108.12	2.70	-2.26	8.62

Table 2.2: FAA noise data at the three certification points for the Boeing 777-200ER with three different engines compared to values predicted with the design tool. All values are in EPNdB.

2.3.5 Comparison to Existing Aircraft

In order to determine the accuracy of estimating certification noise with the design tool and ANOPP, an existing aircraft was simulated and compared to measured FAA certification noise data.

The Boeing 777-200ER was chosen because it is offered with three engine types, allowing for the comparison of identical aircraft with different engine thrust and bypass ratios. Essential data for these engines is summarized in Table 2.1. Table 2.2 includes measured and predicted noise.

While the impact and trend of increasing bypass ratio on certification noise is captured by the design tool, flyover (FO) noise is overpredicted by approximately 3-4 dB. Sideline noise (SL), on the other hand, is underpredicted by 1-3 dB. The largest discrepancy is at the approach point (AP), where the design tool overpredicts noise by approximately 10 dB. In this regime, fan and airframe noise dominate.

A similar trend has been reported as part of an ANOPP validation study completed by General Electric Aircraft Engines [25]. This overprediction is attributed to the Heidmann fan inlet noise prediction method that tends to produce values 11-19 dB over those of the CF6-80C2 engine used for comparison in the report.

The other major contributor to total aircraft noise on approach is airframe noise. The empirical prediction method included in the version of ANOPP used in this research is based on Lockheed L-1011 TriStar data.

2.4 Noise Reduction Scenarios

Because the focus of this research is on studying noise and emissions at the aircraft level, the design tool can be used to study the impact of changing bypass ratio, engine pressure ratio, or other such high-level variables on the aircraft as a whole. As the design of the aircraft progresses, further improvements can be made via the installation of nacelle liners and chevron nozzles, for example. Typically, these modifications do not impact the aircraft configuration as a whole, and can therefore be considered separately during detailed design. Such improvements at the engine or airframe-component level are the focus of programs such as the European X-NOISE project, SILENCE(R) [26], and NASA's Advanced Subsonic Technology Project [27] and Quiet Aircraft Technology Program [28] in the United States.

2.4.1 Bypass Ratio

As noted earlier, jet engines produce most of the sideline and takeoff noise measured during the certification process. It follows that engine design is critical to the noise performance of the aircraft. Advances in liner materials and high-bypass ratio engines have been the largest contributors to aircraft noise reduction (Figure 2.10).

The particular importance of bypass ratios in this respect is well known: increasing the bypass ratio can have a dramatic effect on fuel efficiency, noise, and emissions. By increasing the amount of airflow directed around the combustion chamber relative to the amount of air passing through it, mixing between the flows on exit is increased and exhaust velocities reduced. The result is a considerable decrease in jet noise and overall engine noise (Figure 2.11): increasing bypass ratios from 6 to 14 results in a cumulative noise reduction of 8 dB. These results were obtained with the design tool developed as part of this research (Chapter 4).

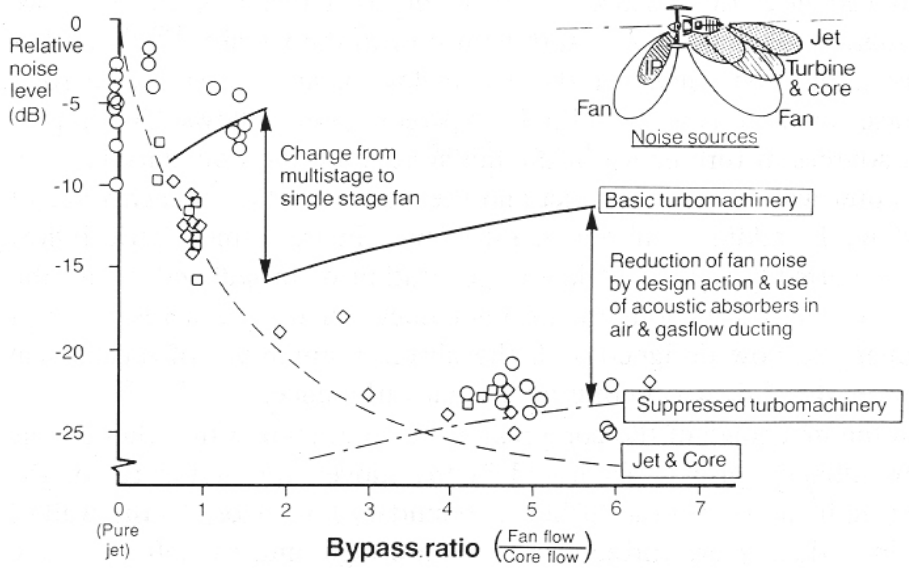

Figure 2.10: Noise reduction technologies [30].

The impact on emissions and operating costs of increasing bypass ratio is not as obvious [31]. Figure 2.11 also illustrates the variations for optimized aircraft in total fuel carried (that largely determines both cost and emissions performance) as a function of the bypass ratio. While fuel consumption improves by about 9% when bypass ratio increases from 4 to 8, it increases again when the bypass ratio exceeds 10. The relative deterioration of the fuel consumption for high bypass engines is caused in part by the significant parasite drag associated with their large fans. In addition, for a given thrust requirement at cruise conditions, high bypass ratio engines will typically have excess sea-level static (SLS) thrust. For instance, an engine with a bypass ratio of 10 may produce about 20% less thrust at 31,000 ft than a engine with a bypass ratio of 6 having identical SLS thrust. As a result, while high bypass ratio engines have low noise emissions because of reduced exhaust velocities, some of this advantage is offset by the need to increase the SLS thrust (i.e. oversize the engines) in order to achieve the required cruising altitude thrust.

The trend of improving fuel consumption (at the engine level) with increasing bypass ratio requires that the fan pressure ratio be optimized for each bypass ratio.

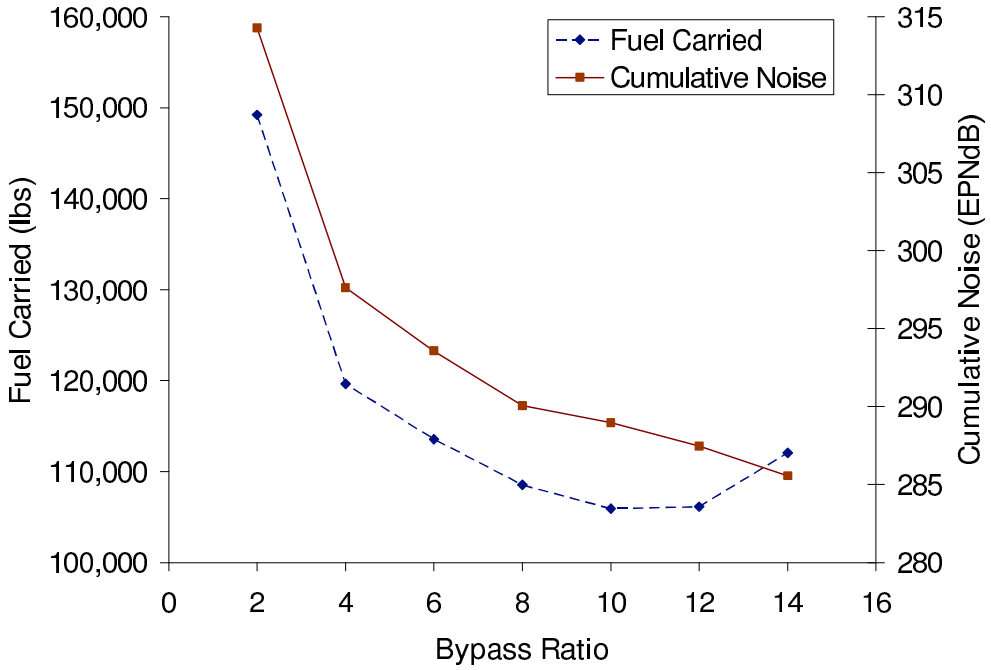

Figure 2.11: Impact of increasing bypass ratio on cumulative certification noise and total fuel required to complete the mission.

Taking into account engine stability and fan surge margins, the variation of optimum fan pressure ratio with BPR from 4 to 15 is shown in Figure 2.12, adapted from [32].

The noise measured at each of the certification points for the same aircraft, as a function of bypass ratio, is shown in Figure 2.13. Note that sideline and flyover noise both gain significantly from the decrease in jet velocities associated with increasing bypass ratios. At the reduced throttle settings required at approach, however, jet noise is not a dominating factor. Airframe and fan noise are the most important contributors in this regime. This is illustrated by the relatively flat approach noise data shown in Figure 2.13. The larger fans associated with high bypass ratio engines tend to have the high tip velocities that engine manufacturers have been able to partially mitigate by sweeping the fan blades, for example.

Having achieved significant progress in reducing jet noise, the focus of most current research is on reducing fan and airframe noise, currently seen as the limiting factors in the manufacturers' present ability to improve aircraft noise performance.

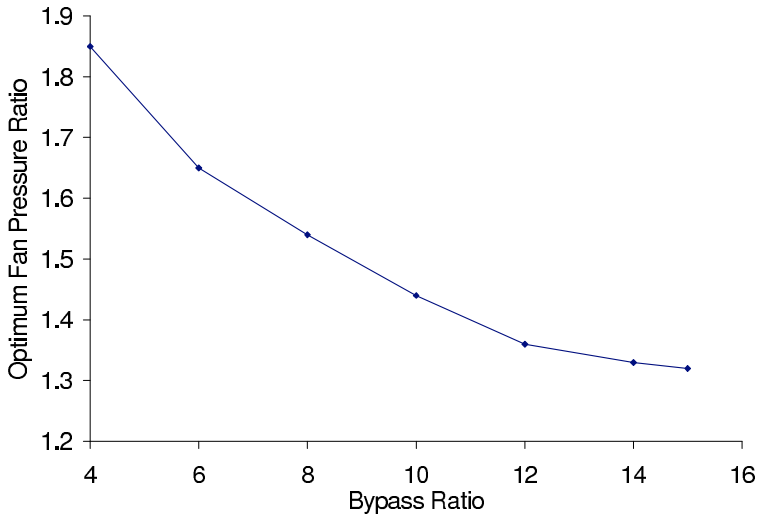

Figure 2.12: Optimum fan pressure ratio as a function of bypass ratio [32].

Aircraft	Total Thrust (lbs)	MTOW (lbs)	T/W	Sideline Noise (EPNdB)	Flyover Noise (EPNdB)
TW1	136,808	372,539	0.367	93.41	85.46
TW2	144,808	377,903	0.383	93.33	84.97

Table 2.3: Total thrust, maximum takeoff weight, thrust-to-weight ratio, and noise performance for two optimized designs simulated with the design tool to study the effects of climb performance on sideline and flyover noise.

2.4.2 Climb Performance

While noise measured at the sideline certification point tends to be controlled by thrust level, flyover noise is strongly affected by the climb performance, and therefore the aircraft thrust-to-weight ratio [33]. This is because, all other things equal, the effect of higher altitude over the flyover measurement point is usually stronger than the effect of higher thrust. To illustrate these effects, the design tool was used to simulate two 280-passenger, twin-engine, 6,000 nm range aircraft, with different total thrust. Data for these aircraft is summarized in Table 2.3.

The additional 8,000 lbs of installed thrust (4,000 lbs per powerplant) for aircraft TW2 translate into heavier engines, resulting in a maximum takeoff weight increase of 1.4% relative to aircraft TW1.

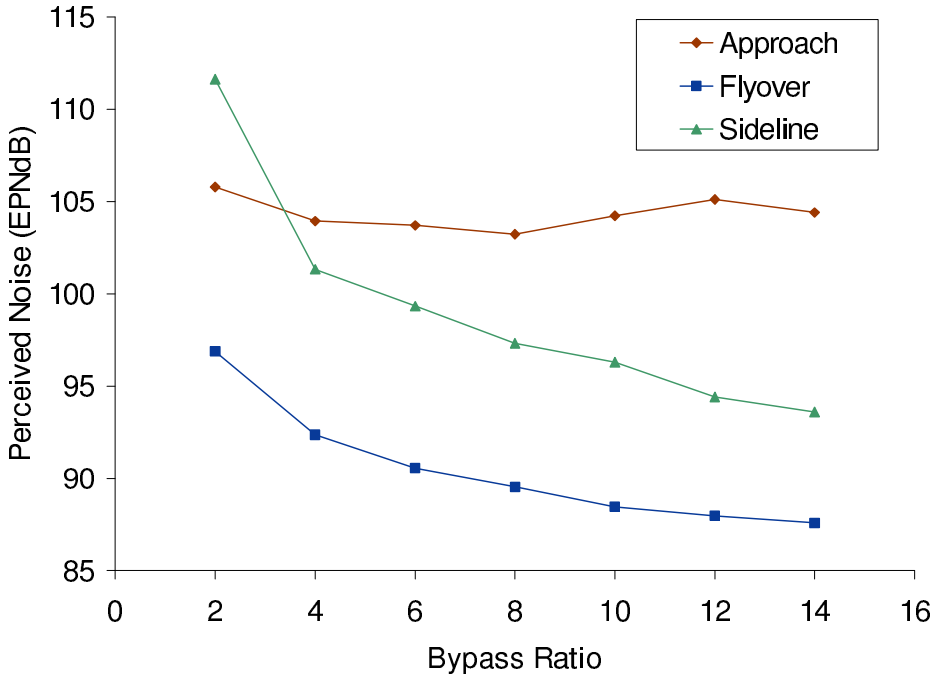

Figure 2.13: Noise measured at the three certification points as a function of bypass ratio.

The thrust-to-weight ratio is nevertheless raised by 4.4% — design TW2 therefore climbs faster, increasing the distance between the aircraft and the ICAO/FAA flyover noise measurement point. Noise computed by ANOPP at this point shows that aircraft TW2 is 0.5 dB quieter than aircraft TW1. As expected, there is no significant change in the sideline noise, since the distance between the aircraft (during the takeoff roll) and the sideline measurement point is fixed.

Chapter 3

Engine Emissions

3.1 Combustion

Both particulate and gaseous pollutants are produced through the combustion of jet kerosene (products in italics stem from non-ideal combustion):

Reactants	Air $N_2 + O_2$
	Fuel $C_nH_m + S$
Products	$CO_2 + H_2O + N_2 + O_2 + \mathit{NO_x} + \mathit{UHC} + \mathit{CO} + \mathit{C_{soot}} + \mathit{SO_x}$

The greenhouse gases carbon dioxide CO_2 and water H_2O are the major products. Minor emissions formed during combustion include nitrous oxides (NO_x), unburned hydrocarbons (UHC), carbon monoxide (CO), and soot (C_{soot}).

3.2 Local Emissions

ICAO regulations for the landing-takeoff (LTO) cycle cover NO_x, CO, unburned hydrocarbons, and smoke emissions [34]. During the LTO cycle, approximately 56% of all commercial aircraft emissions are in the form of NO_x (Figure 3.1). Unburned hydrocarbons typically contribute less than 5%. In fact, significant progress in combustor designs and reducing specific fuel consumption have almost eliminated the issue of particulate matter emissions.

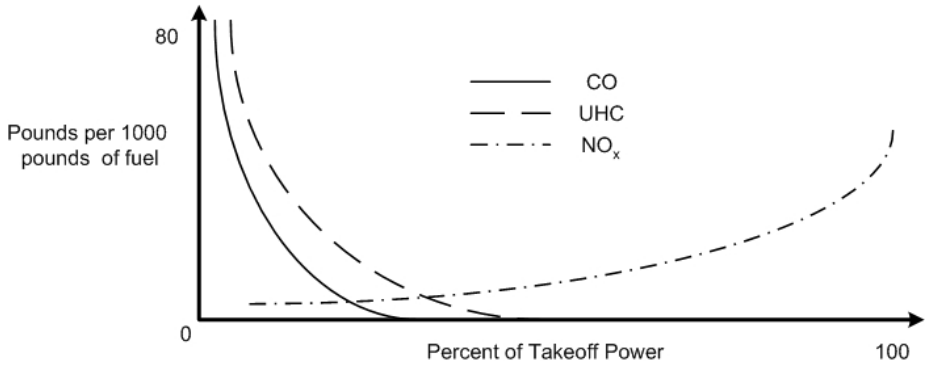

Figure 3.1: Engine emissions as a function of throttle setting [35].

There is considerable pressure to further reduce NO_x emissions from all sources, however, due to their role in the ozone generation and destruction mechanisms.

NO_x emissions are computed based on engine fuel flow (expressed in kg/s) and the combustor emission index (EI, expressed in g of NO_x formed per kg of jet fuel used), both a strong function of power setting, during a take-off and landing cycle involving four different throttle modes: 100% (take off), 85% (climb), 30% (approach) and 7% (idle). Time in mode is simulated as follows: 0.7 minutes for take off, 2.2 minutes for climb, 4 minutes for approach, and 26 minutes for taxi/ground idle. The sum of the emissions at these four conditions (expressed in kg), calculated as shown in Equation 3.1 below, is used to determine the amount of NO_x emitted per LTO cycle.

$$\text{LTO NO}_x = \sum \text{Fuel Flow} \times \text{EI}_{\text{NO}_x} \times \text{Time in Mode} \tag{3.1}$$

3.3 Emissions and the Atmosphere

Gases and particles emitted by aircraft during cruise accumulate in the atmosphere near the busiest flight routes, mainly in the northern mid-latitudes. In addition to altering the concentrations of atmospheric greenhouse gases, aircraft emissions may trigger the formation of contrails, increase cirrus cover, and change other cloud properties. The energy and water budgets of the atmosphere are therefore affected and may contribute to climate change at the local and global scale.

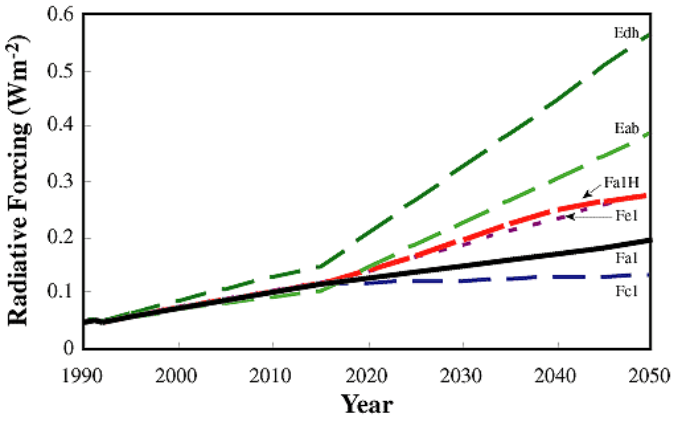

Figure 3.2: Estimates of the globally and annually averaged total radiative forcing associated with aviation emissions for six aviation growth scenarios between 1990-2050 [37].

Subsonic aircraft typically operate in the the region of the atmosphere that includes the upper troposphere, the tropopause, and the lower stratosphere. Because temperature is constant in the stratosphere regardless of altitude, there is no mechanism to drive emissions released in the lower stratosphere or tropopause to higher altitudes. Consequently, the residency time of the combustion products at these altitudes is high.

The direct impact of anthropogenic gases and particles on the climate is to change the absorption and scattering of radiation. Indirect effects that could potentially have serious long-term consequences include chemical and physical changes of clouds and gases, essentially modifying the greenhouse properties of the atmosphere [36].

The impact of different anthropogenic emissions on the climate can be compared using the concept of radiative forcing. Radiative forcing is a measure of the importance of a potential climate change mechanism. It expresses the perturbation or change to the energy balance of the atmosphere in watts per square meter. Positive values imply a net warming, while negative values imply cooling. Highlighting the complexity of modeling the atmosphere and predicting the impact of future aircraft technology, the six future fuel use scenarios shown in Figure 3.2 predict a 2- to 5-fold increase in radiative forcing, depending on the assumptions.

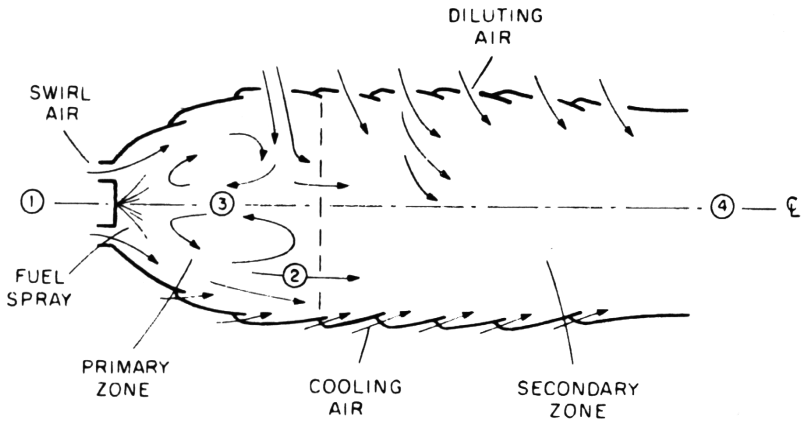

Figure 3.3: Cross section of a combustor liner: upper half shows diluting air holes, lower half shows film-cooling air [41].

During cruise, CO_2 emissions constitute 6% of the total mass flow emerging from the engine, versus 0.3% for NO_x and 0.04% for CO [38]. Jet fuel provides the carbon required for the formation of CO_2, the hydrogen necessary for H_2O, and the sulfur for SO_2. As a result, by changing the amount of fuel required, aircraft can be configured to meet CO_2, H_2O, and SO_2 emissions requirements in addition to the NO_x emissions, cost, and noise constraints already discussed. CO_2, H_2O, and SO_2 trip emissions (in kg) are computed as shown in Equation 3.2.

$$\text{Trip Emissions} = \text{Fuel Flow} \times \text{Emissions Index} \times \text{Trip Time} \tag{3.2}$$

In response to the demands for quantifying emissions generated during cruise, the FAA is developing a System for assessing Aviation's Global Emissions (SAGE) [39] that will permit the computation of the total emissions generated by an aircraft fleet over the entire mission, based on published engine emissions data.

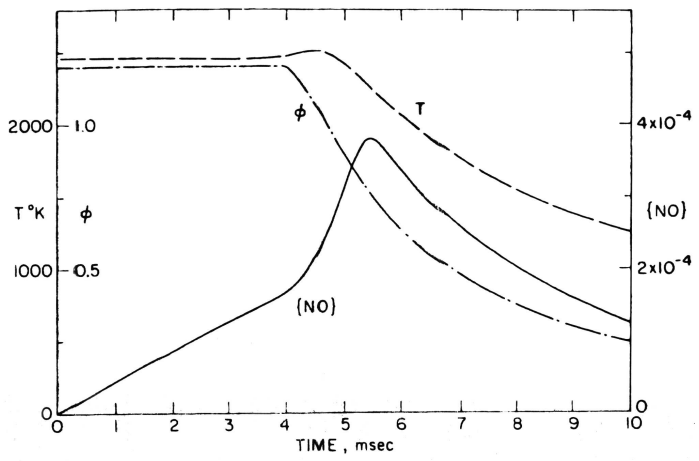

Figure 3.4: Temperature, equivalence ratio, and NO mass fraction as a function of the time spent in the combustor: 0-4 ms corresponds to the primary zone, 4-10 ms corresponds to secondary zone [41].

3.4 Oxides of Nitrogen

3.4.1 Formation

The NO_x formation and destruction process predominantly takes place in the post-flame gases, through chemical reactions involving nitrogen and oxygen atoms and molecules that do not attain chemical equilibrium [40]. As the burned gases cool, the reactions involving NO_x freeze and leave concentrations that exceed the levels that would correspond to equilibrium at combustor exhaust.

The fluid at the upstream end of the primary zone (Figure 3.3) consists of unmixed compressor air and the very-fuel-rich mixture left behind the evaporative droplets. While there is insufficient time for nitric oxide concentrations to reach equilibrium in the primary zone, any design changes that increase the peak temperatures inside the combustor (e.g. increasing engine pressure ratio) will bring NO_x levels in the primary zone closer to equilibrium values.

In the secondary zone, significantly more nitric oxide is formed as air is added and the fuel-to-air equivalence ratio, ϕ, changes from approximately 1.2 to 0.8 (Figure 3.4).

The most important engine variables that affect NO_x emissions are the fuel-to-air ratio and the burned gas fraction. Maximum burn temperature occurs at $\phi = 1.1$. Here, oxygen concentrations are low, hence there is little NO_x formed. As the mixture is diluted with air, the increasing oxygen concentrations initially offset falling gas temperatures and NO_x emissions peak at $\phi = 0.9$. This is a consequence of the competition between fuel and nitrogen for the available oxygen: although the combustion temperature is higher on the slightly fuel-rich side of stoichiometric, the available oxygen is then consumed preferentially by the fuel. As dilution continues and the equivalence ratio decreases further, the temperature drops below the minimum required by the NO_x formation and dissociation mechanisms and the chemistry is effectively frozen.

3.4.2 Prediction

While NO_x formation is mostly a function of equivalence ratio and combustion temperature, obtaining this data requires detailed modeling of the combustion process beyond the capabilities of the engine simulator (NEPP) that forms part of the framework. For the level of detail required by this conceptual design tool, however, a simple NO_x model is sufficient. The correlation used here was developed as part of NASA Glenn's Advanced Subsonic Technology (AST) project, based on internal NASA data and models from industry [42], and estimates the NO_x emissions index for the next generation of jet engines featuring a dual-annular, staged combustor [43]. Only the knowledge of the flow conditions at combustor entry and outlet are required. The correlation for the NO_x emission index (g/kg) is:

$$\mathrm{EI}_{\mathrm{NO}_x} = 0.004194\ T_4\ \left(\frac{P_3}{439}\right)^{0.37} e^{\frac{T_3-1471}{345}} \tag{3.3}$$

where P_3 and T_3 are the burner entrance pressure and temperature and T_4 is the burner exit temperature (units are psia and Rankine).

Emissions	EI (g/kg fuel)
CO_2	3,155
H_2O	1,240
SO_2	0.8

Table 3.1: Emissions Index (EI) of species proportional to fuel consumption.

3.5 Fuel-proportional Emissions

Because CO_2, H_2O, and SO_2 species production is directly proportional to the fuel burnt, modeling these emissions only requires knowledge of fuel consumption and fuel-specific emission indices. For jet kerosene, the emissions indices are shown in Table 3.1.

3.6 Reduction Methods

3.6.1 Combustor and Engine Cycle

The two methods that allow a reduction in emissions at the level of the powerplant include improving the combustor to yield a lower emissions index (that is, reduce the amount of pollutant emitted per kilogram of fuel burned) and choosing an engine cycle that yields lower fuel flow (to reduce the amount of fuel consumed). Increasing the overall engine pressure ratio promotes more complete combustion, resulting in reduced fuel flow. The trade-off is higher NO_x emissions due to the increased combustion temperature, leading to increased dissociation of nitrogen, and consequently a higher NO_x EI.

While improvements to the combustor could decrease the amount of NO_x or CO_2 released into the atmosphere, these are generally conflicting requirements. Typically, changing the operating conditions or combustor configuration to reduce NO_x emissions increases the quantity of CO_2 and unburned hydrocarbons produced [44].

In particular, as the bypass ratio of large turbofans is increased, the resulting power requirements of the larger fan mandates that more energy must be extracted from the low-pressure turbine.

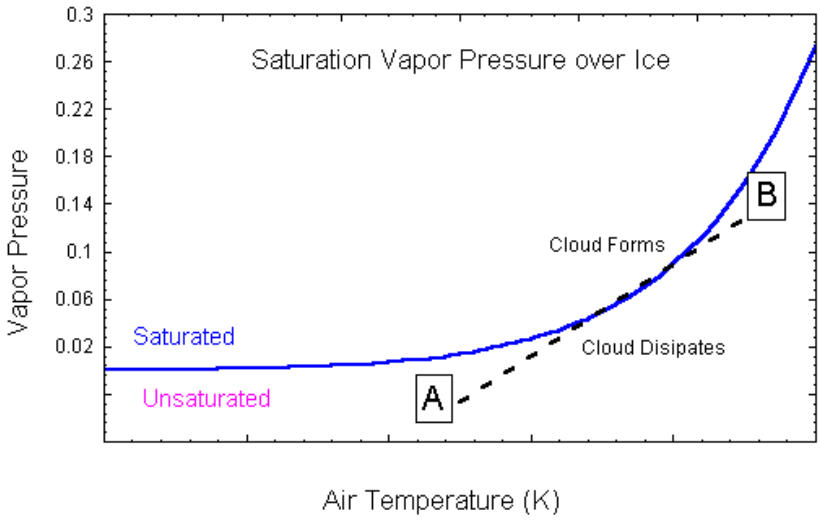

Figure 3.5: The contrail formation mechanism [46].

This typically leads to higher pressures and combustion temperatures, and higher NO_x production. In fact, total aviation NO_x emissions increased faster than total fuel consumption over the last few decades because of the higher pressure ratios (and therefore combustion temperatures) demanded by the more fuel-efficient high-bypass ratio engines. Other types of emissions, however, have decreased per unit of fuel consumption.

This increase in NO_x production can be partially offset through detailed combustor design, and this is beyond the scope of the present conceptual design tool. Advanced double-annular, lean premixed, and rich/quench/lean combustors could all be subsequently incorporated if data were made available relating design parameters (combustion temperature, overall pressure ratio) with emissions indices.

3.6.2 Cruise Altitude Effects

Contrail formation [45] is another issue that is receiving increased attention. While the long-term impact on climate change due to increasing water content at altitude is uncertain, one possible solution to minimize contrails would be to decrease the cruise altitude of commercial aircraft.

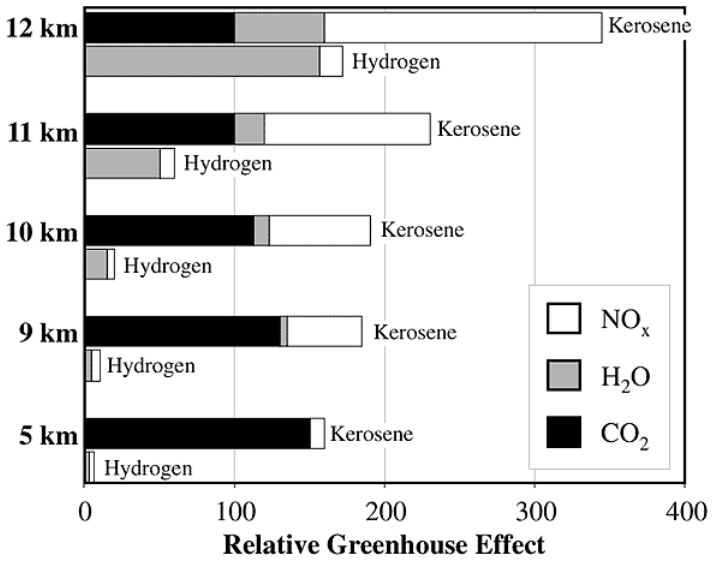

Figure 3.6: Effect of fuel type and altitude on net greenhouse effects [47].

As shown in Figure 3.5, the formation of contrails depends on the jet exhaust temperature (B on the figure), the ambient air temperature (A) and vapor pressure. As the exhaust cools from B to A, intersecting the air saturation curve will result in contrail formation. By decreasing the altitude of the aircraft, the ambient air temperature is increased, and contrails are less likely to form.

The advantages of decreasing cruise altitude are two-fold: contrail formation would be dramatically reduced and the *net* total impact of other emissions could be reduced, as the aircraft would be operating outside of the sensitive tropopause. Figure 3.6 illustrates these effects for two fuels, kerosene and hydrogen. In the case of kerosene, reducing the cruise altitude from 11 km to 9 km reduces the net impact of NO_x by half, because the aircraft is travelling in the troposphere, and H_2O by 75%, because contrail formation is prevented. However, the net impact of operating the aircraft at off-design altitude, from a fuel efficiency perspective, is apparent: CO_2 effects increase by a third. A Boeing study supports this data, concluding that operating an existing aircraft in the 747-400 class at lower altitudes would increase CO_2 production by 15% and NO_x emissions by up to 25% [48]. To minimize this degradation in performance, an aircraft would have to be designed specifically to operate at these lower altitudes.

As a side note, although hydrogen fuel is not considered as part of this research, it is interesting to note that, being the major byproduct of so-called "clean" combustion, water effects would be as much as three times more important than with kerosene fuel at a cruise altitude of 11 km.

3.6.3 Aircraft Aerodynamics

The advantages of reducing fuel flow — at the engine level — on the production of emissions has been discussed previously. At the aircraft level, drag contributes directly to the thrust requirements. Improving the aerodynamic efficiency of an aircraft by reducing drag, and therefore reducing the amount of thrust required, can result in a decrease of required fuel and related emissions.

Reducing the aircraft cruise Mach number is one solution to reducing drag, for example. This must be carefully balanced with other mission requirements, however, and highlights the importance of considering the aircraft as a whole.

New technologies, such as increased laminar flow and induced drag reduction methods, are promising in their ability to increase the aerodynamic efficiency and reduce the fuel consumption of the aircraft. These are discussed in more detail in Chapter 6.

Chapter 4

Aircraft Performance and Design

4.1 Framework Overview

Aircraft design is an extremely complex undertaking that can involve millions of parts and thousands of engineers. The goal of this research was to create a rapid conceptual design tool that, although simplified, nevertheless offered the resolution required to capture environmental concerns and would be amenable to optimization.

The design tool is composed of a library of routines used to analyze key aspects of aircraft design and performance, the Program for Aircraft Synthesis Studies (PASS) [49]. The integration of these multidisciplinary analyses and the optimizer is accomplished using Caffe [50]. The design tool can be quickly reconfigured: adding or removing design variables, objectives, and constraints is done via a simple graphical interface. NASA Langley's Aircraft Noise Prediction Program (ANOPP) is used for noise modeling, and NASA Glenn's Engine Performance Program (NEPP) for predicting engine performance. The engine performance and noise estimation codes are coupled to the programs that compute aircraft performance and operating cost. These methods are well-suited for optimization due to their rapid execution and robustness. An illustration of the framework is shown in Figure 4.1.

The design tool has been created to allow considerable flexibility in the selection of the optimization objectives, variables, and constraints. Common objective functions in aircraft design include takeoff weight, direct operating cost, and range.

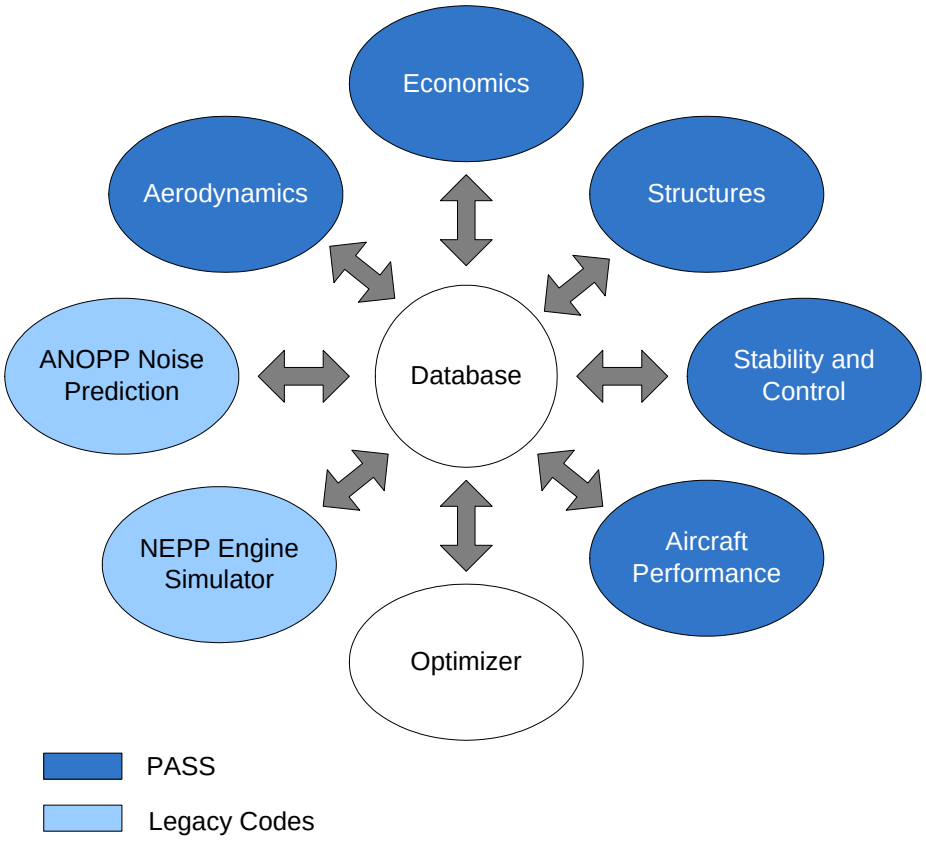

Figure 4.1: The Design Framework: the PASS aircraft design modules, noise prediction, and engine simulator are coupled with an optimizer and a database manager.

Maximum certification noise and allowable emission levels can be included as constraints in the design tool, alongside traditional performance constraints such as range and field performance. This approach allows the user to explicitly specify the level of aircraft environmental acceptability: from slight improvements to 'silent' and 'clean' aircraft. Design variables include parameters pertaining to aircraft configuration, propulsion, and mission profile. These environmental metrics can also be assigned as objectives — one of the useful features of the framework is its ability to allow for any parameter introduced in the database to be set as a variable, constraint, objective, or to a fixed value.

Figure 4.2: Artist rendering of the Boeing Blended-Wing-Body concept (The Boeing Company).

4.2 Unconventional Configurations

The semi-empirical correlations that form the aircraft analysis modules were developed from databases of conventional commercial aircraft. As a result, unorthodox configurations such as flying wings, blended-wing-body aircraft, or multiple lifting surfaces and canard configurations are not attainable.

Such designs, however, would significantly change the landscape of the design space, and possibly enable a dramatic decrease in environmental impact. Blended-wing-body aircraft in particular, due to their higher aerodynamic efficiency and geometry (the engine inlets are shielded by the body), could offer a significant step decrease in measured noise and emissions [51]. Such an aircraft is currently under study at Boeing (Figure 4.2) and the Cambridge-MIT institute has selected a similar configuration as a prime candidate for an ultra-quiet aircraft study [52].

While the design tool created as part of this research is limited to traditional "tube-and-wing" configurations, enough flexibility is allowed in the variables to allow for a wide variation of designs. It is also worth noting that while manufacturers are continually investigating unconventional designs, there is always a desire to favor traditional aircraft that pose less risk and are cheaper to develop.

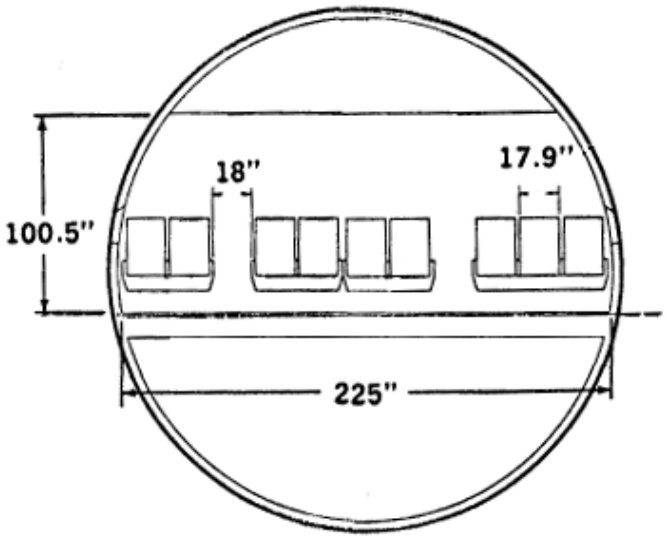

Figure 4.3: A typical commercial aircraft fuselage cross-section.

4.3 Analysis Codes

4.3.1 Introduction to PASS

The Program for Aircraft Synthesis Studies (PASS) is a commercial aircraft conceptual design tool based on a combination of McDonnell-Douglas methods, DATCOM correlations, and new analyses developed specifically for conceptual design. PASS allows the rapid generation of a design and contains modules to compute many aspects of aircraft design and performance: from fuselage and wing geometry, to drag and weight build-ups, and range and stability calculations. In addition, these codes have been specifically designed to be integrated with an optimizer.

PASS forms the basis of a two-quarter graduate-level aircraft design course at Stanford University taught, over the years, by Professors Richard Shevell, Ilan Kroo, and Juan Alonso. Extensive details of the methods introduced below may be found on the AA241 Aircraft Design: Synthesis and Analysis website [53].

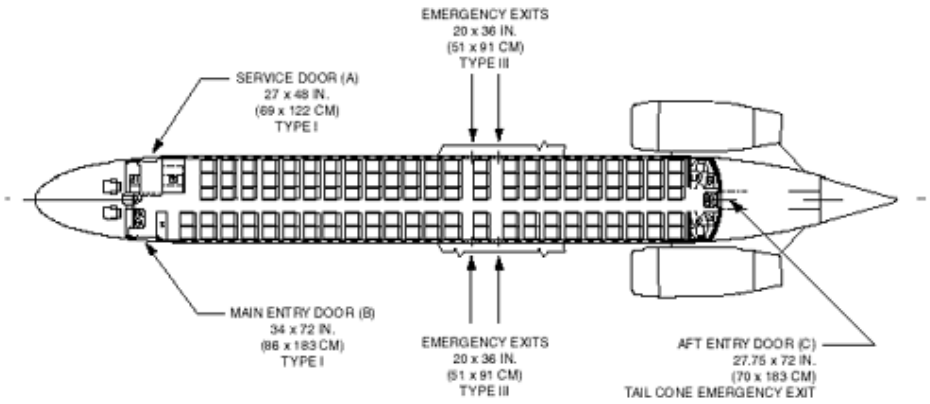

Figure 4.4: The cabin length is a function of the number of passengers, seating arrangement, and safety requirements.

4.3.2 Geometry

The fuselage geometry is determined by first selecting a cross-section layout — while drag is an issue, airline requirements are usually a dominating factor, and a compromise with the aircraft manufacturer is reached early in the design phase.

Most fuselage cross-sections are circular in shape (Figure 4.3). This eliminates corners, hence the flow will not separate at moderate angles of attack or sideslip. A circular cross-section is also desirable due to pressurization, as it will resist the loads with tension stresses, instead of the more severe bending loads inherent to non-circular shapes. The fuselage cross-section, at this early stage of design, is a function of the seat and aisle width, the seating arrangement, and the floor height, usually determined by the underfloor cargo requirements [54]. Airlines may request that a certain type of container be carried as underfloor payload, and this may drive the rest of the cabin cross-section geometry.

Once the cross-section geometry and total number of passengers have been determined, the cabin length calculation is based on seat pitch, cabin amenities, and safety requirements (Figure 4.4). Lavatories, service, and attendant seats must be included. In addition, emergency exits must feature clear aisles that may increase the overall length of the fuselage — these requirements are described in FAA Federal Aviation Regulation (FAR) Part 25 [55].

Each wing geometry parameter affects drag and structural weight as well as stalling characteristics, fuel volume, field, climb, and cruise performance, and many other important characteristics. The overall geometry of the wing is obtained from wing reference area, span, quarter-chord sweep, taper, and leading and trailing edge extensions [56].

4.3.3 High-Lift Systems

A wing designed for efficient high-speed flight requires a different geometry from one designed to provide good take-off and landing characteristics — field lengths are strongly influenced by aircraft stalling speed. It is of course not desirable to cruise with an oversized wing designed for low-speed operation. Other methods of reducing the stalling speed (and therefore improving the field performance of the aircraft) include reducing weight or increasing the maximum lift coefficient of the wing — the latter being the primary purpose of high-lift systems.

Estimating the maximum lift coefficient ($C_{L_{max}}$) is one of the more difficult aspects of aircraft design: it is crucial to sizing the aircraft and accurately computing the aircraft field performance. High-lift systems involve flow that is viscous, compressible, and highly three-dimensional. While the "critical section" method is often used in estimating $C_{L_{max}}$, it must be formulated to include *some* three-dimensional effects around the flap side edges. This is because, according to this method, the sections outboard of the flaps will stall first, while in reality their maximum lift coefficient is increased due to the complex flow geometry around the flaps. It is therefore difficult to obtain accurate maximum lift coefficient values using the critical section method.

In the case of conceptual design, before the lift distribution is computed, it is still possible to make a rough estimate of the maximum lift capability of the aircraft. The method used here involves first computing the maximum lift coefficient of the airfoil and "clean" wing. This is done by estimating the outer-panel lift coefficient and then correcting for the geometry of the wing, including taper ratio and sweep effects, using correlations. At positive wing sweep angles, increasing taper ratio increases the clean-wing lift coefficient.

The deployment of slats suppresses the leading-edge pressure peak by modifying the nose camber, and the gap that is introduced between the device and the wing leading edge re-energizes the boundary layer. As a result, the section lift coefficient is increased dramatically. The specific increase in $C_{L_{max}}$ varies based on the design of the slat, deflection angle θ_{slat}, wing sweep, and gap size. For the purposes of this conceptual design work, the value is estimated based on data from Douglas [57].

Trailing-edge flaps change the airfoil pressure distribution by increasing the effective camber of the airfoil and allowing more of the lift to be carried over the rear portion of the section. The result is that for a given angle of attack, the lift produced is greater than without these trailing-edge devices. Higher lift coefficients are obtained with slotted flaps: the boundary layer is re-energized after travelling over the rest of the airfoil.

4.3.4 Weights

In the conceptual phase, before the detail design of the hundreds of thousands of parts that will eventually form the airplane, little data is available to estimate the structural and operational weights of the aircraft — there are no drawings of the details. The conceptual design engineer can only create a 3-view drawing and some approximate specifications. The rest of the design remains undefined.

The method employed here involves the "build-up" of the weight from the various components: structural analysis and statistical comparisons are combined, with the complexity of the analysis dependent on publicly available information [58].

Wing weight is a function of the fully-stressed bending weight of the wing box and includes the effect of total wing load at the ultimate load factor, span, average airfoil thickness, taper, sweep, and gross wing area. The correlation used is based on data from 15 existing transport aircraft.

The horizontal tail weight, including elevators, introduces both exposed and gross horizontal tail areas as well as the tail length — the distance from the airplane center of gravity to the aerodynamic center of the horizontal tail. The rudder is assumed to occupy 25% of the total vertical tail area and weighs 60% more per unit area.

The weight of surface controls, used for surface actuation, depend primarily on the area of the horizontal and vertical tails.

Fuselage weight is based on gross fuselage wetted area and a pressure-bending load parameter. To account for the distributed support provided by the wing, the effective fuselage length is taken to be the actual fuselage length minus half the wing root chord. From existing aircraft data, the landing gear weight is typically approximately 4.0% of the take-off weight. This includes structure, actuating system, and the rolling assembly consisting of wheels, brakes, and tires.

The propulsion system weight is about 60% greater than that of the dry engine alone. The engine structural section, or nacelle group, and the propulsion group that includes the engines, engine exhaust, reverser, starting, controls, lubricating, and fuel systems are handled together as the total propulsion weight. This weight also includes nacelle and pylon weight. The engine dry weight is computed using correlations based on sea-level static thrust, fan diameter, and engine pressure ratio.

The auxiliary power unit (APU), used to power the aircraft on the ground, is part of the main engine starting mechanism. APU weight is correlated to the passenger capacity of the aircraft. The weight of instruments and navigational equipment, hydraulics and pneumatics lines, electrical systems, electronics, cabin furnishings, air conditioning, anti-ice systems, passengers, cabin and flight crew, and passenger cargo are all included.

4.3.5 Loads

V-n diagrams (Figure 4.5) are used to determine the maximum aircraft loads as a function of airspeed, altitude, and weight. Two diagrams are created: the maneuver diagram for variations in the load factor with airspeed for maneuvers and the gust diagram associated with vertical gusts that must be evaluated over a range of speeds.

Loads associated with vertical gusts are also evaluated over the range of speeds, using a method detailed in the FAR Part 25 regulations. Because the design speed for maximum gust intensity is determined by the gust loads, the process is iterative — various speeds must be considered.

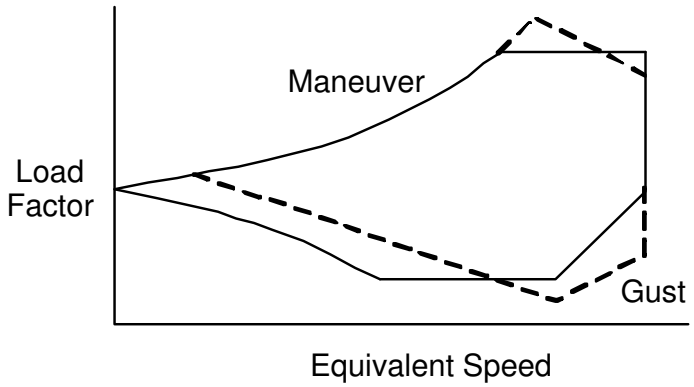

Figure 4.5: Maneuver and gust V-n diagrams.

The FAR Part 25 equation is the result of considering a vertical gust of specified speed and computing the resulting change in lift. The associated incremental load factor is then multiplied by a load alleviation factor that accounts primarily for the aircraft dynamics in a gust. The FAA also specifies the magnitude of the gusts to be used as a function of altitude and speed.

4.3.6 Drag

Parasite Drag

During cruise, the parasite drag of a commercial airplane consists mainly of the skin friction, roughness, and pressure drag of the major components. These include the fuselage, the wing, winglets, and the horizontal and vertical tails. Additional contributors include the fuselage upsweep, gaps in the control surfaces, nacelle base drag, and miscellaneous items. Drag is computed based on the flight conditions of the aircraft, taking into account both Reynolds and Mach number effects.

An overall markup is added to skin friction drag to account for drag increments associated with roughness resulting from smaller items, such as rivets, small gaps, and other construction details. This markup factor has been estimated from flight-test parasite drag. Drag assigned to roughness also includes interference drag, trim drag, drag due to unaligned control surfaces, drag due to landing gear door gaps, and any excess drag of the individual surfaces.

The parasite drag associated with skin friction and pressure drag is determined by incrementing the flat plate results by a factor to account for pressure drag and surface velocities greater than the free-stream.

Most turbofan engines maintain a gap between the engine nozzle and nacelle, where flow separates and creates additional drag. The drag due to the upward curvature of the aft fuselage is the combination of a fuselage pressure drag increase and a drag increment due to loss of lift. Consequently, the airplane must fly at a higher lift coefficient to compensate for this loss, resulting in further induced drag.

In addition to these basic drag components, the drag associated with the environmental systems (miscellaneous inlets and exhausts) and various manufacturing artifacts (rivets, bolts, etc) can be included in the total drag. While it is impractical to account for every last protuberance on the airplane separately, the drag contribution of some of these items can be significant. In the case of this research, at the conceptual design stage, the design of the airplane has not progressed to the point where the drag of these miscellaneous items can be calculated — however, based on existing aircraft data, the drag of these miscellaneous items can be assumed to be about 1.5% of the total airplane parasite drag [59].

Lift-Dependent Drag

Lift-dependent drag is a function of wing twist and planform. The viscous component is due to the increase in skin friction and pressure drag with varying angles of attack. Since the data required for a detailed drag breakdown is usually not available in preliminary design, all airplanes are considered to be geometrically similar to existing designs. Other effects that are not taken into account during the conceptual design phase include fuselage vortex drag, nacelle-pylon interference, and changes in trim drag with angle of attack.

The added lift-dependent drag caused by the modification of the span loading due to the presence of the fuselage is taken into account, as is the interference drag of the wing/tail system (using the Prandtl biplane equation). The viscous part of the induced drag is approximated by a parabolic variation with the lift coefficient.

Compressibility Drag

Compressibility drag consists of the increase in the airplane drag coefficient at Mach numbers greater than approximately 0.5. This includes any variation of the viscous and vortex drag with Mach number, shock-wave drag, and any drag due to shock-induced separation.

The method for estimating compressibility drag involves estimating the crest-critical Mach number (M_{cc}), that is the freestream Mach number at which the component of the local Mach number at the crest first reaches 1.0 [60]. At this early stage of the design process, the detailed airfoil pressure distribution is not available. However, M_{cc} may still be estimated, as a function of airfoil mean thickness ratio, quarter-chord sweep, and aircraft lift coefficient. These correlations are based on studies of various "Peaky" airfoils. A supercritical section might achieve a drag divergence Mach number increment of 0.06 beyond a "Peaky" airfoil. Once the crest-critical Mach number is estimated, the compressibility drag rise can be computed.

4.3.7 Static Stability and Trim

The pitching moment about the center of gravity must become negative as the lift coefficient is increased. The airplane lift curve slope includes contributions from the wing and the horizontal tail — these are determined using a DATCOM correlation.

Once the isolated tail lift curve slope is computed, it is corrected to account for the presence of the wing and the fuselage which produce downwash on the tail. Trim is achieved by setting the incidence of the tail surface to obtain zero pitching moment. Given a stability constraint and a trim requirement, the location of the center of gravity is located and the tail lift is adjusted for trim. The lift from each interfering surface is then computed, along with the combined drag of the system.

4.3.8 Performance

Takeoff field length is very often a critical design constraint. The calculation of take-off field length involves the computation of the distance required to accelerate from full stop to the required take-off speed, plus a climb segment.

Determining the takeoff distance involves multiple scenarios, such as acceleration on all engines, acceleration with one engine inoperative, deceleration after engine failure, and climb with one engine inoperative. Spoilers, the braking system, and rudder will, as a result, affect the FAR take-off field length. For the purposes of this preliminary design tool, correlations of the primary design parameters with actual demonstrated performance are used. Fits of the FAR field length requirements of 2, 3, and 4 engine jet aircraft are used to estimate takeoff field length.

The FAR landing field length is defined as the actual demonstrated distance from a 50 ft. height to a full stop increased by 67%. A correlation, based on the aircraft stall speed, is used to compute landing field length. Mechanical devices, such as spoilers, are crucial in minimizing landing distances by greatly decreasing the lift — the objective is to land the aircraft early so the wheel brakes can be applied.

Constraints on aircraft climb performance are also specified in the federal air regulations. These include a minimum landing climb gradient with all engines running, and minimum climb gradients with one engine inoperative during three take-off segments, an approach segment, and an enroute case. When computing FAR 25 climb performance, the effects of engine-out include a decrease in thrust, the addition of windmilling drag from the inoperative engine(s), and a drag markup due to the increase in rudder and aileron drag associated with counteracting the asymmetric thrust. During the take-off and early climb, the flap and slat drag is taken into account. In the case of engine-out, the aircraft drag is also corrected for the additional trim drag.

The calculation of aircraft range requires that the entire flight profile be described. A typical mission is illustrated in Figure 4.6. For the purposes of this conceptual design tool, the equivalent still-air range (no wind) is computed from a simplified mission profile (Figure 4.7). The fuel required for warm-up, taxi, take-off, approach, and landing segments — maneuver fuel — is estimated as 0.7% of the take-off weight.

For approximate calculations, the additional fuel required to climb to altitude (as compared with cruising the same distance at the cruise altitude) can be approximated by adding an increment to the total cruise fuel. This increment has been estimated for a variety of aircraft, including the Douglas DC-9-30, DC-8-62, and DC-10-10 [62].

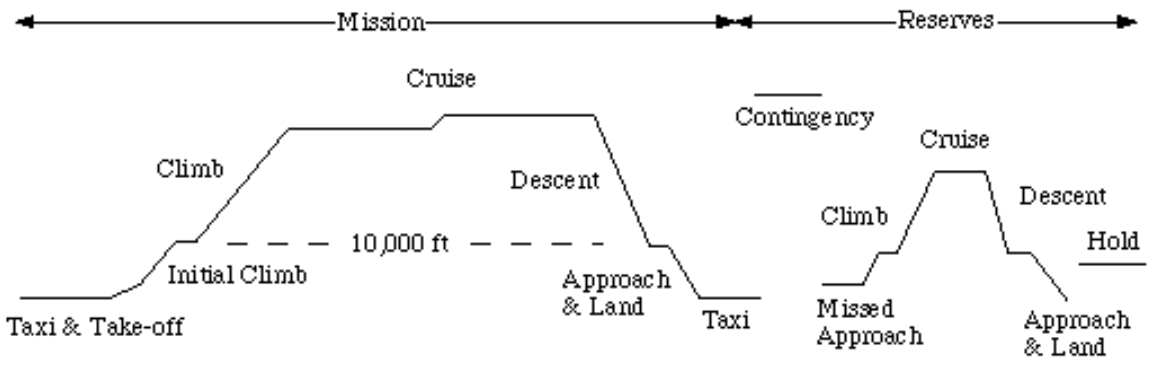

Figure 4.6: A typical commercial aircraft flight profile [61].

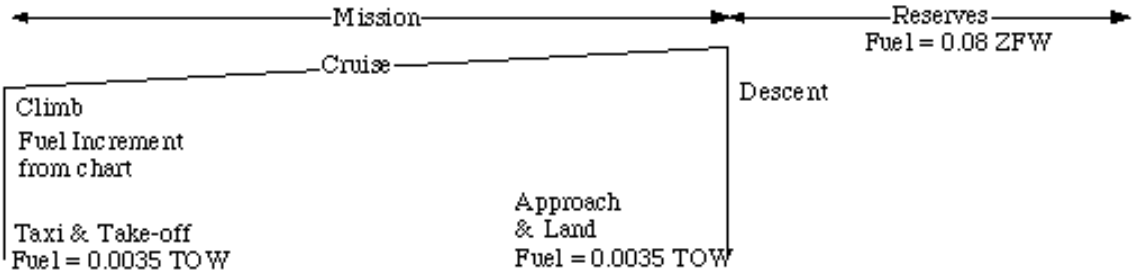

Figure 4.7: Simplified commercial aircraft flight profile [61].

Descent requires slightly less fuel than would be required to cruise the same distance at the final cruise speed and altitude. Hence, in this simplified computation, the cruise extends to the destination airport and the mission is completed at the final cruise altitude. The difference between initial and final cruise weights is the amount of fuel available for cruise. The cruise range of the aircraft is computed given takeoff weight, zero-fuel weight, fuel weight, and engine specific fuel consumption. The range factor is assumed to vary linearly during flight.

4.3.9 Operating Cost

Employing an appropriate cost metric is crucial to understanding the impact of noise and emissions on the aircraft. Total operating cost (TOC) contains direct operating cost (DOC), associated with the direct operation of the aircraft, and indirect operating

	Airbus A320	**Boeing 767-300ER**
Range (n.miles)	2,800	5,500
Pax. Capacity (2-class)	150	260
Wing Span (ft)	112	156
Takeoff Field Length (ft)	6,430	8,900

Table 4.1: Mission requirements and characteristics of the Airbus A320 and Boeing 767-300ER used for comparison with PASS [66].

	Airbus A320			**Boeing 767-300ER**		
	Actual	**PASS**	**% Error**	**Actual**	**PASS**	**% Error**
MTOW (lbs)	162,040	156,173	3.6	401,000	399,763	0.3
SLS Thrust (lbs)	54,000	51,516	4.6	120,000	123,086	2.6
Wing Area (ft^2)	1,320	1,313	0.5	3,050	2,829	7.2

Table 4.2: Comparison of existing aircraft with designs simulated with PASS using identical mission requirements.

cost (IOC), including items that support the operation of the aircraft indirectly.

The most common method of comparing the cost effectiveness of commercial aircraft is direct operating cost. Equations for estimating the *comparative* direct operating costs have been generated by the Air Transportation Association of America (ATA) and are used in the design tool [63]. These equations have been periodically revised by the ATA to match current data. Direct operating cost includes crew costs, maintenance, airframe and engine costs, and depreciation and insurance. To determine aircraft cost, Douglas DC-10 data is used and modified by a weight correction factor to take into account advances in composites and alloys [64].

Indirect operating costs includes the costs that are not directly connected with the actual flight of the aircraft. The following are included: aircraft ground handling, landing fees, service, passenger handling, sales, cargo handling, commissions, advertising, and administration. The value of each of these can only be estimated from statistics and a method developed at Douglas is used here [65].

4.3.10 Comparison to Existing Aircraft

In order to estimate the accuracy of PASS, an Airbus A320 and a Boeing 767-300ER were simulated. Mission requirements were set as constraints (Table 4.1), and the optimizer was run to obtain the lowest-cost designs that meet these requirements. Data is summarized in Table 4.2. Overall, PASS accurately estimates the takeoff weight, maximum thrust, and wing area of the two aircraft. Variations may be due to difficulties in capturing trends in cabin furnishing weight, alloy and composite content, and the details of the high-lift devices.

4.4 NASA's Engine Performance Program (NEPP)

4.4.1 Overview

Developed at NASA Glenn, NEPP is a 1-D steady thermodynamics analysis program. At the design point, NEPP [67] automatically ensures continuity of mass, speed, and energy by varying the scale factors on the performance maps for the compressor and turbine components. Off-design operation is handled through the use of component performance tables and minimization of work, flow, and energy errors. The engine is then balanced by altering free variables of available components.

Variable controls can also be used to obtain a certain performance. For example, airflow or combustion temperature can be varied to reach a desired thrust level. Controls are also used to limit and optimize engine parameters. For the purpose of the design tool, the range of variables has been selected to accommodate technology that would be available by the end of the decade, including increased combustion temperatures and higher turbomachinery efficiencies — for instance, bypass ratios ranging from 4 to 15 are acceptable (in this study, bypass ratio is calculated at sea-level static thrust conditions).

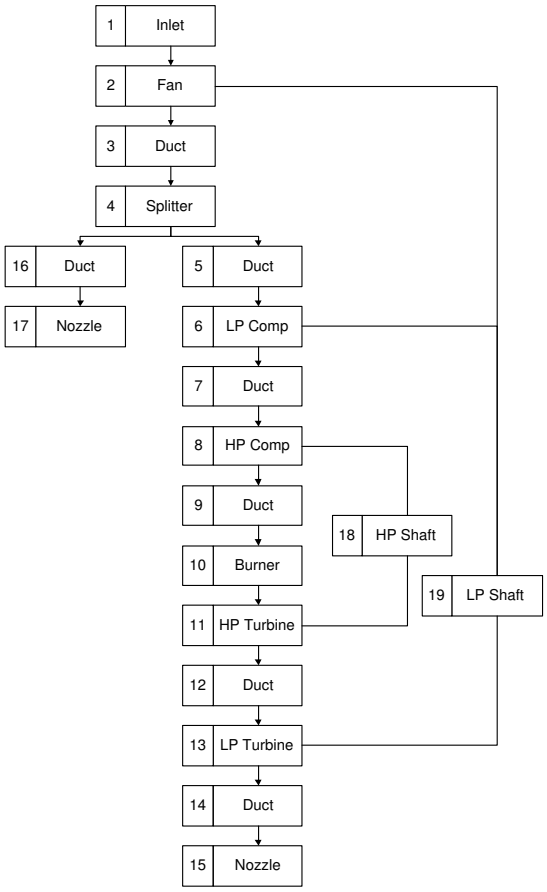

Figure 4.8: NEPP engine diagram.

4.4.2 Comparison to Existing Engines

As part of the NASA-MIT-Stanford Environmental Design Space (EDS) project, existing engines were simulated with NEPP for assessment purposes [68]. Specific fuel consumption at takeoff and cruise conditions was selected as the output metric of interest. Three engines were considered as part of this NEPP assessment study, reflecting various thrust classes and bypass ratios: the CFM56-5A1, the General Electric GE90-90B and the Pratt & Whitney PW4056. Relevant data is shown in Table 4.3.

A series of Monte Carlo simulations was run, with the input data sampled from Gaussian distributions. Results for takeoff thrust specific fuel consumption (TSFC) are shown in Figure 4.9.

Variable	CFM56-5A1	GE90-90B	PW4056
BPR (at SLS conditions)	6.00	8.36	4.70
OPR	26.60	39.38	29.30
TO Mass Flow Rate (lbs/s)	852	3,195	1,705
TO Fuel Flow Rate (lbs/h)	8,333	26,572	19,445
TO Thrust (lbs)	25,000	94,000	56,750
TO TSFC (1/h)	0.333	0.283	0.343

Table 4.3: Reference engine specifications [68].

With 95% confidence, NEPP exactly predicted published engine performance for the three engines. This confidence interval, however, shows significant variability depending on the engine: in this region, specific fuel consumption can be as much as 15% underpredicted for the CFM56, 15% overpredicted for the GE90, and 10% underpredicted for the PW4056.

NEPP accurately captures the performance of the PW4056 and only marginally captures the performance of the CFM56 and the GE90 at takeoff. Sensitivity studies show that for the GE90, changes in the input distribution means and standard deviations could shift the output mean and confidence interval away from the zero-percent error mark. The complex flow schedules of the CFM56 and GE90 are not simulated in NEPP — one reason why results for these two types were not as satisfactory.

4.4.3 On- and Off-design Operations

The engine design point is determined by running NEPP at sea-level static (SLS) condition, given combustor exit temperature, overall pressure ratio, desired sea-level static thrust, bypass ratio, and fan pressure ratio. The engine is run off-design for a variety of conditions, as required for noise prediction, emissions, and overall aircraft performance (Figure 4.10).

At off-design, for example part-power operation, the engine must be balanced using a free variable: burner exit temperature (T_4) is decreased to obtain the desired fraction of maximum thrust.

To determine the amount of thrust available at cruise conditions, for example, the process is as follows:

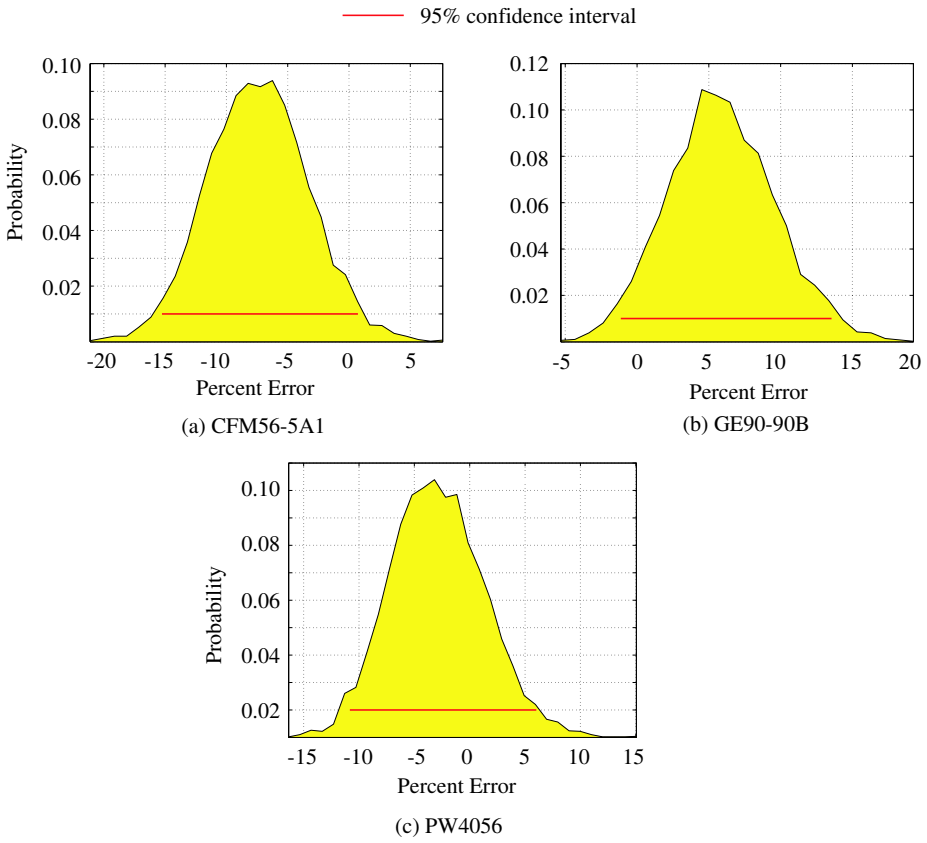

Figure 4.9: Error in computed takeoff TSFC distribution relative to published data [68].

Run 1: Engine at SLS conditions (Alt = 0, Mach = 0, T_4 = max T_4).

Run 2: Automatically vary T_4 until desired cruise thrust is obtained.

Run 3: Run at $T_{4_{cruise}}$ obtained in Run 2 at cruise conditions.

PASS also requires available thrust and fuel consumption at various conditions to compute overall aircraft performance. Engine out performance is required to meet emergency climb requirements.

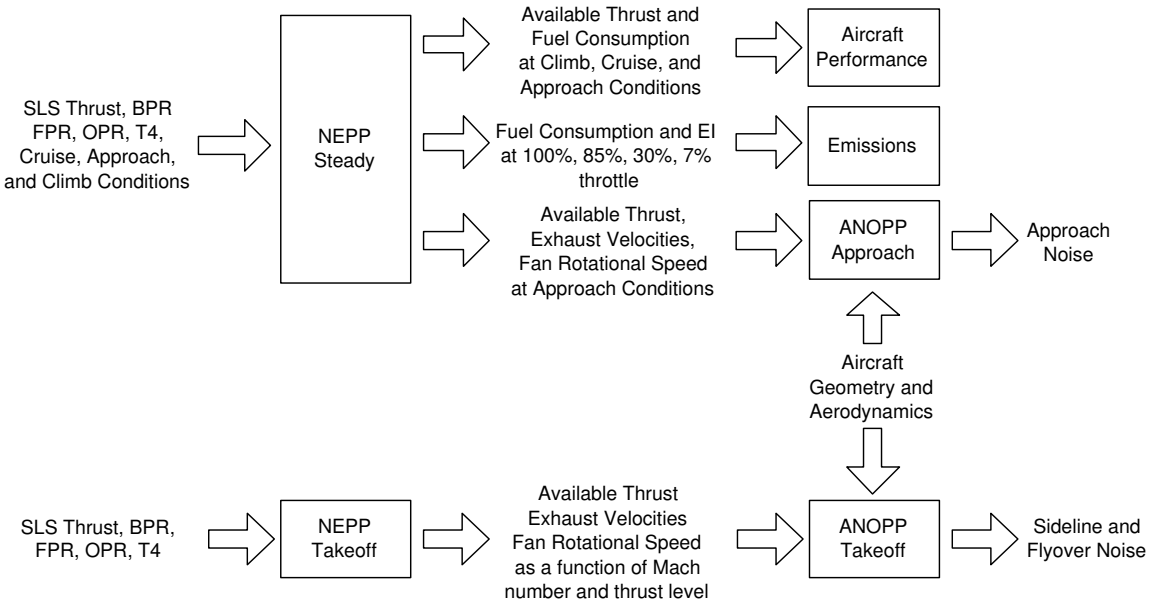

Figure 4.10: ANOPP and NEPP integration in the framework.

Chapter 5

Optimization Methods

5.1 Aircraft Design Optimization

In aircraft design, there is typically a need to minimize or maximize some aspect of the aircraft's performance, for example range or operating cost. It is therefore not surprising that multidisciplinary optimization has been successfully applied to aircraft design at all stages of development, including supersonic aircraft conceptual design [69], sonic boom minimization [70], detailed propulsion-airframe integration [71], and high-fidelity aero-structural optimization of business jets [72], to name just a few examples. In addition, specialized methods have been developed to explicitly capture the particularities of aircraft design including collaborative optimization [73, 74] and graphical interfaces for design space exploration [49].

At the conceptual design stage, optimizing future commercial aircraft for environmental as well as operating performance requires a holistic approach that recognizes the inherently multidisciplinary nature of airplanes, and can consider simultaneously variables and constraints from all relevant disciplines.

Because it is crucial in aircraft design to explore the sensitivity of various objectives and the inevitable inter-disciplinary tradeoffs, the emphasis of this section is on optimization methods that easily accept changes in variables, constraints, and objectives, and propagate them through the multidisciplinary design process, causing other relevant variables to adjust and restore the design to a new optimal state.

5.2 Single and Multiobjective Optimization

A single objective optimization problem can be formulated as follows [75]:

$$\begin{aligned} &\text{Minimize } f(\mathbf{x}) \\ &\text{where } f : \mathbf{x} \in \Omega \subset \Re^n \rightarrow \Re \\ &\text{subject to } \mathbf{g}(\mathbf{x}) \leq 0, \mathbf{h}(\mathbf{x}) = 0 \end{aligned}$$

Ω is the search space, and $f(\Omega)$ is called the objective space. The inequality constraints $\mathbf{g}$ and equality constraints $\mathbf{h}$, must be satisfied.

There are two types of multiobjective optimization problems: cooperative and competing. The optimum solution to a cooperative problem, similarly to single objective optimization, is a single point. When two or more objectives are competing, however, an improvement in one objective causes a degradation in another: a trade-off must take place. The outcome is a finite population of solutions that cannot be decided between because each of these points is better than the others in some objective(s), and worse in the other objective(s). The formulation is as follows:

$$\begin{aligned} &\text{Minimize } \mathbf{f}(\mathbf{x}) \\ &\text{where } \forall f : \mathbf{x} \in \Omega \subset \Re^n \rightarrow \Re \\ &\text{subject to } \mathbf{g}(\mathbf{x}) \leq 0, \mathbf{h}(\mathbf{x}) = 0 \end{aligned}$$

In multi-objective space, there is no ordering of solutions as there is in single objective space. Instead, comparing solutions is based on whether one solution dominates another. Solution $\mathbf{x}_1$ is said to dominate solution $\mathbf{x}_2$ if both conditions below are true [76]:

1. The solution $\mathbf{x}_1$ is no worse than $\mathbf{x}_2$ in all objectives.

2. The solution $\mathbf{x}_1$ is strictly better than $\mathbf{x}_2$ in at least one objective.

When $\mathbf{x}_1$ dominates $\mathbf{x}_2$ (or, conversely, $\mathbf{x}_2$ is dominated by $\mathbf{x}_1$) the design corresponding to $\mathbf{x}_1$ is intrinsically better than the one corresponding to $\mathbf{x}_2$.

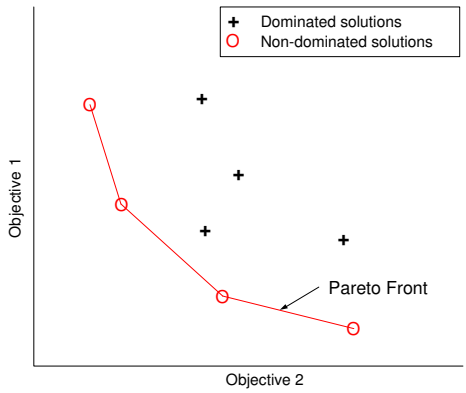

Figure 5.1: An example 2-objective minimization problem.

In cases where $\mathbf{x}_1$ does better than $\mathbf{x}_2$ against some objectives and $\mathbf{x}_2$ does better than $\mathbf{x}_1$ against other objectives, neither solution dominates the other. They are both non-dominated by the other (but can of course be dominated by other solutions).

The set of solutions that are non-dominated by any other solution is called the non-dominated set, or Pareto-optimal set. These solutions correspond to the optimal trade-offs between the various objectives, under the parameters and constraints specified for the problem: any solution in the Pareto Set showing a better score against one objective than another solution inevitably scores worse against another objective.

Figure 5.1 illustrates the concept of Pareto dominance for a problem with two objectives to be minimized. Of the eight solutions to this problem shown in the figure, only four belong to the Pareto Set. Together, they form a *Pareto front*.

5.3 Selecting an Optimizer

Selecting the best optimizer for a real-variable problem is dependent on many factors:

1. Type of objective
2. Topology of the objective space
3. Number of variables
4. Single- or multi- objective

If the objective can be computed analytically, efficient algorithms such as the adjoint method can be used [72]. However, the use of ANOPP and NEPP in this design framework precludes this approach because of the noise such 'black box' codes add to the objective function.

The topology of the objective can have a significant impact on the choice of an optimizer, and gradient methods are most amenable to smooth objective functions. Using sensitivities, these methods can be very efficient, requiring considerably fewer function evaluations than non-gradient methods that only compare objective function values. However, because of the multiple-input, single-output functionality of some of the codes used in the design framework (such as ANOPP) the impact of changing one or more inputs on the output can be difficult to trace (Figure 5.2), and this makes some of the objective functions considered as part of this research not amenable to gradient-based methods. For example, if applied to multi-modal or noisy objectives, gradient methods would have a high probability of converging to local minima. Non-gradient methods, on the other hand, are relatively less efficient, but they can handle any type of topology – there is no requirement of "smoothness".

While non-linear n-dimensional Simplex methods work well with relatively low numbers of variables (up to 8), other methods, in particular population-based ones, are more robust and reliable for the size of problem explored in this research (12-14 variables). Instead of progressing towards the extremum one solution at a time, population-based algorithms employ a set (or population) of solutions. The advantage is that, if the population is initiated correctly, large portions of the design space can be explored simultaneously. Population-based methods tend to be computationally expensive, but they can handle large number of variables and offer a level of robustness not found in sequential methods: in particular, convergence to local extremes can be avoided. Population-based algorithms are the ones most appropriate for the type of optimization problems addressed here. Genetic algorithms, described in more detail in section 5.4 below, are the particular kind of population-based optimizers used for this research.

Finally, there are three approaches to multiobjective (multi-criteria) optimization: weighted composite functions, the ϵ-constraint method, and population ranking.

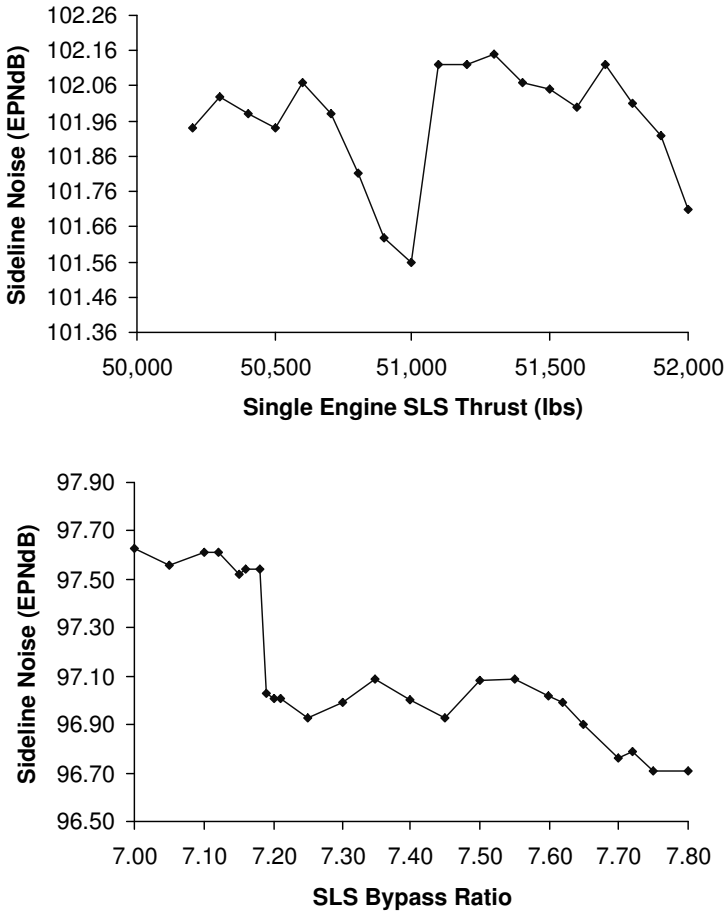

Figure 5.2: ANOPP numerical noise.

In the case of weighted composite functions, a surrogate objective is created via a linear combination of the objectives. This involves assigning a "preference", or weight w_i, to each objective f_i depending on the priority of each objective in the analysis. The problem is essentially reformulated as a single objective (F) problem:

$$F = \sum_i w_i f_i \tag{5.1}$$

If the weights assigned to some objectives are value ranges rather than fixed values, multiple optimization runs will be required to obtain a Pareto set.

The ϵ-constraint approach involves constraining all but one of the objectives f_i to a desired value C_i and repeatedly running the optimizer with a single objective f_j:

$$\min f_j \tag{5.2}$$

$$\text{subject to } f_i = C_i \; \forall i \neq j \tag{5.3}$$

As with the weighted composite function method, this method is computationally expensive and may require a large number of iterations before a satisfactory Pareto set is obtained.

The third approach, population ranking, is particularly well suited to relatively large-scale multiobjective problems. Because multiple solutions are evaluated simultaneously, the Pareto set can be scanned effectively with a limited number of generations.

5.4 Multiobjective Genetic Algorithm

5.4.1 Overview

Genetic algorithms (GA) mimic nature's evolutionary principles to drive a search towards an optimal solution [77]. One of the main differences with traditional search algorithms is that genetic algorithms work with a *population* of solutions (aircraft designs in the context of this research) instead of a sequence of single solutions. At each iteration, GAs produces a new population of solutions that move towards the optimum through a generational process of selection and elimination.

If the problem has a single optimum, all GA population members quickly converge to the optimum. In the case of multiple optimal solutions, typical of multiobjective problems, GAs converge towards a final population (the quality of which does not improve through further iterations) that captures all optimal solutions. Multiobjective GAs have been found particularly successful for optimization scenarios involving noisy objectives: for instance, to study the trade-offs between sonic boom and drag in supersonic aircraft [70].

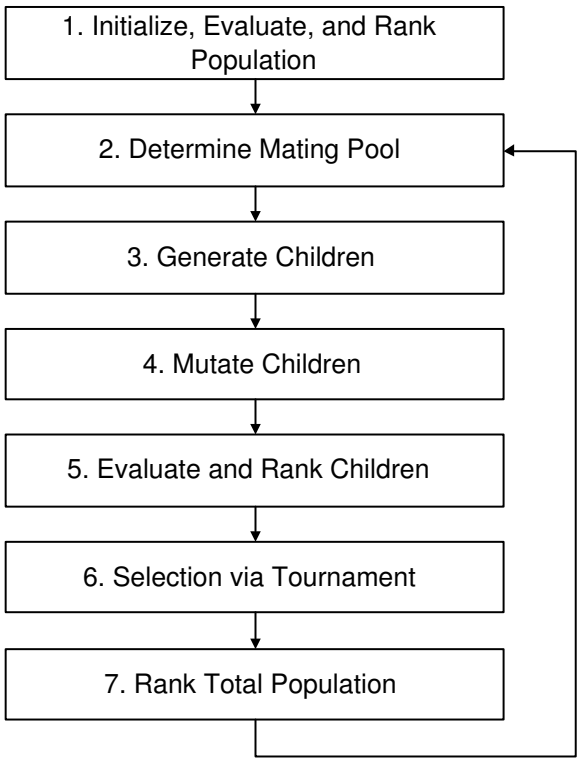

Figure 5.3: An example multiobjective genetic algorithm.

A metric is required to evaluate the relative fitness of each solution produced at each iteration of the GA. A ranking is used for this purpose, based on the dominance concept introduced earlier [78].

Each solution is checked for domination in the population. The rank r_i of solution i is equal to one plus the number of solutions n_i that dominate solution i:

$$r_i = 1 + n_i \tag{5.4}$$

At each iteration, the non-dominated solutions are therefore assigned a rank of 1, and form the Pareto set of that generation. The Pareto set obtained from the final population constitutes the set of optimal solutions to the problem.

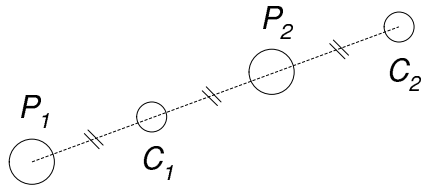

Figure 5.4: Reproduction scheme for generating children C_1 and C_2 from parents P_1 and P_2.

5.4.2 Generational Selection and Elimination

A typical multiobjective genetic algorithm is illustrated in Figure 5.3. The first step is to initiate and evaluate a first population (Box 1), that spans the design space. A random process is normally used to generate this population.

Many 'reproduction' methods are available to produce the next generation of solutions. In the case illustrated in Fig 5.3, a mating population is determined at random (Box 2), and each pair of parents P_1, P_2 generates two children C_1, C_2 (Box 3): one child is created by interpolating between the two parents and the other by extrapolating towards the "fitter" parent (Figure 5.4). To maintain diversity in the population, mutation can be added to the children members as they are generated (Box 4). After the children are evaluated and ranked (Box 5), a tournament takes place in every family, the best child (lower rank) being added to the population for the next reproduction cycle (iteration of the GA) and the worst parent (higher rank) being removed from the population. The above results in a population that remains of constant size through successive generations (or iterations of the GA — Box 6). The entire population is then evaluated and ranked, and the Pareto set of non-dominated solutions (that is, Rank 1 solutions) is identified (Box 7). Next, the reproduction process begins all over again with the updated population, and the selection/elimination process is repeated, each generation of solutions representing a gradual iteration towards the optimum.

In order to maintain diversity among non-dominated solutions, niching is introduced. The concept is to enforce a "minimum distance" between solutions of same rank to avoid clustering around local extrema and ensure that the solution population fills the available design space.

The normalized distance between two solutions i and j of same rank is used as metric for this purpose. It is defined as :

$$d_{ij} = \sqrt{\sum_k \left(\frac{f_k^i - f_k^j}{f_k^{max} - f_k^{min}} \right)^2} \tag{5.5}$$

Where f_k^{max} and f_k^{min} are the maximum and minimum objective function value of the k-th objective, respectively.

The niche count is calculated by summing the sharing function values across all solutions of rank r_i. σ_{share} is set by the user (typical values are 0.2-0.6).

$$nc_i = \sum_{j \in r_i} Sh(d_{ij}) \tag{5.6}$$

$$\begin{aligned} Sh(d_{ij}) &= 1 - \frac{d_{ij}}{\sigma_{share}}, \text{ if } d_{ij} \leq \sigma_{share} \\ &= 0, \text{ otherwise.} \end{aligned}$$

Finally, the shared fitness $F_i^{'}$ of solution i is computed and substituted for raw fitness F_i:

$$F_i^{'} = \frac{F_i}{nc_i} \tag{5.7}$$

Through the generations, the genetic algorithm drives the population towards better solutions. Eventually, the quality of the population stops improving and the resulting Pareto set contains the optimal solutions. This is illustrated in Figure 5.5. In this example, a 200-seat, 6,000nm range aircraft is optimized simultaneously for both minimum cost and maximum cruise Mach number. With each generation, the Pareto front is pushed towards higher Mach numbers and lower costs. Eventually, the front no longer progresses and the set of optimal trade-offs between Mach number and cost is obtained.

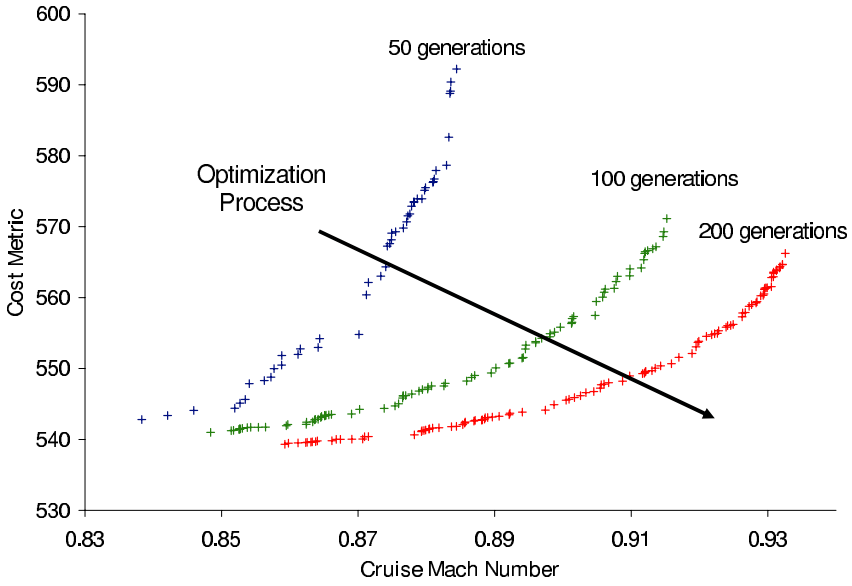

Figure 5.5: The Pareto front indicates the set of non-dominated solutions in a given generation. The optimization process drives the population towards their optimal values.

One of the issues with multiobjective genetic algorithms is the lack of true convergence criteria. The Pareto set simply indicates the best solutions *of a given generation*, but gives no indication of whether global optimality has been reached. The population average rank is a commonly used measure to gauge progress towards the optimal population — an average population rank of 1 would indicate that all population members are non-dominated and lie on the Pareto front.

5.4.3 Handling Constraints

Constraints are an integral part of any engineering problem. In the case of a genetic algorithm-based optimizer, two common methods of handling constraints are:

1. Rejecting the population member that violates one or more constraints
2. Penalizing the member by decreasing its fitness, therefore increasing rank.

The first method requires generating a new population member to replace the one that is rejected.

This can be quite time consuming, especially for early generations, in which a large portion of the population might contravene constraints due to the random nature of the initial population.

As a result, the preferred method involves applying a penalty to each objective i of the population member that violates one or more constraints j. Thus, an infeasible design solution will be recast as a feasible one, albeit with a lower fitness, meaning that it will be less likely to be selected for the next generation. We write:

$$f_i(\mathbf{x}) = f_i(\mathbf{x}) + \sum_j r_j G_j + \sum_j t_j H_j$$

where G_j and H_j are penalty functions of the inequality and equality constraints g_j and h_j, respectively:

$$G_j = \max(0, g_j(\mathbf{x}))^a$$
$$H_j = |h_j(\mathbf{x})|^b$$

The parameters a and b are set by the user. Selecting the appropriate r_j and t_j penalty parameters is crucial: a penalty that is too heavy could reject design solutions that point towards the optimum despite being marginally in contravention of some constraints. Conversely, penalties that are too light will not eliminate infeasible solutions that will be perpetuated in future generations. One method is to set the penalty function to one order of magnitude greater than the raw objective.

5.4.4 Sensitivities

While the Pareto fronts generated during the multiobjective optimization process are typically used to estimate sensitivities in the objective space — such as the impact of increasing Mach number on operating cost, seen previously — they offer limited information on sensitivities in the variable space.

As an example, three adjacent designs are selected from the 200th generation of the Max Mach number — Min cost optimization problem (Figure 5.6).

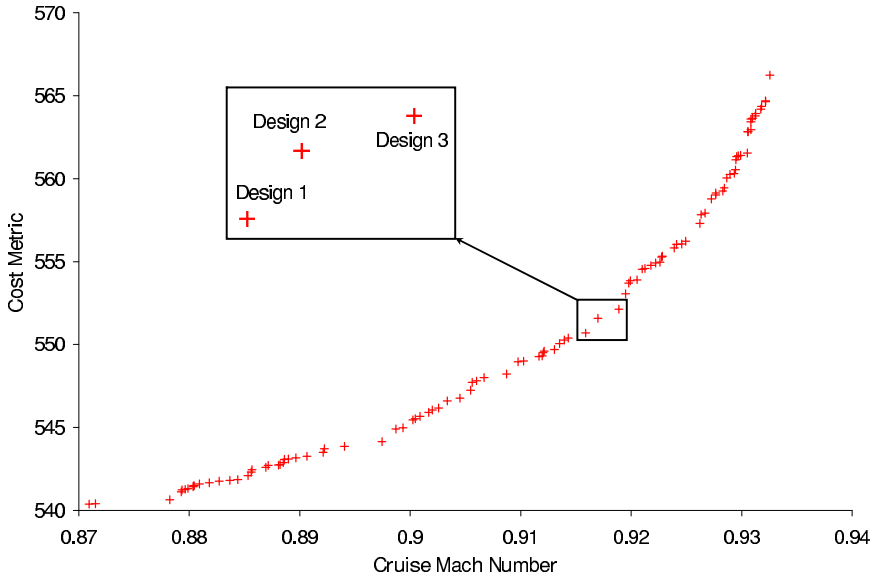

Figure 5.6: Three non-dominated designs are selected to explore variable-space sensitivities.

Design	Objectives		Variables		
	Max. Mach #	Min. Cost	MTOW (lbs)	SLS Thrust (lbs)	BPR
1	0.916	550.7	523,682	91,759	8.62
2	0.917	551.6	525,706	91,761	8.44
3	0.919	552.1	527,834	91,995	8.75

Table 5.1: Objective and variable data for the three aircraft selected for the sensitivity study.

Data for these aircraft, including values for three of the design variables, is summarized in Table 5.1.

The higher drag associated with flying faster demands greater thrust and more fuel: both maximum takeoff weight (MTOW) and sea-level static (SLS) thrust per engine increase as the cruise Mach number is raised. The three designs support this trend. On the other hand, there is no clear trend for the third variable, bypass ratio (BPR). This is typical of variables that are not tightly coupled to the objectives — while thrust and weight directly affect the cruise performance of the aircraft, the impact of bypass ratio in this study is secondary.

Because solutions are solely manipulated by the optimizer based on objective information, any trend that emerges in the variable space is a by-product of the optimization process. A clear trend for variables that have a weak impact on the objectives may not emerge until a significant number of generations has been completed. In the case of bypass ratio, it is very probable that a monotonic trend would emerge following additional generations.

5.4.5 Example: a 2-objective constrained problem

To illustrate the performance of the multiobjective genetic algorithm in solving a constrained problem, the following example problem was solved:

$$\begin{aligned} \text{Minimize: } & f_1 = 4x_1^2 + 4x_2^2 \\ & f_2 = (x_1 - 5)^2 + (x_2 - 5)^2 \\ \text{Subject to: } & c_1 = (x_1 - 5)^2 + x_2^2 \\ & c_2 = (x_1 - 8)^2 + (x_2 + 3)^2 \\ & c_1 \leq 25,\ c_2 \geq 7.7 \\ & 0 \leq x_1 \leq 10,\ 0 \leq x_2 \leq 10 \end{aligned}$$

The population of 20 solutions for select generations is shown in Figure 5.7. Starting from a random initial population (Figure 5.7a), the majority of solutions violate the constraints. Applying the penalty method described above, these infeasible points are recast as feasible solutions of higher rank, proportional to the magnitude of the constraint violation. Since the same penalty weight is applied to both objectives, these infeasible solutions are roughly scattered along an $f_1 = f_2$ line.

As the solutions are driven towards feasible space through the generations, the severity of the constraint violation decreases (Figure 5.7b) and the points approach the growing Pareto front. Infeasible solutions are eventually completely eliminated: all points in Figure 5.7c are feasible (hence the reduced scale of the axes). After 8 generations, all solutions reach rank 1 and span the Pareto front (Figure 5.7d).

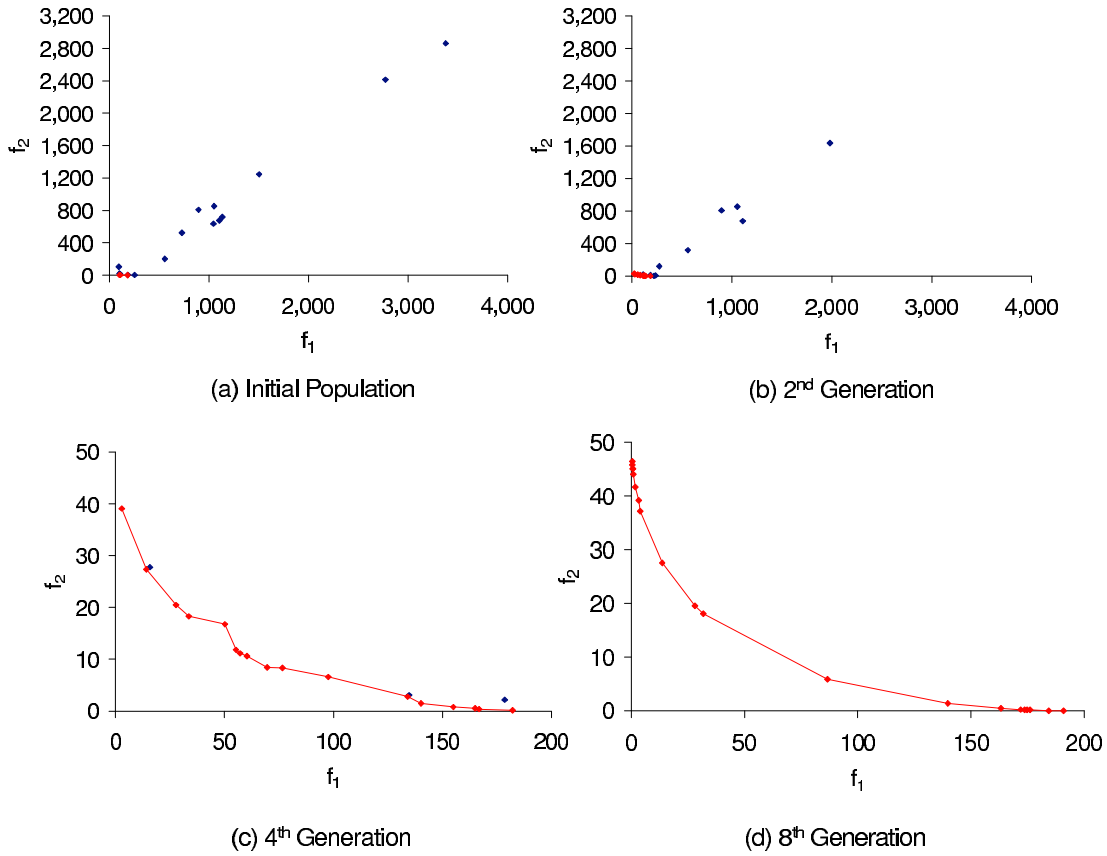

Figure 5.7: Progress of the population towards optimum for the 2-objective minimization example problem with constraints. Solutions in red are of rank 1, all other ranks in blue.

Chapter 6

Multiobjective Trade Studies

6.1 Aircraft Mission, Variables, and Constraints

This section illustrates the optimization process performed by the design tool in the case of a 280-passenger, twin-engine airliner with a 6,000 nm range, and takeoff, cruise, and landing performances in line with industry standards for similarly-sized aircraft. The 15 design variables are listed in Table 6.1, split in three groups: aircraft geometry, engine parameters, and performance. Constraints are shown in Table 6.2.

6.2 Extreme Designs and Sensitivities

6.2.1 Operating Cost vs. Cruise Emissions, LTO NO_x Emissions, and Noise

The process of obtaining a low-rank Pareto front can be significantly accelerated by first computing the extreme points of the fronts. This is done by running a single-objective version of the genetic algorithm. These optimal designs are subsequently inserted into the initial population of the multiobjective problems. The resulting Pareto fronts of fuel carried, NO_x emissions, and cumulative noise margin vs. cost are shown in Figure 6.1. Key parameters for the optimized extreme designs are summarized in Table 6.3.

Variable	**Units**	**Min**	**Max**
Maximum Take-Off Weight	lbs	280,000	550,000
Wing Reference Area	ft^2	1,500	4,000
Wing Thickness-over-Chord	%	0.07	0.20
Wing Location along Fuselage	%	0.2	0.6
Wing Aspect Ratio	—	4.0	15.0
Wing Taper Ratio	—	0.1	0.7
Wing Sweep	deg	0.0	40.0
Horizontal Tail Area	ft^2	225	600
Sea-Level Static Thrust	lbs	40,000	100,000
Turbine Inlet Temperature	°F	3,000	3,300
Bypass Ratio	—	4.0	15.0
Engine Pressure Ratio	—	40.0	60.0
Initial Cruise Altitude	ft	20,000	40,000
Final Cruise Altitude	ft	20,000	50,000
Cruise Mach Number	—	0.65	0.95

Table 6.1: Variable names, units, and minimum and maximum allowable values for the optimization problems.

Constraint	**Units**	**Value**
Cruise Range	n.miles	$\leq$ 6,000
Takeoff Field Length	ft	$\leq$ 9,000
Landing Field Length	ft	$\leq$ 8,000
Engine Out Climb Gradient	—	$\geq$ 0.024
Drag-to-Thrust Ratio	—	$\leq$ 0.88
Stability Margin	—	$\geq$ 0.18
Wing Cruise Lift Coeff. Margin	—	$\geq$ 0.01
Tail Rotation Lift Coeff. Margin	—	$\geq$ 0.01
Tail Cruise Lift Coeff. Margin	—	$\geq$ 0.01
Tail Landing Lift Coeff. Margin	—	$\geq$ 0.01
Wing Span	ft	$\leq$ 260.0

Table 6.2: Constraints for the optimization problems.

	Units	Design A Min Cost	Design B Min Fuel	Design C Min NO_x	Design D Min Noise
Objectives					
Relative Cost	—	1.0	1.02	1.09	1.26
Fuel Carried	lbs	119,018	106,707	134,796	138,840
LTO NO_x	kg	30.88	29.68	14.36	41.09
Relative Noise	EPNdB	0.0	-5.13	3.66	-14.98
Variables					
Max. Take-Off Weight	lbs	372,539	352,515	407,516	473,532
Wing Reference Area	ft^2	3,461	2,942	3,887	3,578
Wing t/c	%	11.7	13.5	12.8	11.5
Wing Location	%	39.2	41.2	48.1	48.2
Wing Aspect Ratio	—	7.38	9.99	8.94	14.43
Wing Taper Ratio	—	0.10	0.10	0.39	0.1
Wing Sweep	deg	33.70	26.17	11.22	14.25
Horizontal Tail Area	ft^2	929	766	953	1,431
SLS Thrust (per engine)	lbs	68,404	67,311	60,264	100,000
Thrust-to-Weight Ratio	—	0.367	0.382	0.296	0.422
Turbine Inlet Temp	°F	3,203	3,215	3,147	3,300
Bypass Ratio	—	9.59	10.35	10.32	14.87
Engine Pressure Ratio	—	59.91	59.63	40.27	59.78
Init. Cruise Altitude	ft	32,937	30,746	28,381	31,674
Final Cruise Altitude	ft	40,790	38,734	33,288	35,486
Cruise Mach Number	—	0.844	0.739	0.669	0.664

Table 6.3: Data for the optimal extreme designs obtained with the single-objective genetic algorithm.

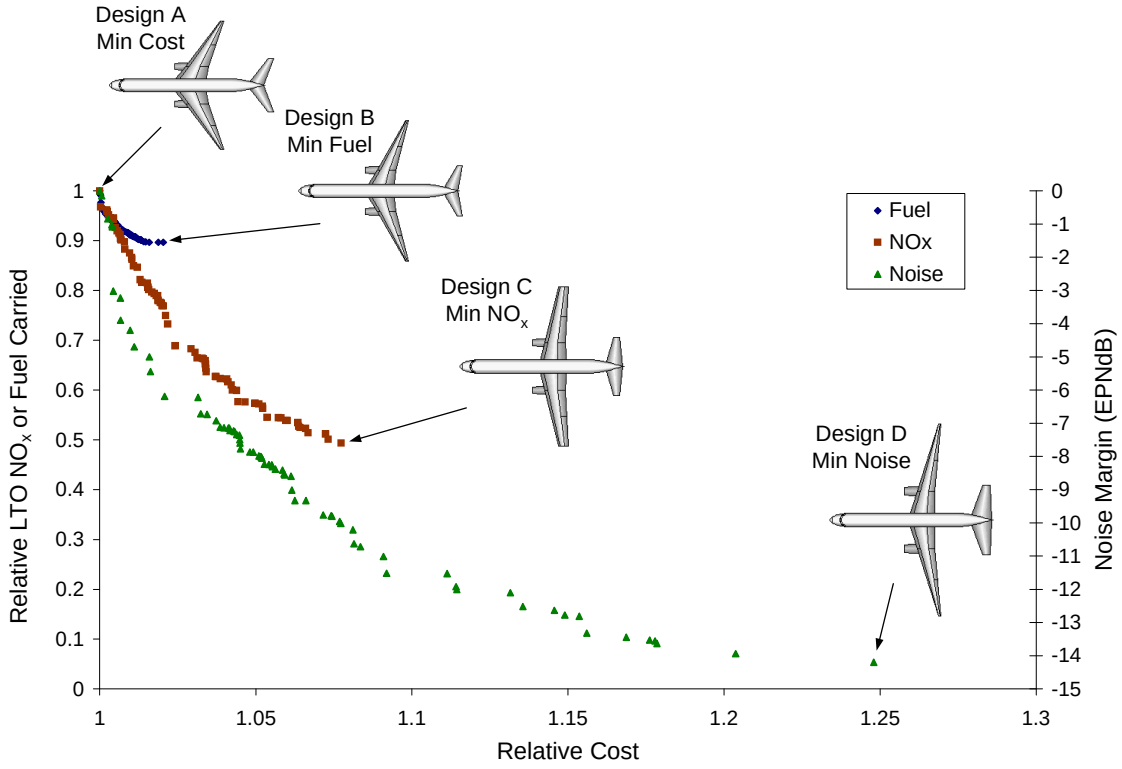

Figure 6.1: Pareto fronts of fuel carried, LTO NO_x, and cumulative certification noise vs. operating cost. Only rank 1 designs are shown. Average rank for all fronts is under 4.

The configuration leading to minimum operating cost (Design A) was computed first by running the design tool without specifying any noise or emissions constraints. This aircraft is considered as the baseline and is representative of existing aircraft. Reflecting the impact of block time on the cost function, the cruise mach number is higher than would be required for minimal fuel burn (Design B). Fuel plays a dominating role in the cost calculation, as illustrated by the similarities in the designs for minimum cost and minimum fuel carried (and therefore, minimum cruise CO_2, SO_2, and H_2O). This tight coupling is also reflected in the relatively small fuel-cost trade space (notice the fuel-cost Pareto front is narrow). At the engine level, noticeably, both designs attain high fuel efficiency via large pressure ratios and high turbine inlet temperatures.

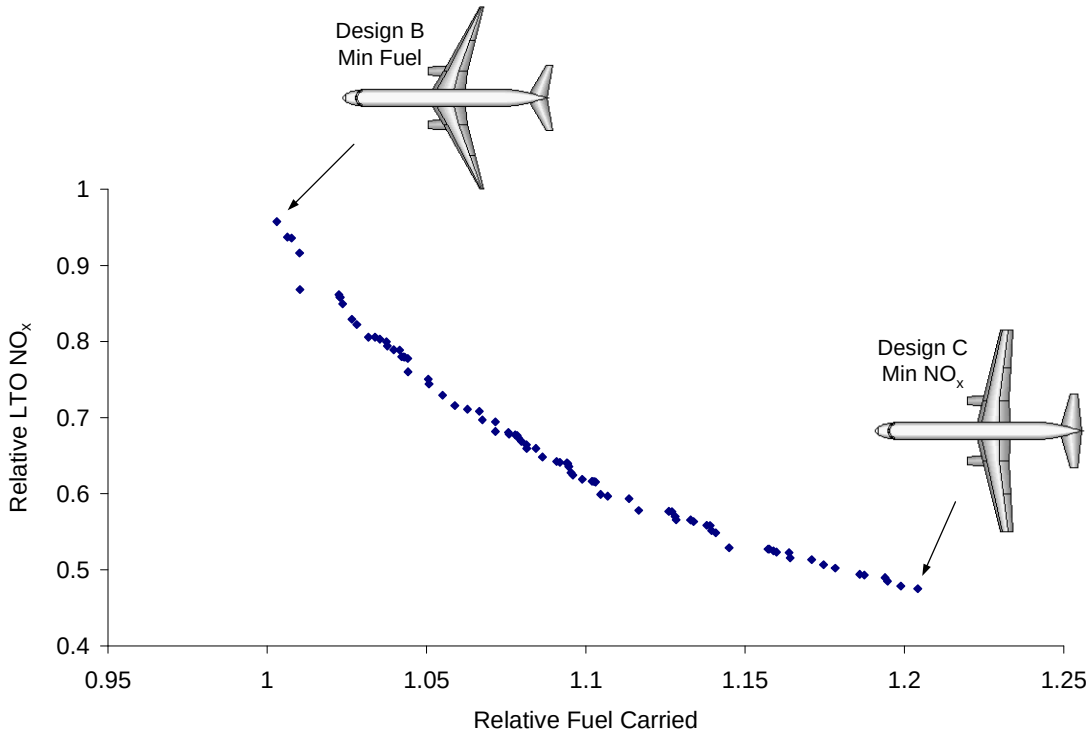

Figure 6.2: Pareto front of LTO NO_x vs. fuel carried. Only rank 1 designs are shown (Average rank = 3.47).

Optimizing the aircraft for lowest fuel yields a 10% decrease in fuel carried (propagating through the design to yield a 5.4% decrease in maximum takeoff weight) for a cost increase of 2% relative to low-cost Design A.

As seen previously (Equation 3.3), the generation of NO_x emissions is a strong function of combustor exhaust temperature and compression ratio. Design C therefore compromises fuel efficiency for low NO_x emissions by reducing the engine overall pressure ratio and combustor temperature. The resulting 12% reduction in sea-level static thrust relative to the low-cost design mandates that the aircraft fly slower (Mach 0.67, close to the lower allowable limit, versus Mach 0.84) and at lower altitudes (the initial cruise altitude is reduced from approximately 33,000 ft to 28,000 ft). The result is a 53.5% drop in LTO NO_x emissions for an 9% and 13% increase in operating cost and fuel consumption, respectively.

These divergent requirements for low-NO_x and low-fuel designs are well illustrated by a wide, and very smooth, Pareto front. As a result of the lower cruise Mach number, wing sweep is reduced from 34 to 11 degrees. With significantly reduced available thrust, the wing taper ratio is increased from 0.10 to 0.39 to increase the maximum lift coefficient during takeoff and initial climb. For similar reasons, the wing area is enlarged by 12%, contributing to an increase in maximum takeoff weight of 9%. Combined with lower available thrust, the climb performance of the low-NO_x design is significantly deteriorated: thrust-to-weight ratio drops to 0.296 — resulting in the highest cumulative certification noise of any design, over 3.5 dB louder than the baseline Design A.

The large fan necessary to reduce noise to the minimum (Design D, with a bypass ratio very close to the maximum allowable value of 15) requires more power, resulting in the selection of the highest allowable combustion temperatures and overall engine pressure ratio. The result is a 15 cumulative EPNdB reduction in noise relative to the low cost design, equivalent to a 25-fold reduction in noise energy. The penalty is a 26% increase in operating cost and 16% in fuel carried, along with NO_x emissions that are 33% higher due to the increased combustion temperature. The higher thrust levels required by this high bypass-ratio engine at altitude are significant: sea level static thrust is raised from 68,404 to 100,000 lbs (the maximum allowable), a 46% increase. Higher thrust enables the aircraft to climb faster, increasing the distance to the flyover certification point and decreasing measured noise.

These enormous, and therefore very heavy, engines cause a 27% maximum takeoff weight increase relative to Design A. The large frontal area, and therefore increased drag of the design, leads the aircraft to fly slower than the low cost candidate (Mach 0.66 vs. Mach 0.83). Similarly to the low NO_x aircraft, the reduced cruise Mach number results in a reduced sweep of 14 degrees. A summary quantifying the trades between designs is shown in Table 6.4.

For this increase in cost	Can reduce one of these by		
	Fuel Carried	LTO NO_x	Cumulative Noise
1%	7%	10%	3 EPNdB
2%	10%	20%	6 EPNdB
9%	10%	51%	10 EPNdB
25%	10%	51%	15 EPNdB

Table 6.4: Fuel carried, LTO NO_x, or cumulative noise can be traded with operating cost.

6.2.2 Cruise Emissions vs. LTO NO_x Emissions

To explore the interrelationship between the conflicting requirements of reducing NO_x and fuel-based emissions (CO_2, H_2O, and SO_2), the multiobjective optimizer was applied to the min-NO_x/min-fuel problem. The resulting Pareto front is shown in Figure 6.2, with Design B (low-fuel) and Design C (low-NO_x) the extreme points discussed previously. According to these results, a decrease in LTO NO_x of 12% (as recommended by ICAO for new aircraft after 2008 under CAEP/6) would require an increase of approximately 2% in fuel consumption and related emissions. As the demand for reductions in NO_x increase, this penalty grows: the next 12% require a further 4% increase in fuel. These results illustrate the delicate trade-off that must be resolved as new regulations come into play: what is the "value" of trading one type of emissions for another?

6.2.3 Noise vs. Cruise vs. LTO NO_x Emissions

This trade-off approach is expanded to include a third objective, cumulative noise. The surface that is obtained, as well as the location of the three extreme points, are shown in Figure 6.3. The conflicting design requirements for the min noise (Design D) and min NO_x (Design C) aircraft are well illustrated here: the low-noise aircraft is also the design with highest NO_x, and conversely, the aircraft with lowest min NO_x is the noisiest. Indeed, Designs D and C are costly to obtain and require almost complete deterioration of the other two objectives. The minimum fuel design (Design B), however, is obtained without entirely forgoing gains in noise or NO_x emissions.

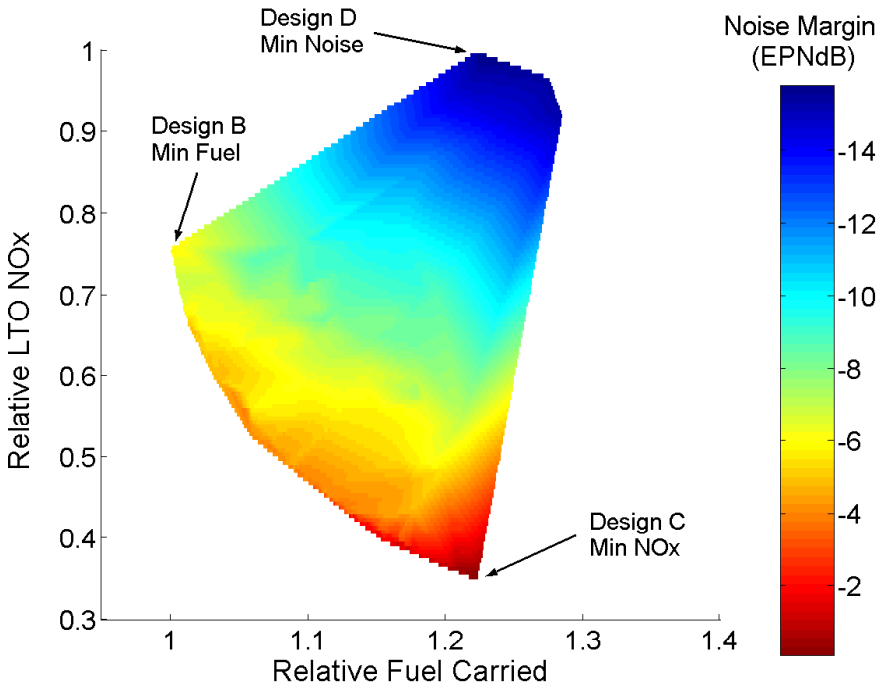

Figure 6.3: Pareto surface of LTO NO_x vs. Fuel Carried vs. Cumulative Noise. Only rank 1 designs are shown.

The usefulness of this Pareto surface is not limited to the extreme designs. Every design on the surface is optimized for a combination of noise, fuel, and NO_x performance; the impact of reducing one objective on the two others can be estimated directly from the surface.

Displaying three objectives also allows the selection of the objective to forgo in order to improve the design. If the goal is to trade noise and fuel efficiency for a 20% decrease in NO_x, for example, a whole family of designs is applicable. Each aircraft features a different fuel and noise trade in order to attain the desired reduction in NO_x. The final decision for selecting the appropriate design lies with the user: higher-level information, such as certification or operational requirements, is required.

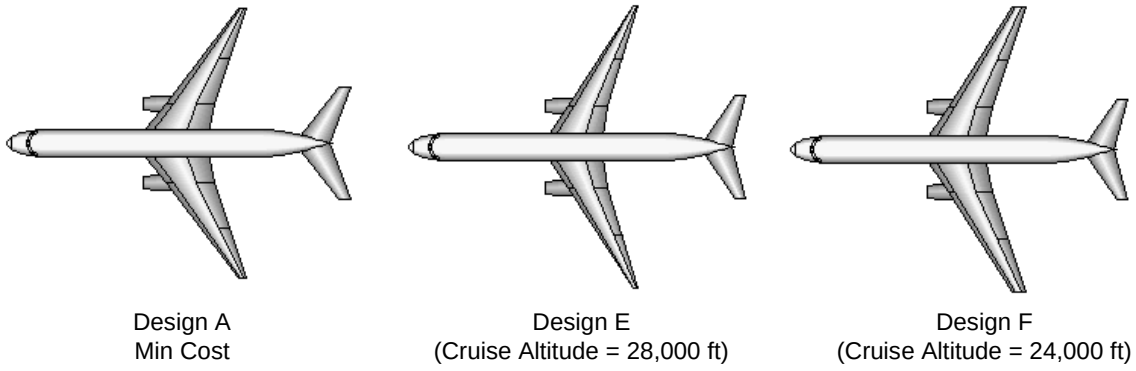

Figure 6.4: Top view of aircraft optimized for cruise at altitudes of 28,000ft (Design E), 24,000 ft (Design F), and minimum cost Design A.

6.3 Cruise Altitude Study

Reducing the cruise altitude of commercial aircraft would reduce contrail formation and potentially reduce the net impact of aircraft emissions. Today's aircraft operate at 30-40,000 ft, the optimal altitudes considering range and cruise speed. In order to minimize the impact on fuel economy, the aircraft needs to be designed to operate at these altitudes.

The single-objective version of the genetic algorithm was run with the initial cruise altitude fixed to 24,000 ft and 28,000 ft. A maximum cruise climb of 4,000 ft is allowed. Data for the optimized designs is shown in Table 6.5.

As expected, Designs E and F are designed to fly slower (Mach 0.762 and 0.728) in order to negotiate the increased drag inherent to lower altitude cruise. The corresponding increase in operating cost is 4% for Design E and 7% for Design F. The amount of fuel carried to complete the mission is decreased by 5% if the aircraft is designed to fly at 28,000 ft (a similar altitude to the aircraft optimized for lowest-fuel, Design B) and increased by 7% for a design altitude of 24,000 ft. Changes in NO_x production are minimal: with all three designs optimized for minimal operating cost, the optimizer is driven to select high pressure ratios and combustion temperatures, regardless of cruise altitude.

	Units	Design A	Design E	Design F
Relative Cost	—	1.00	1.04	1.07
Fuel Carried	lbs	119,018	112,950	127,069
LTO NO_x	kg	30.88	31.74	29.85
Relative Noise	EPNdB	0.0	-3.87	1.85
Variables				
Max. Take-Off Weight	lbs	372,539	357,802	374,525
Wing Reference Area	ft^2	3,461	2,955	3,502
Wing t/c	%	11.7	14.8	13.6
Wing Location	%	39.2	40.6	39.2
Wing Aspect Ratio	—	7.38	9.39	8.15
Wing Taper Ratio	—	0.10	0.10	0.22
Wing Sweep	deg	33.70	29.41	29.51
Horizontal Tail Area	ft^2	929	778	732
SLS Thrust	lbs	68,404	71,106	63,602
Turbine Inlet Temp	°F	3,203	3,220	3,228
Bypass Ratio	—	9.59	9.88	9.59
Engine Pressure Ratio	—	59.91	59.61	60.00
Init. Cruise Altitude	**ft**	**32,937**	**28,000**	**24,000**
Final Cruise Altitude	ft	40,790	33,023	29,531
Cruise Mach Number	—	0.844	0.762	0.728

Table 6.5: Data for the cost-optimized designs with initial cruise altitude fixed at 28,000 ft (Design E) and 24,000 ft (Design F) compared to the optimized design for minimum cost (Design A).

The purpose of operating aircraft at lower altitudes would be to reduce the net impact of the emissions on the atmosphere. Accurately estimating these net effects requires more information than the amount of emissions generated by the engines. Indeed, to truly understand the effects of the combustion products on the atmosphere, a detailed study of the propagation and absorption characteristics of the upper troposphere would be required.

6.4 Contribution of Fuel Cost to Total Cost

Increasing the cost of fuel by 25%, from \$0.96 per gallon to \$1.20 per gallon, the Pareto front illustrating the optimal trade-off between fuel carried and operating cost is shifted towards higher operating cost (Figure 6.5).

	Units	Design A Min Cost	Design B Min Fuel	Design G Min Cost	Design H Min Fuel
Fuel Cost	**$/gallon**	**0.96**	**0.96**	**1.20**	**1.20**
Objectives					
Relative Cost	—	1.0	1.02	1.03	1.04
Fuel Carried	lbs	119,018	106,707	116,592	106,430
LTO NO_x	kg	30.88	29.68	30.18	28.30
Relative Noise	EPNdB	0.0	-5.13	-1.49	-5.90
Variables					
Max. Take-Off Weight	lbs	372,539	352,515	367,881	356,868
Wing Reference Area	ft^2	3,461	2,942	3,451	3,184
Wing t/c	%	11.7	13.5	12.7	13.7
Wing Location	%	39.2	41.2	38.6	40.4
Wing Aspect Ratio	—	7.38	9.99	7.54	9.97
Wing Taper Ratio	—	0.10	0.10	0.10	0.10
Wing Sweep	deg	33.70	26.17	34.59	27.31
Horizontal Tail Area	ft^2	929	766	882	779
SLS Thrust (per engine)	lbs	68,404	67,311	67,791	64,732
Thrust-to-Weight Ratio	—	0.367	0.382	0.369	0.363
Turbine Inlet Temp	°F	3,203	3,215	3,219	3,220
Bypass Ratio	—	9.59	10.35	10.30	10.98
Engine Pressure Ratio	—	59.91	59.63	59.91	59.79
Init. Cruise Altitude	ft	32,937	30,746	32,198	30,805
Final Cruise Altitude	ft	40,790	38,734	41,668	39,219
Cruise Mach Number	—	0.844	0.739	0.832	0.755

Table 6.6: Data for the optimized designs with fuel cost at $0.96 per gallon (Designs A and B) and $1.20 per gallon (Designs G and H).

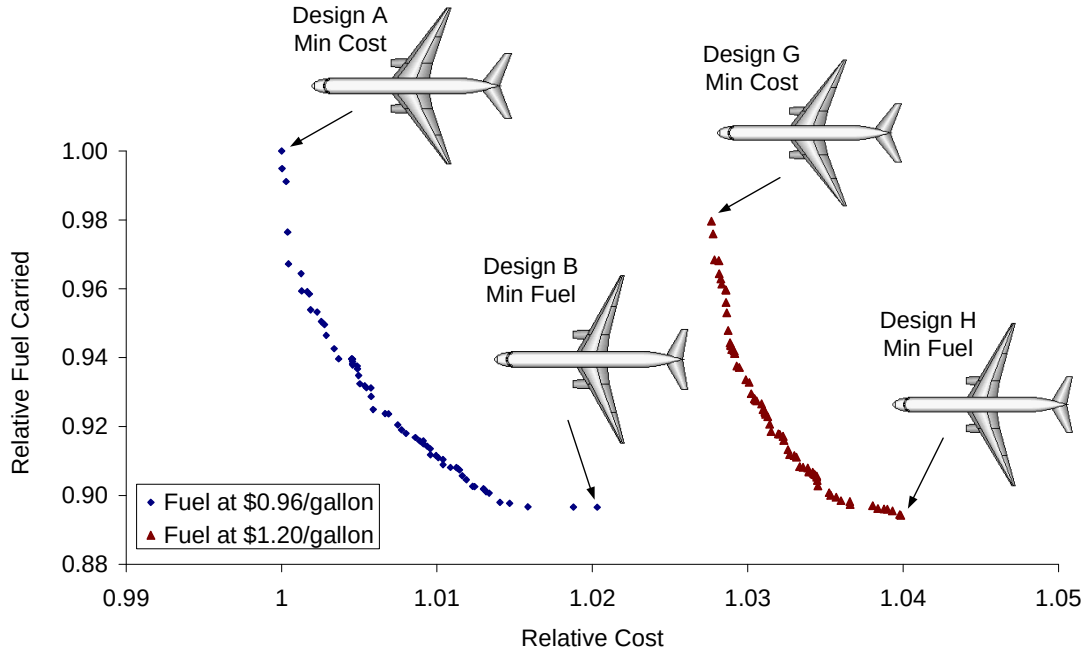

Figure 6.5: The impact of increasing fuel cost by 25% is reflected on the fuel-operating cost Pareto front.

Data for Designs A, B, G, and H is summarized in Table 6.6. As can be expected, Design B (min fuel carried at $0.96 per gallon) and Design H (min fuel carried at $1.20 per gallon) carry an essentially identical fuel load — they are both optimized for lowest fuel carried, regardless of fuel cost.

The minimum cost design with fuel at $1.20 per gallon (Design G), on the other hand, carries 2% less fuel than the minimum cost design at $0.96 per gallon (Design A): with increasing fuel costs, designs that carry less fuel are preferred. The decreased drag that yields this reduction in required fuel stems from the lower cruise speed (0.832 vs. 0.844), that, however, causes an increase in block time and overall operating costs. Overall, the 25% increase in fuel price results in only a 3% increase in operating cost. The two low-fuel and low-cost aircraft are geometrically very similar — reflecting the relatively low importance of fuel cost as a design driver.

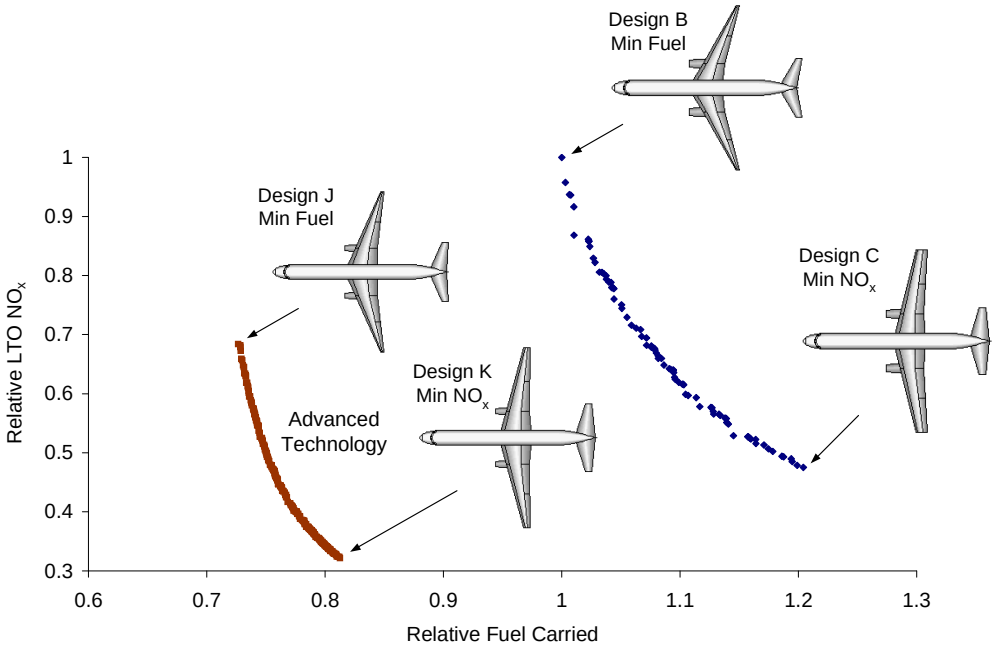

Figure 6.6: The benefits of increased laminar flow, reduced induced drag, and lower structural weight are illustrated on the fuel-cost Pareto front.

6.5 Impact of Future Technologies

Increased laminar flow, advanced materials, and reduced induced drag are three examples of advanced technologies studied with the design tool.

- Increased laminar flow: for wing sweeps less than 20 degrees, laminar flow is assumed to extend over 60% of the chord.
- Advanced materials: a factor of 0.8 is applied to the aircraft structural weight.
- 10% reduction in induced drag.

These technologies, meant to improve aerodynamic efficiency or reduce structural weight, are of interest because they also have significant impact on the environmental performance of the aircraft. Figure 6.6 illustrates the changes to the aircraft fuel-NO_x performance.

	Units	Design B Min Fuel	Design C Min NO_x	Design J Min Fuel	Design K Min NO_x
Objectives					
Relative Cost	—	1.02	1.09	0.96	1.00
Fuel Carried	lbs	106,707	134,796	78,243	87,485
LTO NO_x	kg	29.68	14.36	20.18	9.47
Relative Noise	EPNdB	-5.13	3.66	-5.50	-0.80
Variables					
Max. Take-Off Weight	lbs	352,515	407,516	304,611	333,634
Wing Reference Area	ft^2	2,942	3,887	3,122	3,855
Wing t/c	%	13.5	12.8	12.9	12.8
Wing Location	%	41.2	48.1	41.3	44.7
Wing Aspect Ratio	—	9.99	8.94	10.00	9.96
Wing Taper Ratio	—	0.10	0.39	0.10	0.21
Wing Sweep	deg	26.17	11.22	19.81	12.10
Horizontal Tail Area	ft^2	766	953	870	1,099
SLS Thrust (per engine)	lbs	67,311	60,264	46,525	41,120
Thrust-to-Weight Ratio	—	0.382	0.296	0.422	0.246
Turbine Inlet Temp	°F	3,215	3,147	3,222	3,135
Bypass Ratio	—	10.35	10.32	11.50	12.18
Engine Pressure Ratio	—	59.63	40.27	59.36	40.05
Init. Cruise Altitude	ft	30,746	28,381	32,372	30,114
Final Cruise Altitude	ft	38,734	33,288	40,097	38,718
Cruise Mach Number	—	0.739	0.669	0.725	0.669

Table 6.7: Data for optimized low-fuel and low-NO_x conventional Designs B and C and advanced technology Designs J and K.

Data for the extreme designs is summarized in Table 6.7. The advanced technology lowest-NO_x aircraft (Design K) produces 34% less NO_x per LTO cycle than the conventional low-NO_x aircraft (Design C), at 9% lower operating cost. Similarly, the advanced low-fuel candidate (Design J) requires 27% less fuel (and therefore produces 27% fewer fuel-proportional emissions) to complete the mission while releasing 32% fewer NO_x emissions than the conventional lowest-fuel aircraft (Design B). Taking advantage of the drag benefits associated with increased laminar flow, the two advanced designs feature wing sweep under 20 degrees — without any impact on cruise Mach number, thanks to the thinner wing afforded by the reduced fuel capacity requirement.

Incorporating these advanced technologies negates some of the adverse effects of optimizing the aircraft for low-noise or low-emissions. Indeed, the advanced low-NO_x aircraft (Design K) generates 30% of the NO_x emissions generated by the conventional low-cost design (Design A), at the same operating cost. From the reduced structural weight and fuel load (and therefore maximum takeoff weight), the two advanced designs require approximately 30% less installed thrust, resulting in a cumulative noise margin of 5.5 EPNdB for Design J and 0.8 EPNdB for Design K.

Chapter 7

Fleet Design

7.1 Introduction

As was discussed previously, the introduction of noise-based restrictions at airports worldwide has led airlines to demand, and adopt, low-noise aircraft. These restrictions can fundamentally change an airline's routing strategy: the noise performance of each type must be taken into account during the assignment process.

A simple fleet design tool was developed to select the optimal aircraft types, determine the fleet mix, and route the aircraft to meet passenger demand, at minimum operating cost. The emphasis is on the impact of airport noise restrictions: if an airport adopts noise regulations, for example, how should the airline re-allocate aircraft?

While this tool does not feature the level of complexity required to capture all aspects of fleet assignment, it does allow the user to understand the implications of noise regulations at the airline level, and points to the importance of further system-level environmental studies.

7.2 Aircraft Routing and Fleet Assignment

The introduction of noise and emissions landing and takeoff fees has driven airlines to consider aircraft environmental performance as part of their acquisition plans — as in the case of the Airbus A380.

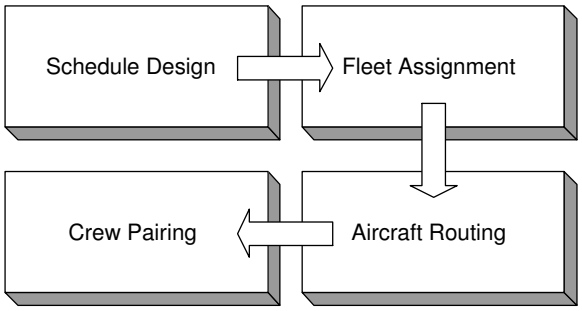

Figure 7.1: Airline schedule development.

While airport fees based on aircraft noise and emissions performance are not currently legal in the US, they have been in place in Europe for some time: London Heathrow, Brussels National, and Madrid Barajas are just a few of the airports that include aircraft certification noise level as part of landing and takeoff fees.

Schedule development, a crucial aspect of profitable airline management, involves many steps, including schedule design, fleet assignment, aircraft routing, and crew pairing [79]. Here we assume that schedule design has been finalized; the focus is on *fleet assignment*, that is the assignment of available aircraft to the scheduled flights, and on *aircraft routing*, the sequence of flights to be flown by each aircraft throughout the day (Figure 7.1). Typical fleet assignment objectives include minimizing assignment cost or maximizing the profit from each flight. In our case, the objective is to meet the passenger demand throughout the day with the lowest total landing and takeoff (LTO) costs.

Fleet assignment problems can be classified as either "warm start", in which case an existing assignment is used as a starting point, or "cold start", in which only the fleet size, aircraft types, and passenger demand are known [80]. Fleet assignment and aircraft routing problems have been solved using various optimization methods, including integer linear programming [81, 82], neighborhood search [83], genetic algorithms [84], and collective intelligence [85].

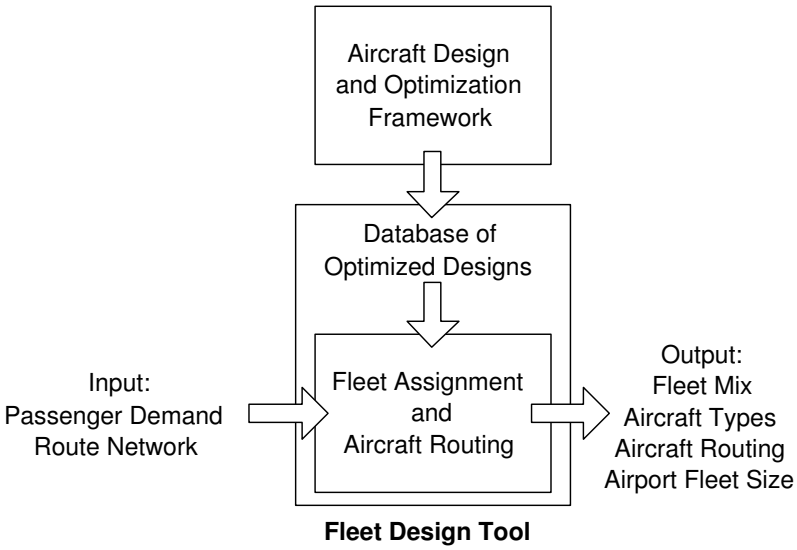

Figure 7.2: The fleet design tool includes a database of optimized aircraft designs and a fleet assignment and aircraft routing module.

7.3 The Fleet Design Tool

7.3.1 Overview

Combining the conceptual aircraft design tool with an aircraft routing algorithm allows the user to study various fleet-level scenarios, such as the impact of changing noise fees at an airport, modifying the fleet mix or size, and how best to respond to changes in passenger demand, for example. This "System of Systems" framework is shown in Figure 7.2. A database of optimal aircraft designs is created before solving the fleet design problem.

The objective is to determine the types of aircraft, the fleet mix, and the aircraft routing and resident fleet size at each airport that minimizes the landing and takeoff fees levied by airports while meeting demand. The 9-airport, 20-flight arc sample problem (Figure 7.3) is used to demonstrate the performance of the approach. Airports D and H feature landing and takeoff fees that are a function of the noise performance of the aircraft. Only the quietest types of aircraft are allowed to operate in and out of airport B.

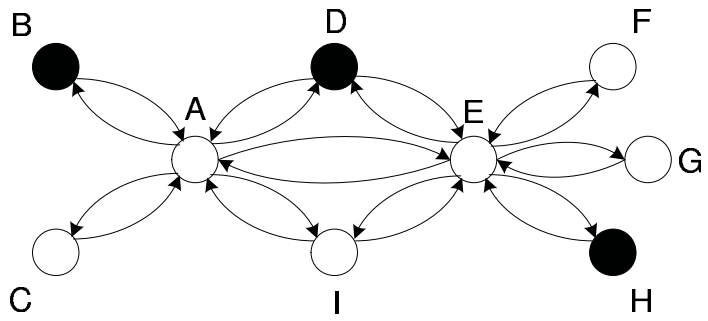

Figure 7.3: The 9-airport, 20-arc problem. The LTO fees at airports D and H (in black) include noise fees. Only the quietest aircraft (Noise Category 3) can operate in and out of airport B.

The passenger demand on each arc is given as a function of time (determined as part of the schedule design). The day is split into six 4-hour segments. It is assumed that each arc can be flown and the aircraft turned around in one time segment.

7.3.2 Formulation

The optimization problem is as follows:

MINIMIZE:	Total LTO Fees
VARIABLES:	Number of aircraft of each type, on each arc, at each time segment
	Resident fleet of each type, at each airport
	Passenger capacity of each aircraft type
	Noise category of each aircraft type
CONSTRAINTS:	Passenger demand
	Assignment continuity of each aircraft type
	Resident fleet conservation of each aircraft type
	Acquisition budget

The four types of variables are: $u_{i,j,m}$, the number of aircraft of type m assigned to flight arc i at time segment j, $v_{k,m}$, the number of resident aircraft of type m at airport k. p_m and n_m are the passenger capacity and noise category of aircraft type m (based on certification noise), respectively.

Noise Margin	Noise Cat. n_m	Environmental Factor E			
		Airport B	Airport D	Airport H	Others
0 dB	1	N/A	1.7	1.5	1.0
6 dB	2	N/A	1.5	1.2	1.0
12 dB	3	1.0	1.0	1.0	1.0

Table 7.1: The environmental factor E is a function of the noise performance of the aircraft.

Time Segment j	Day/Night Factor D_j
1 (24:00 - 03:59)	2
2 (04:00 - 07:59)	2
3 (08:00 - 11:59)	1
4 (12:00 - 15:59)	1
5 (16:00 - 19:59)	1
6 (20:00 - 23:59)	1

Table 7.2: The Day/Night factor is a penalty applied to aircraft operating during noise-sensitive hours.

The resident fleet is the number of airplanes at each airport at the start and end of the day, which must be the same to repeat the schedule the next day.

The allowable ranges for the variables are:

$$0 \leq u_{i,j,m} \leq 15 \tag{7.1}$$

$$0 \leq v_{k,m} \leq 30 \tag{7.2}$$

$$p_m \in \mathrm{P} = \{100,\ 200,\ 300\} \tag{7.3}$$

$$n_m \in \mathrm{N} = \{1,\ 2,\ 3\} \tag{7.4}$$

In the example problem presented here, we have 20 arcs i and 6 time segments j, with 9 airports k and 2 aircraft types m, yielding a total of 262 variables.

As part of this study, a model based on the landing and takeoff charge at Brussels National was used as the objective. It is shown below:

$$C_{LTO} = W_m \times E_{i,m} \times D_j \tag{7.5}$$

Noise	Pax Cap. p_m		
Cat. n_m	**100**	**200**	**300**
1	48	80	138
2	51	85	145
3	56	93	161

Table 7.3: Maximum takeoff weight W_m, in tons, as a function of passenger capacity p_m and noise category n_m.

W_m is the maximum takeoff weight of aircraft type m, in tons. The maximum allowable value of this factor is 175 tons, regardless of the actual aircraft weight. The environmental factor, $E_{i,m}$, is a function of the aircraft's noise category n_m and the airport in question, i (Table 7.1). Note that only aircraft belonging to noise category 3 are allowed to operate in and out of airport B. Finally, D_j is the day/night factor for time segment j, as can be seen in Table 7.2.

The total landing takeoff fees for all flights, a non-linear objective, can be written as follows:

$$\min_{u_{i,j,m},v_{k,m},E_{i,m},n_m} \left(G = \sum_{i,j,m} u_{i,j,m} E_{i,m} W_m D_j \right) \tag{7.6}$$

W_m is obtained from the optimized designs database for a combination of aircraft passenger capacity (p_m) and noise factor (n_m). The database entries are shown in Table 7.3.

Constraints are required to ensure that passenger demand $D_{i,j}$ is met in full by capacity $C_{i,j,m}$ for each aircraft type, arc, and time segment. There are 20 arcs and 6 time segments, for a total of 120 passenger demand constraints. For these non-linear constraints to be satisfied:

$$D_{i,j} - \sum_m C_{i,j,m} \leq 0 \tag{7.7}$$

with:

$$C_{i,j,m} = p_m \cdot u_{i,j,m} \tag{7.8}$$

Assignment continuity ensures that an aircraft of a type can only be assigned to an arc if an aircraft of that same type is available at the originating airport.

With 9 airports, 6 time segments, and 2 aircraft types, 108 continuity constraints are included. Defining $S_{k,j,m}$ as the state of the fleet of aircraft of type m at airport k, at the beginning of time increment j, we require:

$$-S_{k,j,m} \leq 0 \tag{7.9}$$

where:

$$S_{k,j,m} = S_{k,j-1,m} + \sum_i M_{out_{k,i}} \cdot u_{i,j,m} + \sum_i M_{in_{k,i}} \cdot u_{i,j-1,m} \tag{7.10}$$

The M_{out} matrix is used to tally outbound aircraft for each airport during a time segment.

Likewise, M_{in} is used to determine the inbound aircraft to be added to an airport pool. For example, for our 9-city, 20-arc case:

$M_{out} =$

	AB	AC	...	BA	...	IE
A	-1	-1	...	0	...	0
B	0	0	...	-1	...	0
C	0	0	...	0	...	0
⋮	⋮	⋮	⋱	⋮	⋱	⋮
I	0	0	...	0	...	-1

(7.11)

$M_{in} =$

	AB	AC	...	BA	...	IE
A	0	0	...	1	...	0
B	1	0	...	0	...	0
C	0	0	...	0	...	0
⋮	⋮	⋮	⋱	⋮	⋱	⋮
I	0	0	...	0	...	0

(7.12)

The resident fleet size of aircraft type m, $SI_{k,m}$ at each airport k must equal the number of airplanes of the same type, $SF_{k,m}$ at the end of the day so the schedule can be restarted the following day. In equation form, we require:

$$-SI_{k,m} + SF_{k,m} \leq 0 \tag{7.13}$$

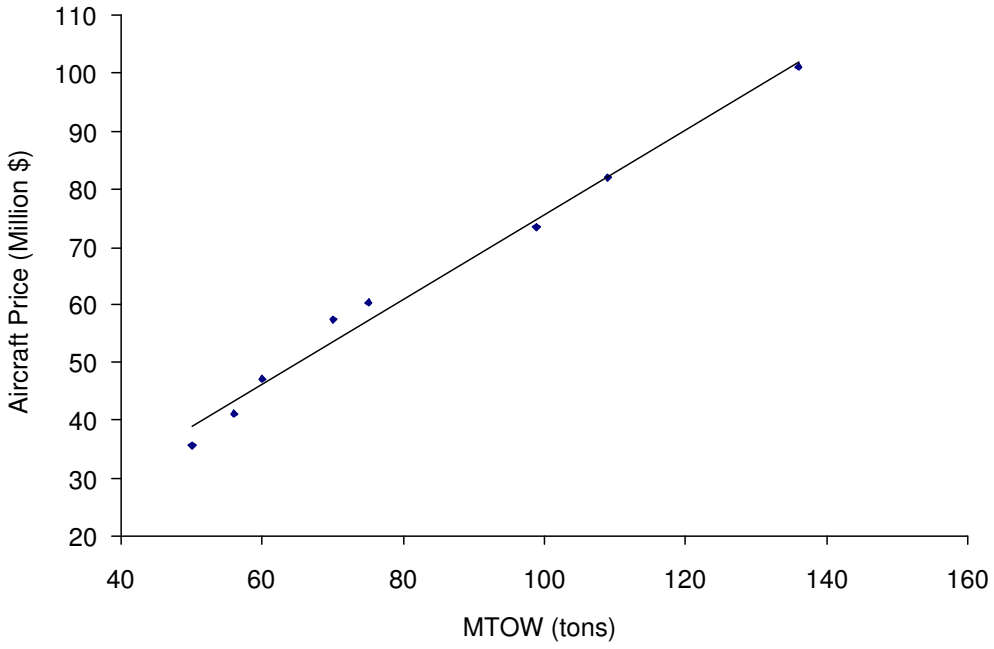

Figure 7.4: Aircraft cost is closely correlated to maximum takeoff weight [86].

with:

$$SI_{k,m} = v_{k,m} \tag{7.14}$$

$$SF_{k,m} = \sum_{i} M_{in_{k,i}} \cdot u_{i,j_{final},m} \tag{7.15}$$

The airports in this sample problem contribute 18 resident fleet constraints.

The aircraft cost is based on a maximum takeoff-weight correlation, shown in Figure 7.4. The cost of one aircraft, in millions of dollars, is:

$$H = 0.7337W_m + 2.1788 \tag{7.16}$$

Finally, the total acquisition budget B is enforced with:

$$\sum_{m} \sum_{k} H(W_m) \cdot SI_{k,m} \leq B \tag{7.17}$$

This results in a total of 247 constraints.

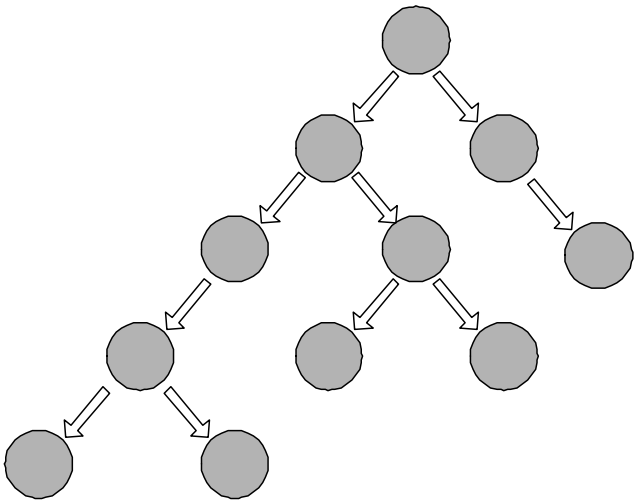

Figure 7.5: The Branch and Bound search tree.

7.4 Integer Programming

AMPL-CPLEX 8.0 features the Branch and Bound technique for solving integer problems. The objective and constraints must be linear [87, 88]. In the current formulation of the fleet design problem, the total daily LTO cost is a function of the variables aircraft weight, noise factor, and segments flown, resulting in a non-linear objective that CPLEX cannot manage.

To resolve this issue, the problem was linearized by removing the aircraft type components from the objective; the fleet assignment and aircraft routing problem was run for every combination of designs for the two aircraft types. The passenger capacity constraints are also linearized in the process. With 9 designs possibilities for each aircraft type, a total of 81 runs was required. The combination of designs that yields the minimum cost after fleet assignment and aircraft routing is considered the global optimum.

The branch-and-bound technique has proven to be reasonably efficient on practical problems. The optimizer maintains a search tree of related linear programming subproblems (Figure 7.5). The algorithm starts with the top node, whose associated subproblem is the relaxation of the integer program — the linear problem that results when all integrality restrictions are dropped.

If this relaxation happens to have an integer solution, then it would provide an optimal solution to the integer program. Normally, however, the optimum for the relaxation has some fractional-valued integer variables. A fractional variable is then chosen for branching, and two new subproblems are generated, each with more restrictive bounds for the branching variable.

Most likely each of these subproblems also has fractional-valued integer variables, in which case the process is repeated, producing the tree structure shown above. Because a single integer program generates many LP subproblems, even small instances can be very computation-intensive and require significant amounts of memory.

The number of linearized fleet design problems grows with the number of aircraft types m, as well as with the number of passenger capacities (P) and noise factors (N), according to:

$$\text{No. of Runs} = (\text{P} \times \text{N})^m \tag{7.18}$$

Hence, as the number of aircraft types and configurations for each type is increased, the number of CPLEX runs required to determine global optimum becomes very large. If 5 aircraft types were to be designed, each with 16 possible combinations of passenger capacity and noise performance (4 choices each), over 1 million AMPL-CPLEX runs would be required.

7.5 Results

The 9-airport, 20-arc network sample problem introduced above is used to demonstrate the performance of the approach. The asymmetric, time-dependent passenger demand, as a function of time and flight arc (route), is shown in Table 7.4.

With an acquisition budget of $1,800 million, the fleet composition, selected aircraft types, and minimized daily LTO fees are shown on the first line of Table 7.6, marked Case 1. The number of flights covered by the two types for every arc and time increment is shown in Table 7.5. To illustrate the impact of these operating noise restrictions and fees, the same problem was solved, except that the Noise Category 3 requirement was removed at Airport B.

	Time Segment					
Arc	**1**	**2**	**3**	**4**	**5**	**6**
AB	100	200	200	200	100	100
AC	200	100	175	100	200	200
AD	200	200	200	200	250	200
AE	400	630	800	800	550	300
AI	100	100	200	100	100	100
BA	100	100	200	200	200	100
CA	200	260	100	100	100	200
DA	200	200	200	225	200	200
DE	200	200	200	200	200	200
EA	400	600	800	800	600	400
ED	200	200	200	200	200	200
EF	100	0	100	100	130	100
EG	100	100	100	100	100	100
EH	200	200	200	200	200	200
EI	100	100	100	100	100	125
FE	100	125	100	100	100	100
GE	100	100	100	180	210	100
HE	200	200	200	200	200	200
IA	100	200	100	150	100	100
IE	100	125	100	100	100	100

Table 7.4: Passenger demand for each arc as a function of time.

	Aircraft Type 1 # Flights						Aircraft Type 2 # Flights					
	Time Segment						Time Segment					
Arc	**1**	**2**	**3**	**4**	**5**	**6**	**1**	**2**	**3**	**4**	**5**	**6**
AB	1	2	2	2	1	1	0	0	0	0	0	0
AC	0	1	2	1	0	0	1	0	0	0	1	1
AD	0	0	0	0	1	0	1	1	1	1	1	1
AE	0	1	0	0	0	1	2	3	4	4	3	1
AI	1	1	0	1	0	1	0	0	1	0	1	0
BA	1	1	2	2	2	1	0	0	0	0	0	0
CA	0	1	1	1	1	0	1	1	0	0	0	1
DA	0	0	0	1	0	0	1	1	1	1	1	1
DE	0	0	0	0	0	0	1	1	1	1	1	1
EA	0	0	0	0	0	2	2	3	4	4	3	1
ED	0	0	0	0	0	0	1	1	1	1	1	1
EF	1	0	1	2	0	1	0	0	0	0	1	0
EG	1	1	1	0	1	1	0	0	1	1	0	0
EH	0	0	0	0	0	0	1	1	1	1	1	1
EI	1	1	1	1	1	0	0	0	0	0	0	1
FE	1	0	1	1	1	1	0	1	0	0	0	0
GE	1	1	1	0	1	1	0	0	0	1	1	0
HE	0	0	0	0	0	0	1	1	1	1	1	1
IA	1	0	1	0	1	1	0	1	0	1	0	0
IE	1	0	1	1	1	1	0	1	0	0	0	0

Table 7.5: Case 1: Number of flights assigned to each arc at each time segment. Airports D and H feature noise-based fees and only noise category 3 aircraft may operate out of and into airport B (Acquisition Budget: $1,800 million).

Case	Airports with Noise Restrictions	LTO Cost ($)	Aircraft Type 1			Aircraft Type 2		
			Fleet Size	Pax. Cap.	Noise Cat.	Fleet Size	Pax. Cap.	Noise Cat.
1	B,D,H	28,688	18	100	3	17	200	1
2	D,H	27,763	15	100	1	20	200	1

Table 7.6: Total LTO cost and optimal fleet mix for Cases 1 and 2.

	Aircraft Type 1 # Flights						**Aircraft Type 2 # Flights**					
	Time Segment						**Time Segment**					
Arc	**1**	**2**	**3**	**4**	**5**	**6**	**1**	**2**	**3**	**4**	**5**	**6**
AB	1	**0**	**0**	**0**	1	1	0	**1**	**1**	**1**	0	0
AC	0	1	2	1	0	0	1	0	0	0	1	1
AD	0	0	0	0	1	0	1	1	1	1	1	1
AE	0	1	0	0	0	1	2	3	4	4	3	1
AI	1	1	0	**0**	**1**	1	0	0	1	**1**	**0**	0
BA	1	1	**0**	**0**	**0**	1	0	0	**1**	**1**	**1**	0
CA	0	1	1	1	1	0	1	1	0	0	0	1
DA	0	0	0	1	0	0	1	1	1	1	1	1
DE	0	0	0	0	0	0	1	1	1	1	1	1
EA	0	0	**2**	0	0	**0**	2	3	**4**	4	3	**2**
ED	0	0	0	0	0	0	1	1	1	1	1	1
EF	1	0	1	2	0	1	0	0	0	0	1	0
EG	1	1	1	0	1	1	0	0	1	1	0	0
EH	0	0	0	0	0	0	1	1	1	1	1	1
EI	1	1	1	1	1	0	0	0	0	0	0	1
FE	1	0	1	1	1	1	0	1	0	0	0	0
GE	1	1	1	0	1	1	0	0	0	1	1	0
HE	0	0	0	0	0	0	1	1	1	1	1	1
IA	1	0	1	0	1	1	0	1	0	1	0	0
IE	1	0	1	1	1	1	0	1	0	0	0	0

Table 7.7: Case 2: Number of flights assigned to each arc at each time segment. Restrictions at Airport B have been removed. Changes relative to Case 1 are shown in **bold** (Acquisition Budget: $1,800 million).

Hence, only airports D and H feature noise-based landing and takeoff fees. The results of this second case are shown on the second line of Table 7.6 and the fleet assignment schedule is shown in Table 7.7.

The fleet composition in both cases includes a 100 passenger aircraft and a 200 passenger aircraft. In the first case, however, the smaller aircraft is of noise category 3, enabling it to operate in and out of every airport in the network, including airport B. As a result, the type 1 fleet size for case 1 is slightly larger than for case 2 (18 vs. 15): these additional aircraft are used to operate solely between airports A and B, and are supplemented by other type 1 aircraft as required by passenger demand. In both cases, the larger type 2 aircraft cover the trunk routes, while the smaller type 1 aircraft are used on the thinner spokes.

As can be seen from the fleet assignment schedules, the introduction of restrictive noise requirements — even at a single, non-hub airport — can have dramatic effects as the type assignment changes propagate through the network.

This is an example of the type of preliminary study that can be accomplished with this fleet design tool. By combining the aircraft design framework with a fleet assignment solver, as was done here, many types of scenarios can be studied. Clearly, managing noise-based operating restrictions at airports and integrating low-noise aircraft into the fleet requires careful consideration of passenger demand, aircraft routing, and fleet composition.

Chapter 8

Conclusion and Future Work

8.1 Conclusion

The objective of this research was to determine the feasibility of including environmental performance during the initial phase of aircraft design. A design tool was developed using multidisciplinary optimization to quantify the trade-offs between noise, emissions, and operating cost, both at single aircraft and fleet levels. Engine and noise models available from NASA were integrated into the optimization framework. The application of this design approach was successful in producing optimal solutions. The ability of a conceptual tool to predict the consequences of design changes, however, is heavily dependent on validation: because of the uncertainty in modeling noise and emissions, it is important that the design tool be compared to additional experimental results and existing, usually proprietary, databases.

The study established a tradeoff between noise, emissions, and cost performance. The resolution of these diverging requirements will largely depend on the environmental regulations applying in the markets served by the aircraft. Significant reductions in emissions and perceived noise were found to be possible for aircraft specifically optimized with these objectives in mind. For an increase in operating cost of 9%, NO_x emissions could be reduced by as much as 50%, while cumulative certification noise could be lowered by up to 15 EPNdB for a cost increase of 26%.

There is little doubt that the market would be unwilling to accept these drastic trades unless regulatory bodies mandated increased environmental responsibility from the airline industry. Considering the recent explosive growth of public complaints, however, increasingly severe and restrictive operational measures at airports seem unavoidable.

The one trend that emerges amongst the seemingly conflicting objectives of noise, fuel consumption, and NO_x emissions is the opportunity for significant reductions in environmental impact by designing the aircraft to fly slower and at lower altitude. The larger fan frontal area of low-noise designs, the reduced thrust capabilities of low-NO_x engines, and the reduced drag mandated by the low-fuel aircraft — all these requirements point towards "Slower, Lower, Greener".

Finally, it is worth noting that the results presented here fully support the 'Balanced Approach' adopted by the ICAO that deems that reductions in the environmental nuisances associated with commercial aviation will be achieved most effectively by a combination of quieter and cleaner aircraft, appropriate flight procedures, suitable government regulations and — for the long-term — adequate land-use planning.

8.2 Future Work

While unconventional designs were not considered, certain configurations, such as blended-wing-body aircraft, have shown enormous potential for reduced environmental impact. Although these aircraft would require the development of new design modules independent of the databases and validated correlations available for the conventional designs studied here, the general methodology would still be applicable. As noise and emissions become ever more important design drivers, these unconventional designs may offer the only viable solution to ensure commercial aviation continues its spectacular growth. In addition, unconventional aircraft may eventually offer truly ultra-quiet and -clean operations, potentially revolutionizing air transport by enabling aircraft to operate closer to major cities than ever before.

With the eventual adoption of cruise emissions restrictions, developing an appropriate metric is essential.

As we have seen, simply quantifying the amount of emissions generated by the aircraft is not sufficient; the properties of the atmosphere means that the diffusion and mixing of the emissions are crucial. Accurate models of these mechanisms near the troposphere are critical in understanding the net impact of aircraft emissions on the global atmosphere. Enhancing the design tool by adding details of the mission profile would allow for a more accurate estimate of the emissions release schedule.

The uncertainty associated with the approximate methods used in this conceptual design tool could be propagated through the optimization process. The outcome would be a distribution of solutions, as opposed to the current single-point deterministic result for each design. This probabilistic approach would allow the user to understand — and quantify — the impact of modeling error on the conceptual design process. The computing cost associated with generating such a Pareto 'band' (as opposed to a well-defined front) would be considerable.

With significant reductions in emissions and noise, slower and lower-flying aircraft could be introduced into the fleet. In this situation, in addition to new challenges for air traffic control, integrating these new designs with potentially vastly different cruise speeds would require extensive schedule and equipment assignment changes. This would prohibit the decoupling of the design and assignment portions of the problem: aircraft design would have to be completed "in the loop" of fleet assignment. Such a large scale System-of-Systems approach may prove ideal for collaborative optimization frameworks: properly capturing seemingly weak coupling between variables (engine bypass ratio and takeoff time slots, for example) would become critical in obtaining truly optimal solutions.

Efforts in creating civil supersonic aircraft have highlighted the critical importance of environmental concerns. Balancing the objectives of low sonic boom, low certification noise, and low emissions with competitive cost performance is expected to demand extremely difficult trades due to the highly conflicting requirements of these objectives on an engine designed for supersonic flight. New technologies, such as variable bypass ratio, multi-stage fans, and ultra-low emissions combustors will, hopefully, enable a new generation of supersonic transports to succeed where Concorde failed.

Bibliography

[1] Penner, J.E., *Aviation and the Global Atmosphere*, Cambridge University Press, 1999, pp. 1-15.

[2] Sietzen Jr., F., "New Blueprint for NASA Aeronautics," Aerospace America, August 2002, p.25.

[3] Erickson, J. D., "Environmental Acceptability," Office of Environment and Energy, presented to the Federal Aviation Administration, 2000.

[4] Smith, M.J.T., *Aircraft Noise*, Cambridge University Press, 1989.

[5] Penner, J.E., *Aviation and the Global Atmosphere*, Cambridge University Press, 1999, p. 6.

[6] Boeing Current Market Outlook 2002 [Online],
URL: http://www.boeing.com/commercial/cmo,
The Boeing Company, 2002 [Cited April 8 2003].

[7] Emission charges at Swedish airports [Online],
URL: http://www.lfv.se/site/lfv/environment/eng/emission_charges.asp,
Swedish Civil Aviation Administration, October 2000 [Cited April 8 2003].

[8] Pacull, M., "Transport Aircraft Noise Technologies," *Proceedings of the International Symposium: Which Technologies for Future Aircraft Noise Reduction?*, Arcachon, France, October 2002.

[9] FAA's Preliminary Briefing on CAEP/6 [Online],
URL: http://www.ueet.nasa.gov/toi/viewtoi.php?id=119,
NASA Glenn Research Center, February 2004 [Cited May 17 2004].

[10] Kroo, I.M., Aircraft Design: Synthesis and Analysis [Online],
URL: http://adg.stanford.edu/aa241/AircraftDesign.html,
Chapter 12.1, Desktop Aeronautics, January 2003 [Cited May 17 2004].

[11] Night Restrictions at Heathrow, Gatwick and Stansted [Online],
URL: http://www.aviation.dft.gov.uk/consult/night/index.htm,
UK Department of the Environment, Transport and the Regions, January 1999 [Cited April 8 2003].

[12] McGregor, D.L. and Wat, J.K., "Efficient Low-Noise Airplane Operations", Presented at Jet Set Go — Environmental Aviation Takes Off, Palm Springs, CA, February 29 - March 4, 2004.

[13] Elmer, K., et al, "A Continuous Descent Approach Study Using Ames B747-400 Flight Simulator," AIAA's Aircraft Technology, Integration, and Operations (ATIO) 2002, Los Angeles, CA, Oct. 1-3 2002, AIAA Paper 2002-5869.

[14] Erkelens, L.J., "Advanced Noise Abatement Procedures for Approach and Departure," AIAA Guidance, Navigation, and Control Conference and Exhibit, Monterey, CA, Aug. 5-8 2002, AIAA Paper 2002-4858.

[15] Elmer, K., et al, "Community Noise Reduction Using Continuous Descent Approach: A Demonstration Flight Test at Louisville ," 9th AIAA/CEAS Aeroacoustics Conference and Exhibit, Hilton Head, SC, May 12-14, 2003, AIAA Paper 2003-3277.

[16] Anon., *ICAO Annex 16 Volume I — Aircraft Noise, Third Edition*, International Civil Aviation Organization, 1993.

[17] Gillian, R.E., *Aircraft Noise Prediction Program User's Manual*, NASA Langley Research Center, 1982.

[18] Smith, M.J.T., *Aircraft Noise*, Cambridge University Press, 1989, pp. 62-63.

[19] Ibid., pp. 66-67.

[20] Heidmann, M.F., "Interim Prediction Method for Fan and Compressor Source Noise," NASA Technical Memorandum X-71763, 1979.

[21] Stone, J.R., Groesbeck, D.E., and Zola, C.L., "An Improved Prediction Method for Noise Generated by Conventional Profile Coaxial Jets," 7th AIAA Aeroacoustics Conference, Palo Alto, CA, Oct 5-7 1981, AIAA Paper 81-1991.

[22] Fink, M.R., *Airframe Noise Prediction Method*, Federal Aviation Administration FAA-RD-77-29, 1977.

[23] Kendall, J.M. and Ahtye, W.F., "Noise Generation by a Lifting Wing/Flap Combination at Reynolds Numbers to 2.8E6," 18th AIAA Aerospace Sciences Meeting, Pasadena, CA, AIAA Paper 80-0035, 1980.

[24] Fink, M.R. and Schlinker, R.H., "Airframe Noise Component Interaction Studies," 5th AIAA Aeroacoustics Conference, Seattle, WA, AIAA Paper 79-0668, 1979.

[25] Konot, K.B., Janardan, B.A., Gliebe, P.R., "Improved NASA-ANOPP Noise Prediction Computer Code for Advanced Subsonic Propulsion Systems — Volume 1: ANOPP Evaluation and Fan Noise Model Improvement," NASA Contractor Report 195480, August 1996.

[26] The X-NOISE Network Homepage [Online],
URL: http://www.x-noise.net/, [Cited August 19 2004].

[27] Advanced Subsonic Technology Project [Online],
URL: http://www.lerc.nasa.gov/WWW/AST/ast.htm,
NASA Glenn Research Center [Cited August 19 2004].

[28] Quiet Aircraft Technology Program [Online],
URL: http://avst.larc.nasa.gov/projects_qat.html,
NASA Langley Research Center [Cited April 8 2003].

[29] Aviation Emissions Individual Datasheets [Online],
URL: http://www.qinetiq.com [cited 11 July 2004],
Qinetiq Combustion and Environment Group, Farnborough, UK.

[30] Smith, M.J.T., *Aircraft Noise*, Cambridge University Press, 1989, p. 260.

[31] Antoine, N.E., and Kroo, I.M., "Aircraft Optimization for Minimal Environmental Impact," AIAA Journal of Aircraft, Volume 41, Number 4, pp. 790-797, July-August 2004.

[32] Zimbrick, R.A., Colehour, J.L., *Investigation of very high bypass ratio engines for subsonic transports*, Journal of Propulsion and Power, Volume 6, pp. 3002, July-Aug. 1990.

[33] Hubbard, H.H., *Aeroacoustics of Flight Vehicles: Theory and Practive — Volume 2: Noise Control*, Acoustical Society of America, 1995, pp. 399-400.

[34] Anon., *ICAO Annex 16 Volume II — Aircraft Engine Emissions, Second Edition*, International Civil Aviation Organization, 1993.

[35] Lefebvre, A., *Gas Turbine Combustion*, Taylor & Francis, Philadelphia, PA, 1999, p. 318.

[36] Penner, J.E., *Aviation and the Global Atmosphere*, Cambridge University Press, 1999, pp. 185-217.

[37] Ibid., p. 8.

[38] Green, J.E., "Greener by Design — the technology challenge," *The Aeronautical Journal*, Volume 106, Number 1056, February 2002, p. 72.

[39] Locke, M. and Morales, A., System for assessing Aviation's Global Emissions [Online]
, URL: http://www.aee.faa.gov/emissions/global/sage.htm [cited 8 April 2003]

[40] Heywood, J.B., *Internal Combustion Engine Fundamentals*, McGraw-Hill, 1988, pp. 567-667.

[41] Heywood, J.B., Fay, J.A., and Linden, L.H., *Jet aircraft air pollutant production and dispersion*, AIAA Journal, 9(5):841-850, May 1971.

[42] Personal communication with Scott Jones, Aerospace Engineer, Airbreathing Systems Analysis Office, NASA Glenn Research Center, OH.

[43] Lukachko, S.P. and Waitz, I.A., "Effects of Engine Aging on Aircraft NO_x Emissions," ASME International Gas Turbine and Aeroengine Congress and Exhibition, June 2-5, 1997, ASME Paper 97-GT-386.

[44] Lefebvre, A., *Gas Turbine Combustion*, Taylor & Francis, Philadelphia, PA, 1999, pp. 331-335.

[45] Penner, J.E., *Aviation and the Global Atmosphere*, Cambridge University Press, 1999, pp. 76-79.

[46] Ackerman, S., Contrails [Online],
URL: http://cimss.ssec.wisc.edu/wxwise/class/contrail.html [cited 17 May 2004].

[47] Penner, J.E., *Aviation and the Global Atmosphere*, Cambridge University Press, 1999, p. 257.

[48] Garrison, M., DuBois, D., and Baughcum, S., "Aircraft Emission Inventories & Scenarios", presented to the Ultra-Efficient Engine Technology Program (UEET) Technology Forum, Westlake, OH, October 27-29, 2003.

[49] Kroo, I.M., "An Interactive System for Aircraft Design and Optimization," AIAA Aerospace Design Conference, Irvine, CA, Feb 3-6 1992, AIAA Paper 92-1190.

[50] Kroo, I.M. and Manning, V.M., "Collaborative Optimization: Status and Directions," 8th AIAA/USAF/NASA/ISSMO Symposium on Multidisciplinary Analysis and Optimization, Long Beach, CA, Sept. 6-8 2000, AIAA Paper 2000-4721.

[51] Clark, L.R. and Gerhold, C.H., "Inlet Noise Reduction by Shielding for the Blended-Wing-Body Airplane," 5th AIAA/CEAS Aeroacoustics Conference, Greater Seattle, WA, May 10-12 1999, AIAA Paper 99-1937.

[52] The Cambridge-MIT Silent Aircraft Initiative [Online],
URL: http://sai.eng.cam.ac.uk/,
Silent Aircraft Initiative, 2004 [Cited June 18 2004].

[53] Kroo, I.M., "AA241 Aircraft Design: Synthesis and Analysis," Course Notes [Online],
URL: http://adg.stanford.edu/aa241/AircraftDesign.html,
January 2003 [Cited August 1 2004].

[54] Kroo, I.M., "AA241 Aircraft Design: Synthesis and Analysis," Fuselage Layout Course Notes [Online],
URL: http://adg.stanford.edu/aa241/fuselayout/fuselayout.html,
January 2003 [Cited August 1 2004].

[55] Federal Aviation Administration Regulatory and Guidance Library, Part 25 — Airworthiness Standards: Transport Category Airplanes [Online],
URL: http://http://www.airweb.faa.gov/rgl, 2004 [Cited Augist 4 2004].

[56] Kroo, I.M., "AA241 Aircraft Design: Synthesis and Analysis," Wing Design Course Notes [Online],
URL: http://adg.stanford.edu/aa241/wingdesign/wingdesign.html,
January 2003 [Cited August 4 2004].

[57] Kroo, I.M., "AA241 Aircraft Design: Synthesis and Analysis," High Lift Systems Course Notes [Online],
URL: http://adg.stanford.edu/aa241/highlift/highlift.html,
January 2003 [Cited August 4 2004].

[58] Kroo, I.M., "AA241 Aircraft Design: Synthesis and Analysis," Aircraft Structures Course Notes [Online],
URL: http://adg.stanford.edu/aa241/structures/structures.html,
January 2003 [Cited August 4 2004].

[59] Kroo, I.M., "AA241 Aircraft Design: Synthesis and Analysis," Parasite Drag Course Notes [Online],

URL: http://adg.stanford.edu/aa241/drag/parasitedrag.html, January 2003 [Cited August 4 2004].

[60] Kroo, I.M., "AA241 Aircraft Design: Synthesis and Analysis," Transonic Compressibility Drag Course Notes [Online],
URL: http://adg.stanford.edu/aa241/drag/compressibledrag.html,
January 2003 [Cited August 20 2004].

[61] Kroo, I.M., "AA241 Aircraft Design: Synthesis and Analysis," Cruise Performance and Range Course Notes [Online],
URL: http://adg.stanford.edu/aa241/performance/cruise.html,
January 2003 [Cited August 5 2004].

[62] Kroo, I.M., "AA241 Aircraft Design: Synthesis and Analysis," Climb Performance Course Notes [Online],
URL: http://adg.stanford.edu/aa241/performance/climb.html,
January 2003 [Cited August 5 2004].

[63] Anon., *Standard Method of Estimating Comparative Direct Operating Costs of Turbine Powered Transport Airplanes*, Air Transportation Association of America, December 1967.

[64] Schaufele, R., *The Elements of Aircraft Preliminary Design*, Aries Publixations, Santa Ana, CA, 2000, pp. 311-323.

[65] Kroo, I.M., "AA241 Aircraft Design: Synthesis and Analysis," Operating Cost Course Notes [Online],
URL: http://adg.stanford.edu/aa241/cost/cost.html,
January 2003 [Cited August 5 2004].

[66] Jackson, P., *Jane's All the World's Aircraft*, Jane's Information Group, Coulsdon, Surrey, 1998.

[67] Klann, J.L. and Snyder, C.A., *NEPP User's Manual*, NASA Glenn Research Center, March 1997.

[68] Barter, G.E., *Exploration and Assessment of the Environmental Design Space for Commercial Aircraft and Future Technologies*, M.S. Thesis, Massachussetts Institute of Technology, June 2004.

[69] Manning, V.M., *Large-Scale Design of Supersonic Aircraft via Collaborative Optimization*, Ph.D. Thesis, Stanford University, 1999.

[70] Chan, M.K., *Supersonic Aircraft Optimization for Minimizing Drag and Sonic Boom*, Ph.D. Thesis, Stanford University, August 2003.

[71] Rodriguez, D.L., *A Multidiscplinary Optimization Method for Designing Boundary Layer Ingesting Inlets*, Ph.D. Thesis, Stanford University, January 2001.

[72] Martins, J.R.R.A., *A Coupled-Adjoint Method for High-Fidelity Aero-Structural Optimization*, Ph.D. Thesis, Stanford University, October 2002.

[73] Braun, R.D., *Collaboration Optimization: An Architecture for Large-Scale Distribution Design*, Ph.D. Thesis, Stanford University, May 1996.

[74] Kroo, I.M., "Decomposition and collaborative optimization for large scale aerospace design". In *Multidisciplinary Design Optimization: State of the Art*, SIAM, 1996.

[75] Sweeney, F.D., *New Smapling Distributions for Evolution Algorithms*, Ph.D. Thesis, Stanford University, August 2003.

[76] Deb, K., *Multi-objective Optimization Using Evolutionary Algorithms*, Wiley, 2001, pp. 28-41.

[77] Goldberg, D.E., *Genetic Algorithms in Search, Optimization, and Machine Learning*, Addison Wesley, 1989.

[78] Deb, K., *Multi-objective Optimization Using Evolutionary Algorithms*, Wiley, 2001, pp. 190-196.

[79] Etschmaier, M. and Mathaisel, D., "Airline Scheduling: An Overview," Transportation Science 19, 1985, pp. 127-138.

[80] Rushmeier, R. and Kontogiorgis, A., "Advances in the Optimization of Airline Fleet Assignment," Transportation Science 31, 1997, pp. 159-169.

[81] Abara, J., "Applying integer linear programming to the fleet assignment problem," Interfaces 19, 1989.

[82] Hane, C., et al., "The fleet assignment problem: Solving a large-scale integer program," Mathematical Programming 70, 1995, pp. 211-232.

[83] Ahuja, R., et al., "A very large scale neighborhood search algorithm for the quadratic assignment problem," Submitted to INFORMS Journal on Computing, 2002.

[84] Chung, T. and Chung J., "Airline Fleet Assignment Using Genetic Algorithms," GECCO2002, 2002 Genetic and Evolutionary Computation Conference, New York, New York, July 11-13, 2002, p. 255.

[85] Antoine, N.E. et al., "Fleet Assignment Using Collective Intelligence," 42nd AIAA Aerospace Sciences Meeting and Exhibit, Reno, NV, January 5-8 2004, AIAA Paper 2004-0622.

[86] Boeing Commercial Airplane Prices [Online],
URL: http://www.boeing.com/commercial/prices/,
Boeing, 2004 [Cited August 16 2004].

[87] Fourer, R., Gay, D., and Kernighan, B., *AMPL: a Modeling Language for Mathematical Programming*, Boyd and Fraser, 1993.

[88] Anon., *ILOG AMPL CPLEX System User's Guide*, ILOG, 2002.